

AD-A266 421

AFOSR-91-0117 0458



2

**EXPERIMENTAL STUDY OF NONASSOCIATED FLOW AND  
INSTABILITY OF FRICITIONAL MATERIALS**

by

Poul V. Lade and Jerry A. Yamamuro

Department of Civil Engineering  
University of California  
Los Angeles, California 90024-1593

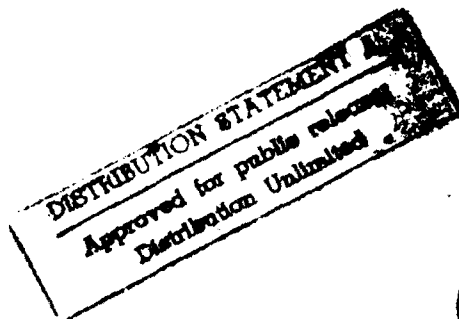
**FINAL REPORT**

AFOSR Grant No. 91-0117

Prepared for

Air Force Office of Scientific Research

Principal Investigator: Poul V. Lade




May 1993

DTIC  
ELECTE  
JUN 23 1993  
S B D

# REPORT DOCUMENTATION PAGE

Form Approved  
OMB No. 0704-0188

Public reporting burden for this collection of information is estimated to average 1 hour per response, including the time for reviewing instructions, searching existing data sources, gathering and maintaining the data needed, and completing and reviewing the collection of information. Send comments regarding this burden estimate or any other aspect of this collection of information, including suggestions for reducing this burden, to Washington Headquarters Services, Directorate for Information Operations and Reports, 1215 Jefferson Davis Highway, Suite 1204, Arlington, VA 22202-4302, and to the Office of Management and Budget, Paperwork Reduction Project (0704-0188), Washington, DC 20503.

1. AGENCY USE ONLY (Leave blank)		2. REPORT DATE May 1993		3. REPORT TYPE AND DATES COVERED Final (Dec 1990 - Mar 1993)	
4. TITLE AND SUBTITLE Experimental Study of Nonassociated Flow and Instability of Frictional Materials				5. FUNDING NUMBERS AFOSR 91-0117 2302/CS	
6. AUTHOR(S) Poul V. Lade and Jerry A. Yamamoto					
7. PERFORMING ORGANIZATION NAME(S) AND ADDRESS(ES) University of California, Los Angeles Department of Civil Engineering				8. PERFORMING ORGANIZATION REPORT NUMBER	
9. SPONSORING/MONITORING AGENCY NAME(S) AND ADDRESS(ES) AFOSR/NA Bolling AFB, DC 20332-6448				10. SPONSORING/MONITORING AGENCY REPORT NUMBER AFOSR- 91-0117	
11. SUPPLEMENTARY NOTES					
12a. DISTRIBUTION/AVAILABILITY STATEMENT  93-14657 					
13. ABSTRACT (Maximum 200 words) Experimental investigations and analyses have been performed to study the behavior of granular materials with respect to their nonassociated flow and instability under certain loading conditions. All experiments have been performed in triaxial compression and extension at high as well as at low confining pressures. Major topics that were studied include: strain localization in triaxial extension tests; drained and undrained stress-strain and strength behavior from low to high pressures in triaxial extension and compression; instability of granular materials at high pressures in triaxial compression and extension; the determination of Skempton's pore pressure parameter B at high pressures; strain rate effects of granular materials at high pressures in drained and undrained conditions; examination of the effective stress principle at high pressures; particle breakage at high pressures; behavior of sand in one-dimensional compression tests at very high pressures; determination of values of $K_0$ , the coefficient of earth pressure at rest, at high pressures; evaluation of the elastic modulus and Poisson's ratio at high pressure levels; correlations of high pressure soil behavior with stress-dilatancy, critical state, and input energy; static instability and liquefaction of loose fine sandy slopes; stability of granular materials in post peak softening regime; instability of dilating sand; and creep effects on static and cyclic instability of granular soils.					
14. SUBJECT TERMS Frictional materials; high pressures; instability; nonassociated flow; pore pressures; stress-strain behavior				15. NUMBER OF PAGES 853	
				16. PRICE CODE	
17. SECURITY CLASSIFICATION OF REPORT Unclassified	18. SECURITY CLASSIFICATION OF THIS PAGE Unclassified	19. SECURITY CLASSIFICATION OF ABSTRACT Unclassified	20. LIMITATION OF ABSTRACT UL		

## TABLE OF CONTENTS

	Page
INTRODUCTION	1
SUMMARY OF ATTACHMENT NO. 1	3
High Pressure Testing Equipment	3
Strain Localization	3
Stress-Strain Behavior at High Pressure	14
Instability of Soils at High Pressure	28
B-Values, The Effective Stress Principle, and Strain Rate Effects	37
Particle Breakage at High Pressures	45
One-Dimensional Compression Tests and Elastic Parameters	65
General Soil Behavior at High Pressures	75
SUMMARY OF ATTACHMENT NO. 2	105
Static Instability and Liquefaction of Loose Fine Sandy Slopes	105
Stability of Granular Materials in Post Peak Softening Regime	105
B-Value Measurements for Granular Materials at High Confining Pressures	108
Effects of Strain Rate on Instability of Granular Soils	108
Instability of Dilating Sand	108
Creep Effects on Static and Cyclic Instability of Granular Soils	110
Technical Journal Publications	116
Manuscripts in Preparation	116
Professional Personnel	117
Interactions	117

## INTRODUCTION

Extensive experimental investigations and analyses have been performed to study the behavior of granular materials with respect to their nonassociated flow and instability under certain loading conditions. All experiments have been performed in triaxial compression and extension at high as well as at low confining pressures.

The report takes the form of an executive summary with two attachments. Attachment no. 1 in essence contains the Ph.D. dissertation of the second author of this summary, and Attachment no. 2 contains journal papers that have been produced, published, or accepted for publication with support from AFOSR under this grant. These papers all deal with aspects of nonassociated flow and instability of frictional materials. The studies contained in these papers may be considered as additional investigations whose importance were realized and then researched in the overall process of this project.

Attachment no. 1 presents the results of an extensive experimental investigation of granular materials at high pressures. Among the many types of experiments performed are drained and undrained triaxial compression and extension tests with an overall confining pressure range of 0.25 to 68.9 MPa. One-dimensional compression tests up to 900 MPa axial stress level were also performed.

Major topics that were studied include: strain localization in triaxial extension tests; drained and undrained stress-strain and strength behavior from low to high pressures in triaxial extension and compression; instability of granular materials at high pressures in triaxial compression and extension; the determination of Skempton's pore pressure parameter  $B$  at high pressures; strain rate effects of granular materials at high pressures in drained and undrained conditions; examination of the effective stress principle at high pressures; particle breakage at high pressures; behavior of sand in one-dimensional compression tests at very high pressures; determination of values of  $K_0$ , the

coefficient of earth pressure at rest, at high pressures; evaluation of the elastic modulus and Poisson's ratio at high pressure levels; and correlations of high pressure soil behavior with stress-dilatancy, critical state, and input energy.

Attachment no. 2 deals with individual topics such as: Static instability and liquefaction of loose fine sandy slopes; stability of granular materials in post peak softening regime; B-value measurements for granular materials at high pressures; effects of strain rate on instability of granular soils; instability of dilating sand; and creep effects on static and cyclic instability of granular soils.

The following executive summary refers to the relevant chapters in Attachment no. 1, and the figure numbers are also maintained for easy reference to Attachment no. 1.

In the same manner, the summary of papers contained in Attachment no. 2 utilizes figures with the same figure numbers as in the papers.

Accession For	
NTIS GRA&I	<input checked="checked" type="checkbox"/>
DTIC TAB	<input type="checkbox"/>
Unannounced	<input type="checkbox"/>
Justification	
By	
Distribution/	
Availability Codes	
Dist.	Avail and/or Special
A-1	

## SUMMARY OF ATTACHMENT NO. 1

### High Pressure Testing Equipment (Chapter 3)

A high pressure testing system has been developed and continuously refined at University of California, Los Angeles (Chamieh, 1990; Yamamuro, 1990). The basic components of the system consist of a one meganewton loading frame, high pressure triaxial cell, two axes of motion control, instrumentation, signal conditioning, and a microcomputer. The system is schematically depicted in Figures 3-2, showing the process control loop, and Figure 3-1, which indicates the loading system. The two axes of control consist of hydraulic cylinders that are actuated by stepping motors through reduction gears and ball-screw jacks. The whole system is close-looped-controlled by a microcomputer, which operates an analog-to-digital converter for data acquisition, and a stepping motor controller to control the stepping motors, all supervised by custom control programs. Load is measured by a load cell, displacement by an LVDT, and cell and pore pressures by pressure transducers. All instrumentation signals are conditioned through amplifiers and active filters before entering the microcomputer. The first control axis controls either the true vertical stress or strain, by feeding hydraulic fluid into the loading frame's hydraulic cylinder, which raises or lowers the frame's table. The second control axis operates the confining pressure, by feeding hydraulic fluid into the high pressure triaxial cell. The high pressure triaxial cell and instrumentation can test the specimens in either compression or extension, and has experienced confining pressures of up to 100 MPa. Custom control software has been developed to perform a wide variety of tests under both true strain and true stress control.

### Strain Localization (Chapter 4)

A series of conventional extension tests (tests with only membranes surrounding the specimen) was performed. Strain localization severely affected the results of conventional triaxial

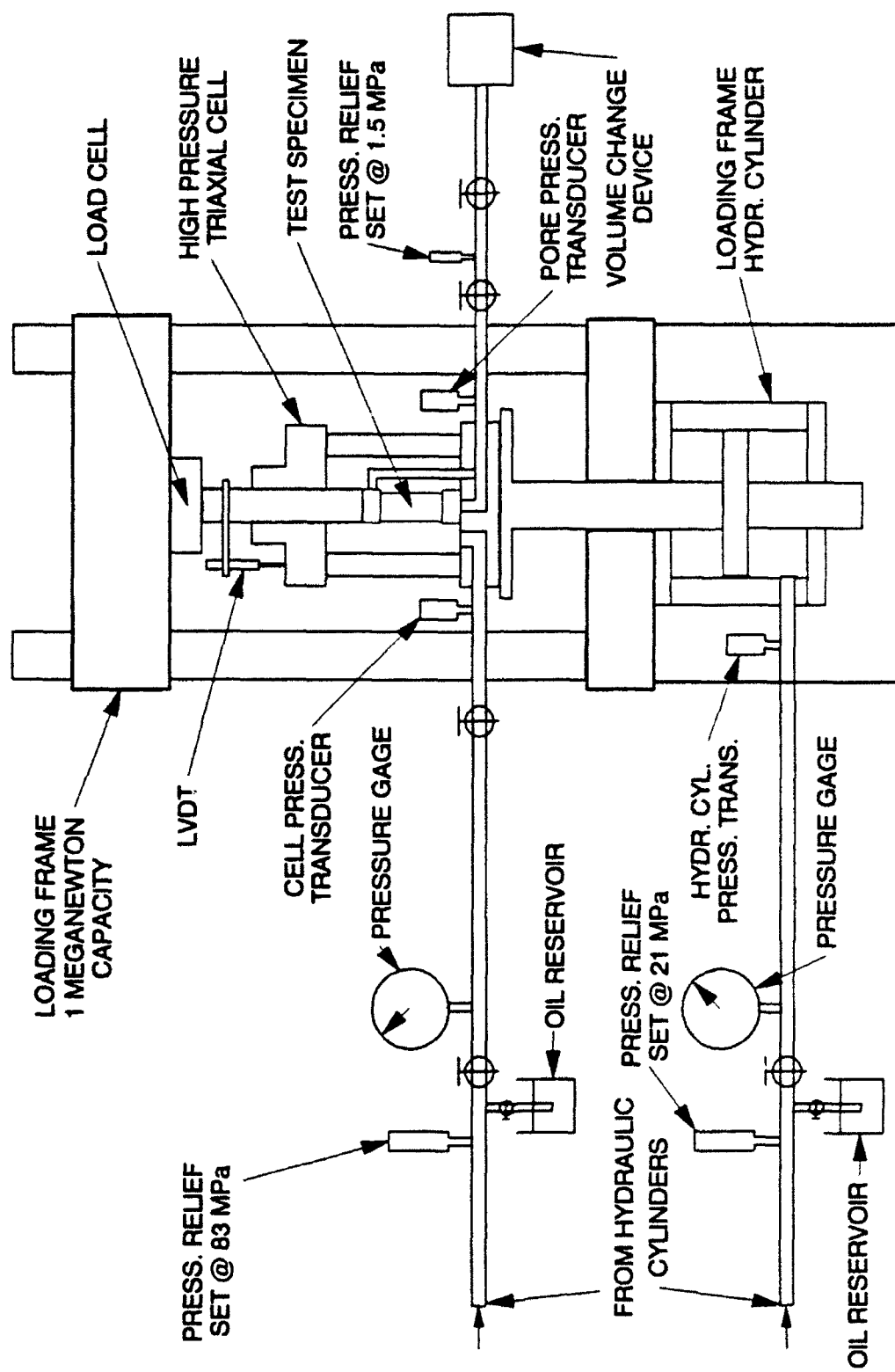


FIGURE 3-1 HIGH PRESSURE TESTING LOADING SYSTEM

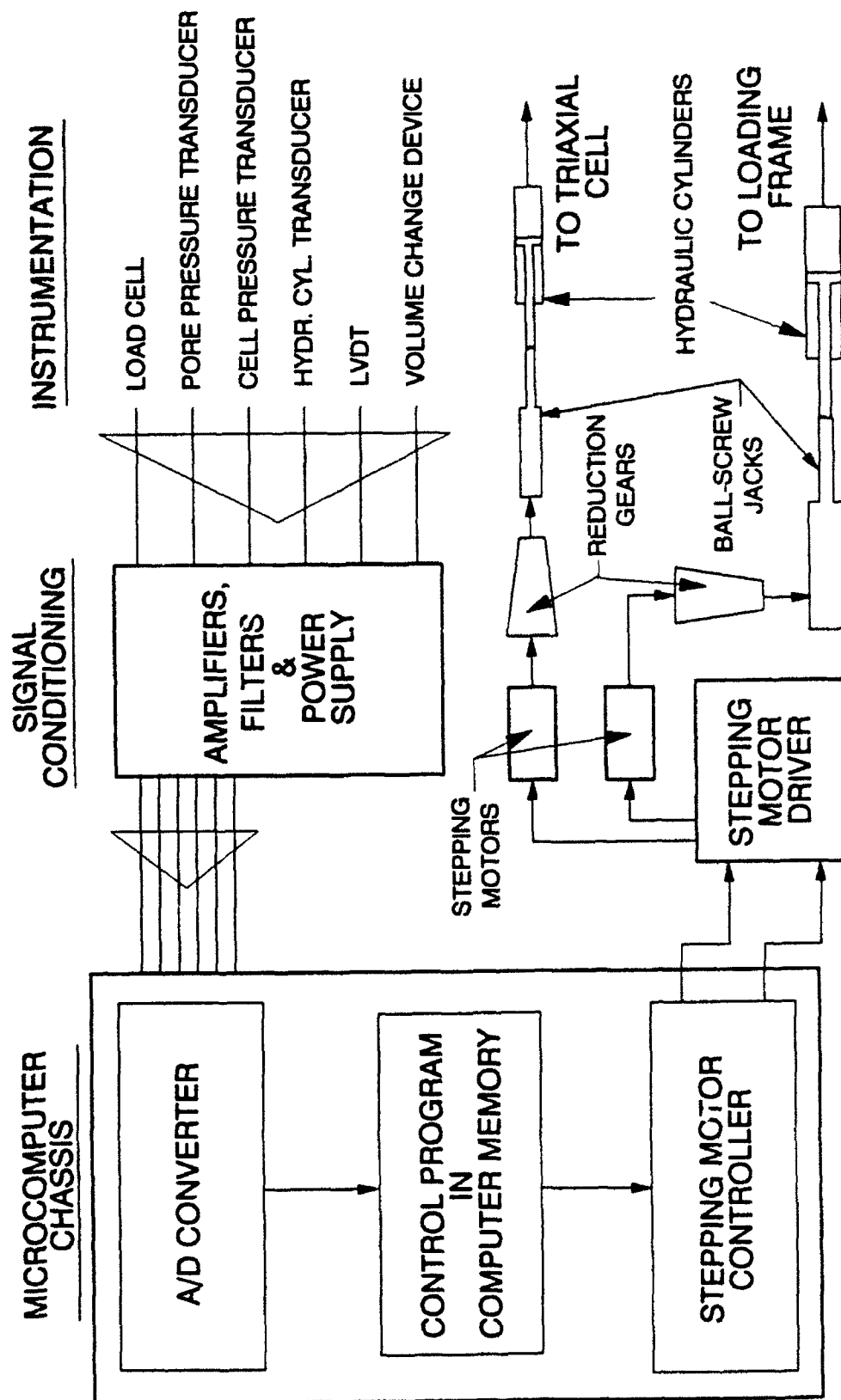


FIGURE 3-2 HIGH PRESSURE TESTING SYSTEM-PROCESS CONTROL FLOW

extension tests, with failure being precipitated by necking in all tests performed (Figure 4-15). The conventional extension test was determined to be an inherently unstable test (Figure 4-17), because it concentrates the stresses (and therefore strains) at the weakest portion of the specimen, and it is not deemed to be an appropriate means to evaluate the strength characteristics of soil in extension.

A series of conventional extension tests was performed and terminated at different axial strains, whereupon the specimen was carefully measured. It was determined that strain localization developed very early in the extension test, possibly near zero axial strain (Figure 4-15). Increasing levels of isotropic consolidation was also seen to enhance the development of strain localization.

An experimental method was developed to enforce uniform strains in the cylindrical extension test. The method consists of encasing the test specimen with layers of overlapping small steel plates bent to fit the curvature of the specimen and sandwiched between greased membranes (Figure 4-18). Upon application of cell pressure, the plates interlock to form a flexurally rigid jacket, resulting in uniform strains being enforced. Friction is not induced because the plates can slide relative to each other on the greased membranes that separate them. Friction was shown to be insignificant, because the initial slope of the stress-strain curve is essentially the same as in conventional extension tests.

Drained uniform strain extension test results indicate that the volumetric strains (in the volumetrically compressing region) and the principal strains to failure are generally larger than in conventional extension tests (Figures 4-35 and 4-36). Also, the effective stress friction angles are generally higher in both drained or undrained uniform extension tests, as compared with those from strain localized tests (Figure 4-34).

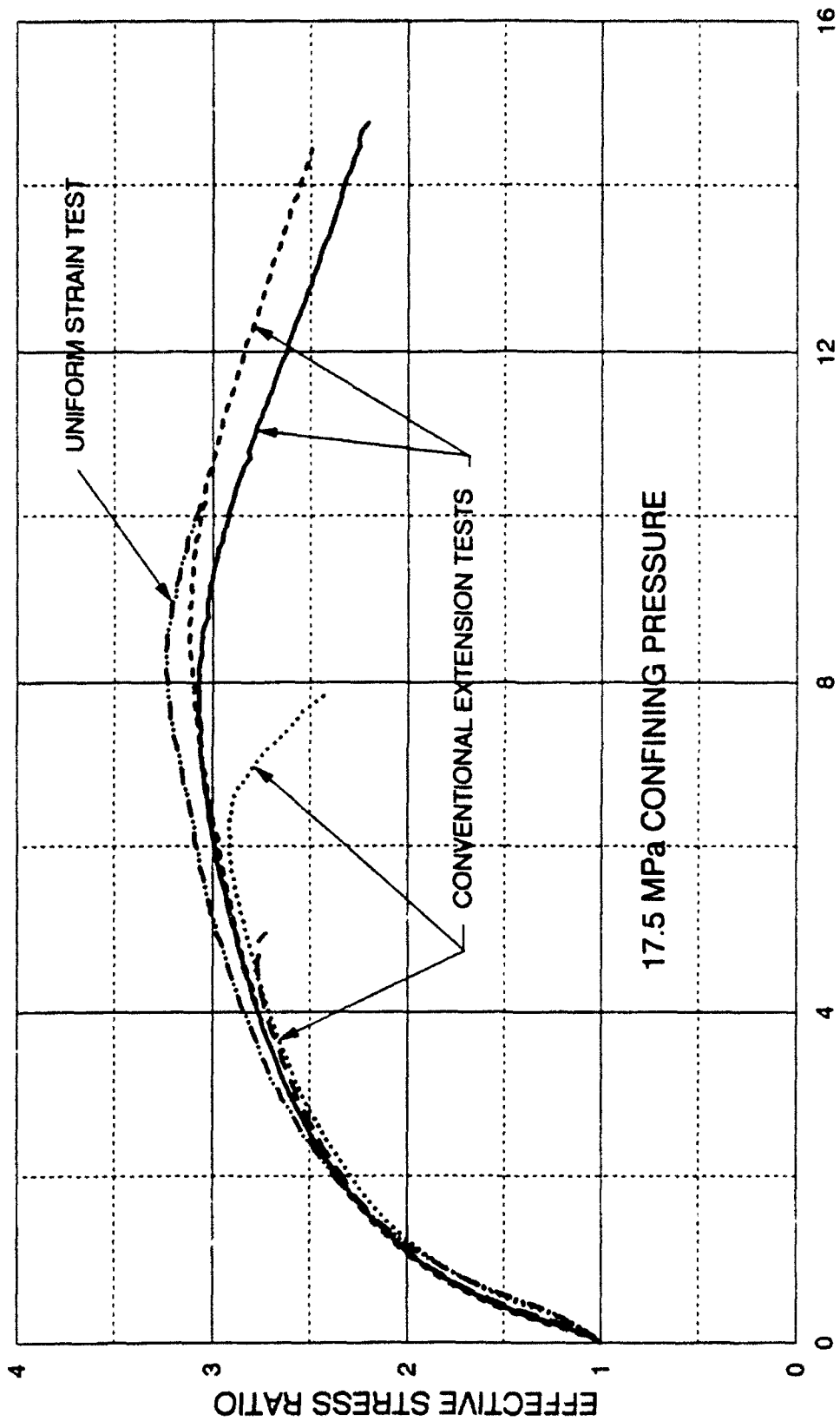
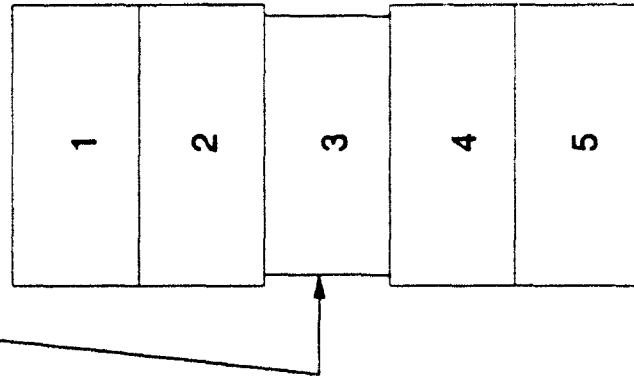


FIGURE 4-15 - STRESS RATIO AT 17.5 MPa  
SEVERAL DIFFERENT DRAINED EXTENSION TESTS  
DENSE CAMBRIA SAND

## TENSION TEST (EXTENSION)

GEOMETRIC OR  
MATERIAL DEFECT.



BEFORE LOAD APPLIED

$AREA(1,2,4,5) > AREA(3)$

$STRESS(3) > STRESS(1,2,4,5)$

CROSS-SECTIONAL AREA DECREASES

RELATIVE TO OTHER SECTIONS.

INITIAL DIFFERENCE IN STRESSES

ACTUALLY INCREASE.

UNTIL,

STRESSES & DEFORMATIONS

CONCENTRATE ENOUGH THAT

SOIL FAILS IN NECK REGION.

UNSTABLE TEST

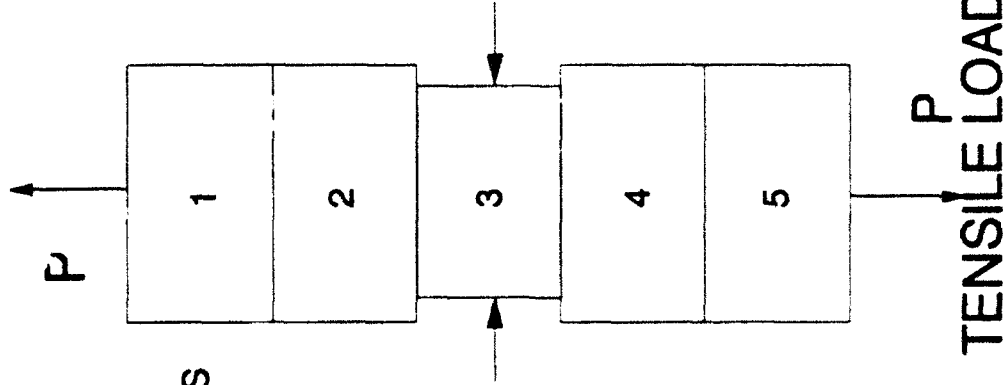


FIGURE 4-17 - DIAGRAM SHOWING TENSION TEST  
IS AN UNSTABLE TEST.

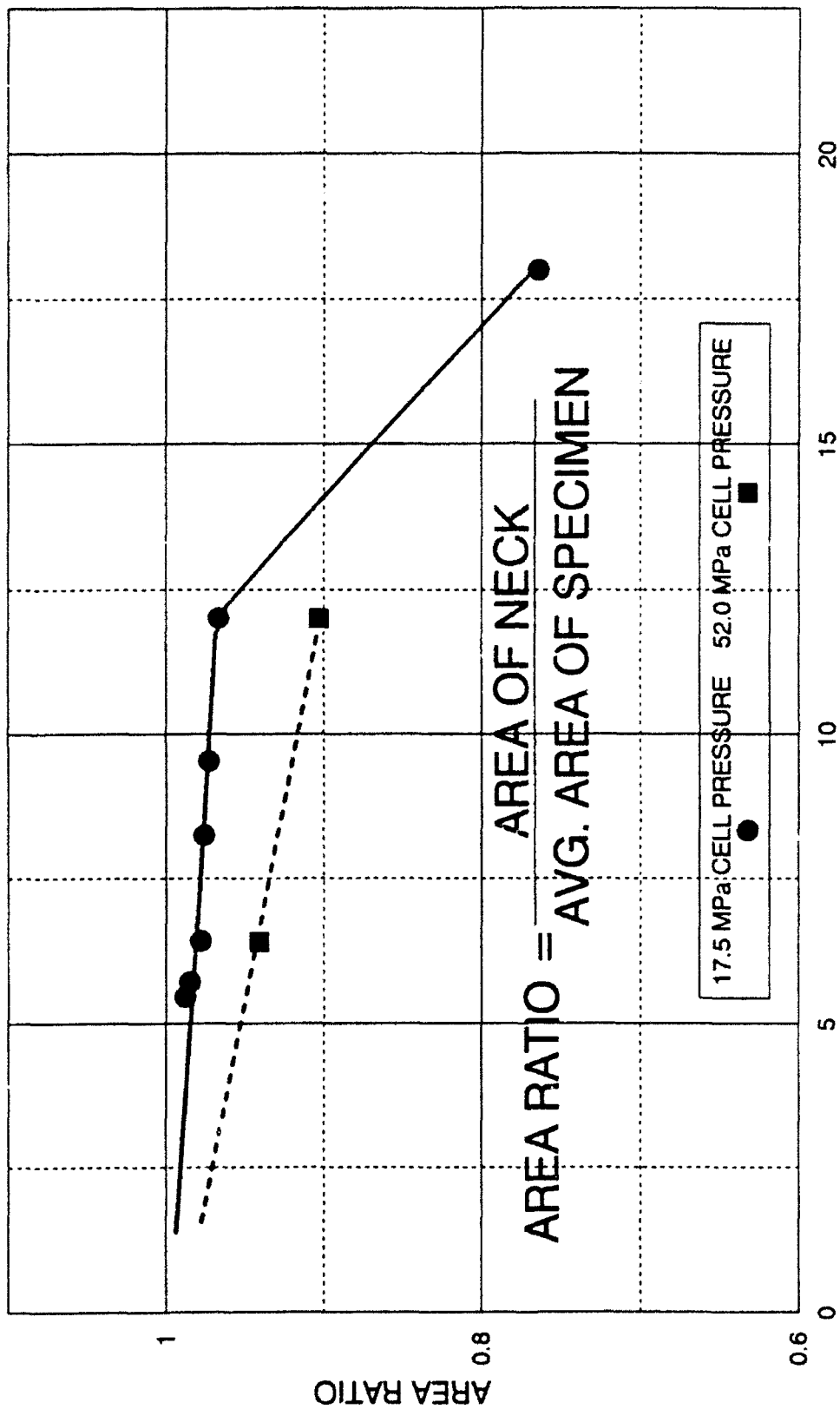


FIGURE 4-14 - AREA RATIO: STRAIN LOCALIZATION  
CONVENTIONAL DRAINED TRIAXIAL EXTENSION  
DENSE CAMBRIA SAND

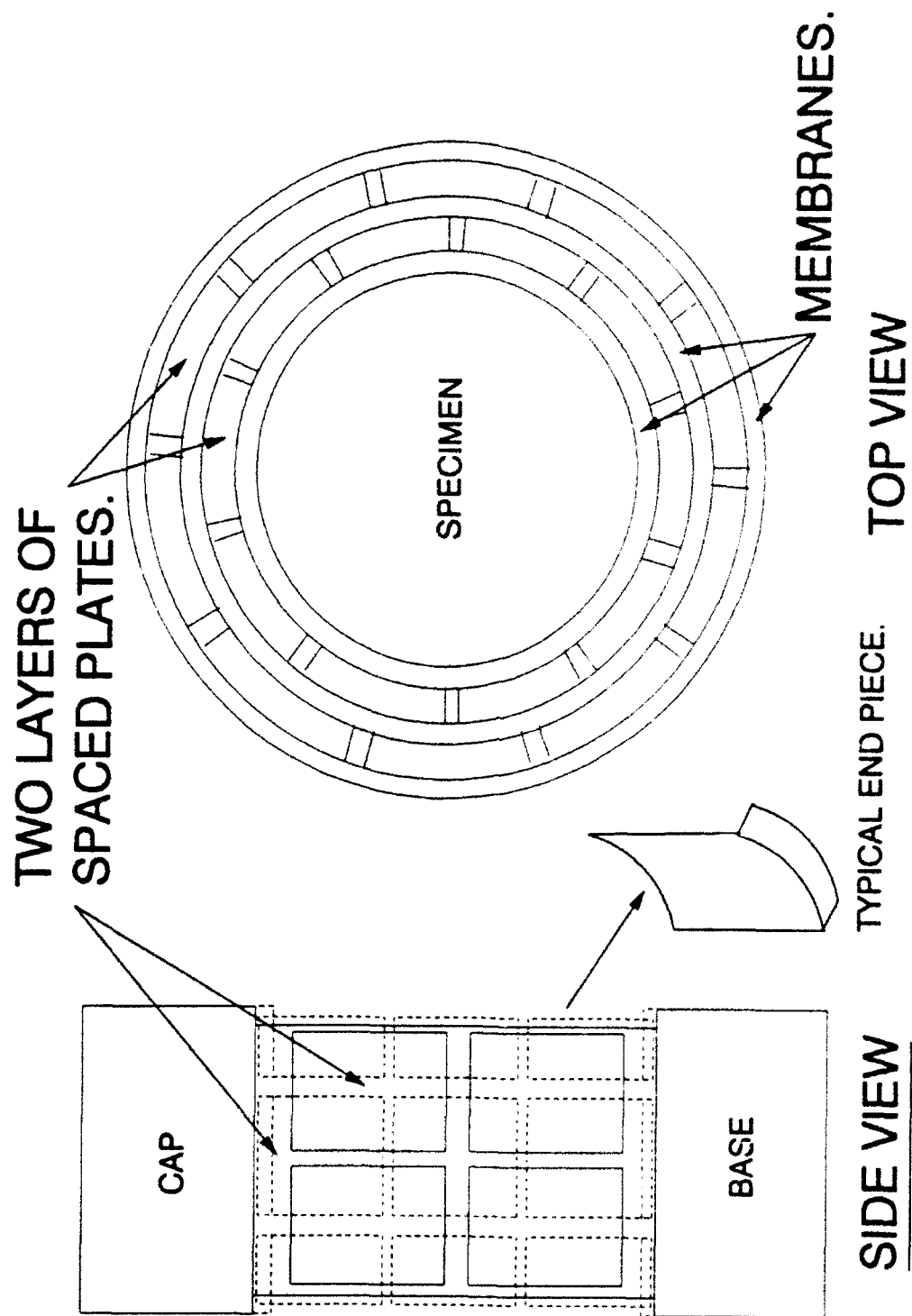


FIGURE 4-18 - METHOD USING STEEL PLATES FOR ENFORCING UNIFORM STRAINS IN EXTENSION.

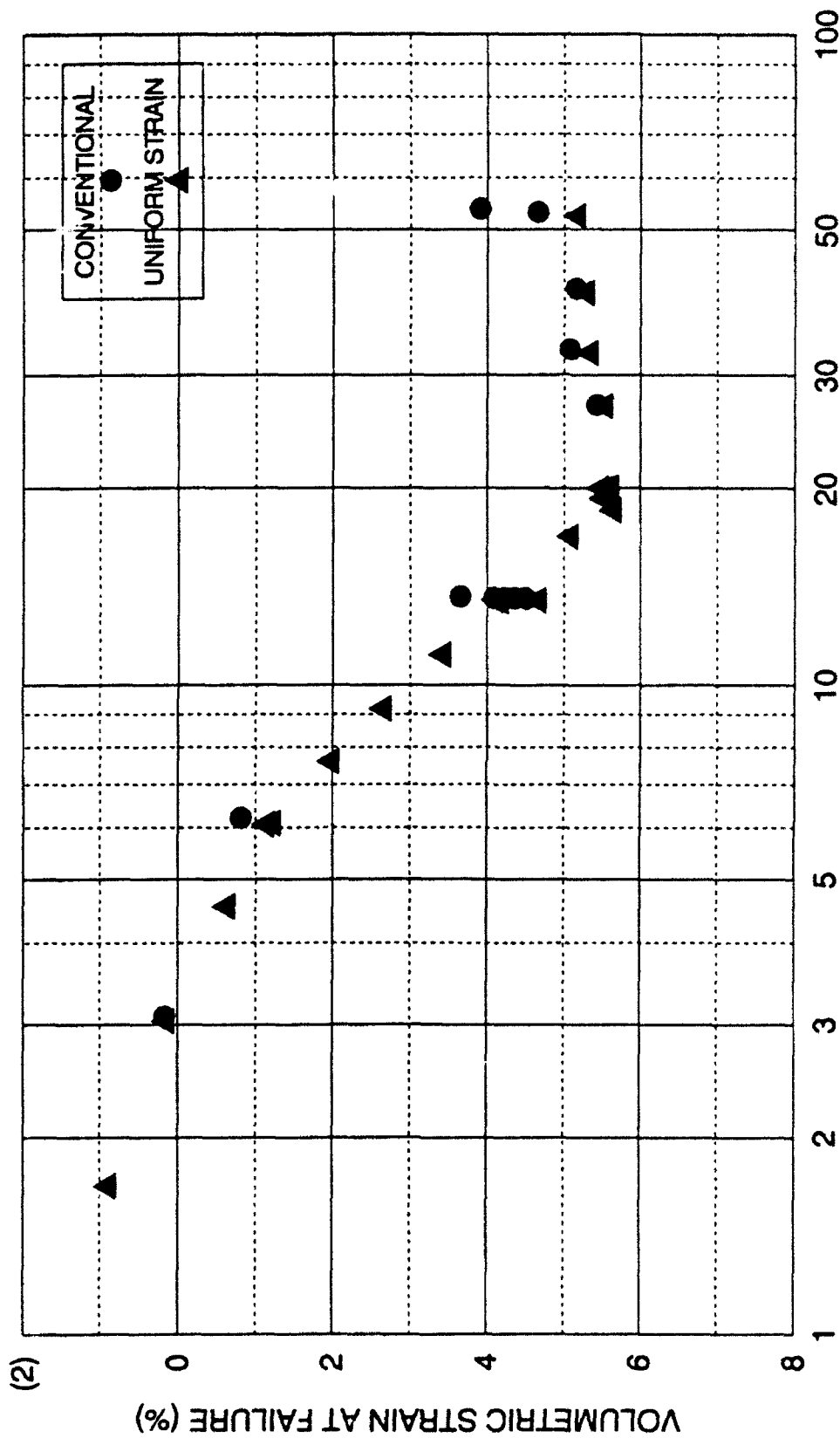


FIGURE 4-35 - COMPARISON OF VOLUMETRIC STRAIN AT FAILURE

CONVENTIONAL AND UNIFORM STRAIN EXTENSION TESTS

DENSE CAMBRIA SAND

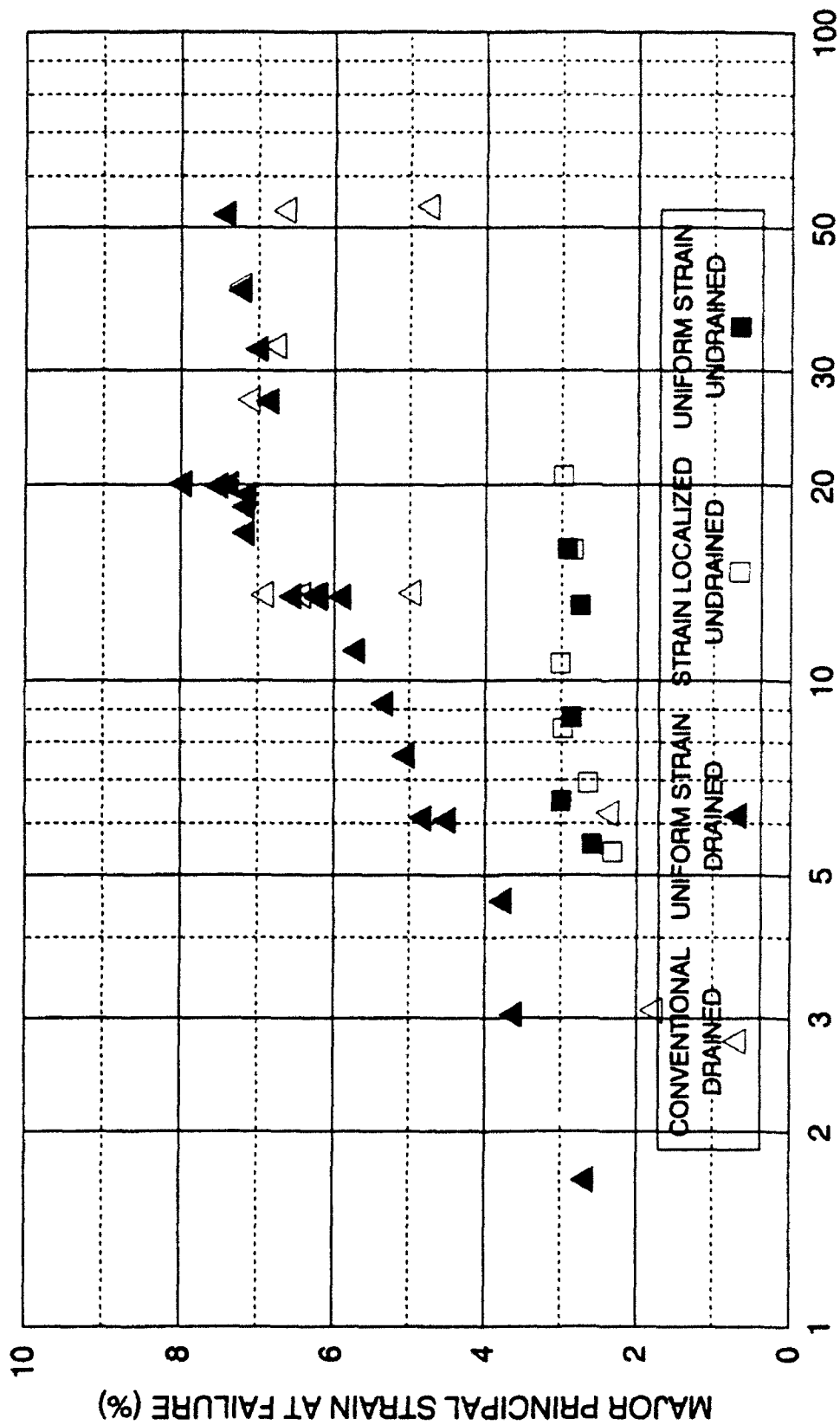
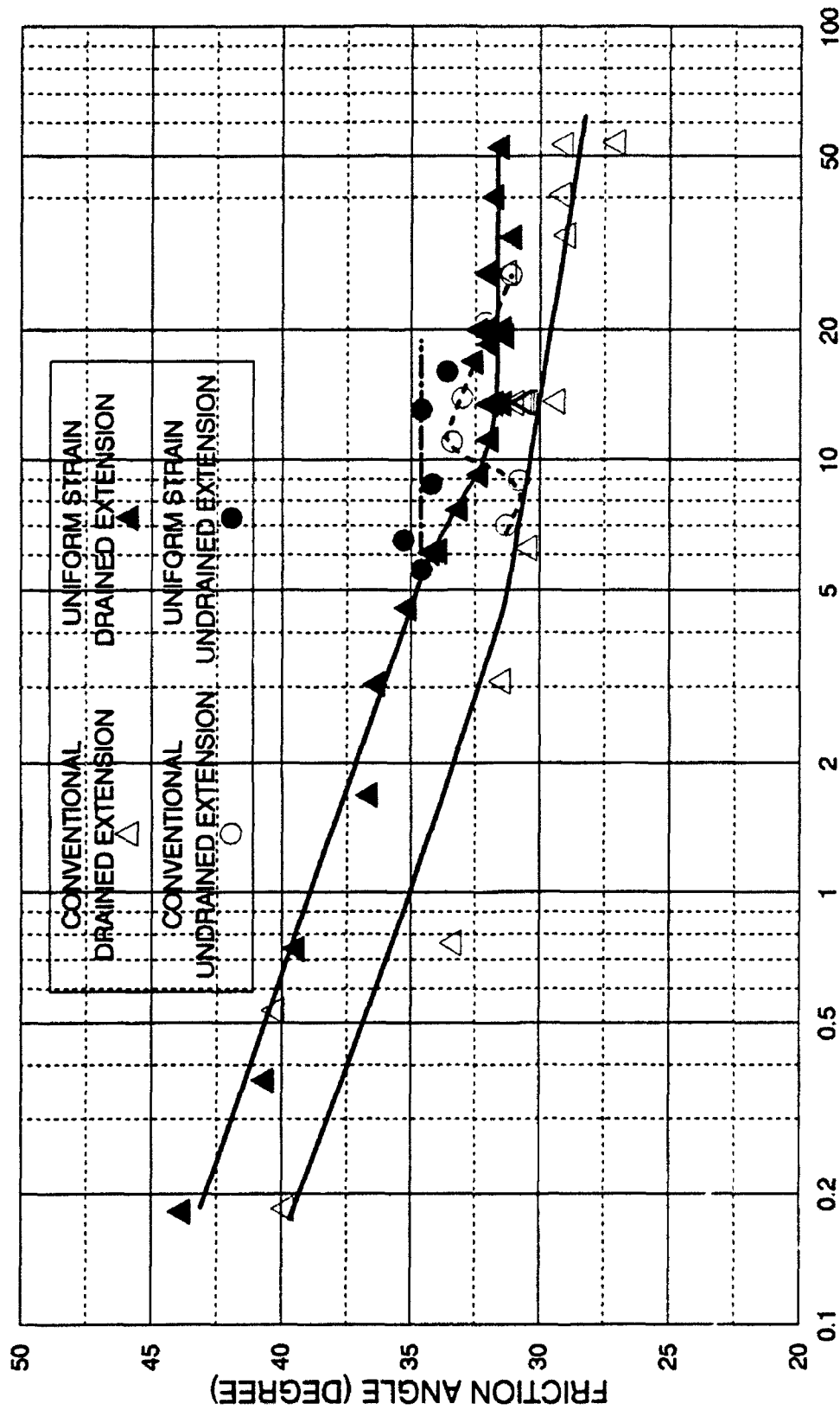


FIGURE 4-36 - COMPARISON OF PRINCIPAL STRAIN AT FAILURE

ALL CONVENTIONAL AND UNIFORM STRAIN EXTENSION TESTS

DENSE CAMBRIA SAND



EFFECTIVE MEAN NORMAL STRESS AT FAILURE (MPa)

FIGURE 4-34 MOHR-COULOMB SECANT FRICTION ANGLES

DRAINED AND UNDRAINED EXTENSION TESTS

WITH & WITHOUT STRAIN LOCALIZATION ON DENSE CAMBRIA SAND

### Stress-Strain Behavior at High Pressure (Chapter 5)

A series of drained and undrained triaxial compression and extension tests were performed to evaluate the stress-strain behavior of Cambria sand at high pressures (up to 68.9 MPa confining pressure). The normalized stress-strain curves from drained triaxial compression and extension tests were seen to become flatter with increasing confining pressure (Figures 5-1 and 5-22). The volumetric strains at failure and the principal strains to failure also increase with confining pressure (Figures 5-32 and 5-34), and this was attributed to increasing amounts of particle crushing and rearranging (Figure 5-33). As confining pressure continues to increase, the volumetric strains at failure and the principal strains to failure reach a maximum level, and start to decrease as particle crushing reaches a maximum level. This stress magnitude was seen to coincide with a steepening of the normalized stress-strain curve.

At high pressures the deviator stress curves from undrained triaxial compression and extension tests generally exhibit a maximum value at very low principal strain levels (Figures 5-12 and 5-29), but actually reach effective stress failure at large principal strains (Figures 5-11 and 5-28). This is caused by the rapid development of positive pore pressures (Figures 5-13 and 5-30).

The drained friction angles in triaxial compression and extension clearly relate directly to the rate of dilation at failure (Figures 5-35 and 5-36). As the confining pressure increases, the rate of dilation increases (increasing volumetric compression) due to higher levels of particle breakage resulting in more volumetric compression. At low pressures the soil is more dilatant at failure in extension, resulting in higher drained friction angles than in compression, but the two curves eventually cross. The stress at the crossing point correspond to the point where the drained friction angles in compression and extension are equal. As the stress magnitude increases and particle crushing slows down in compression, the friction angle increases up to a stable value where it remains constant, even at the highest stress magnitudes employed. In extension, where

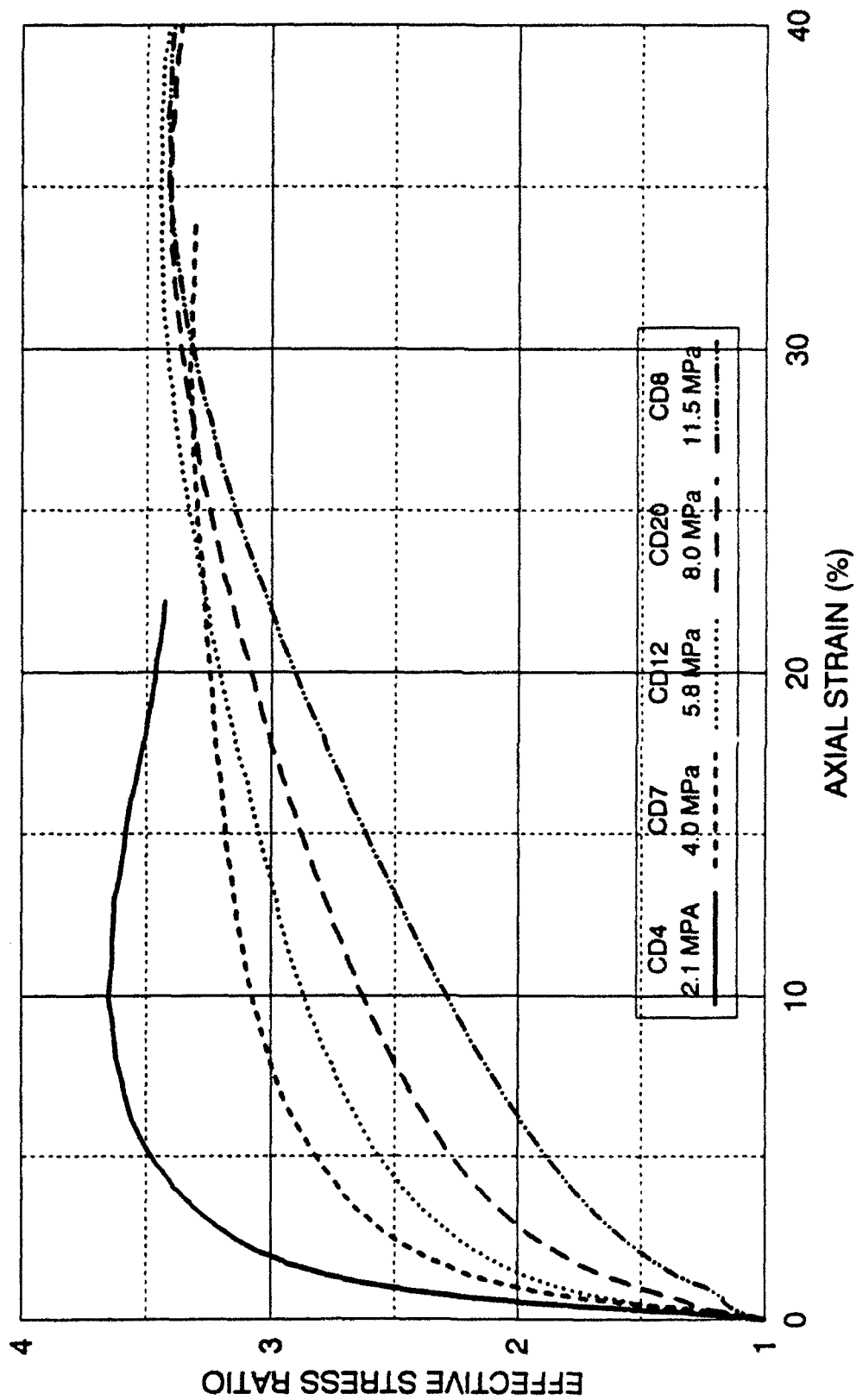
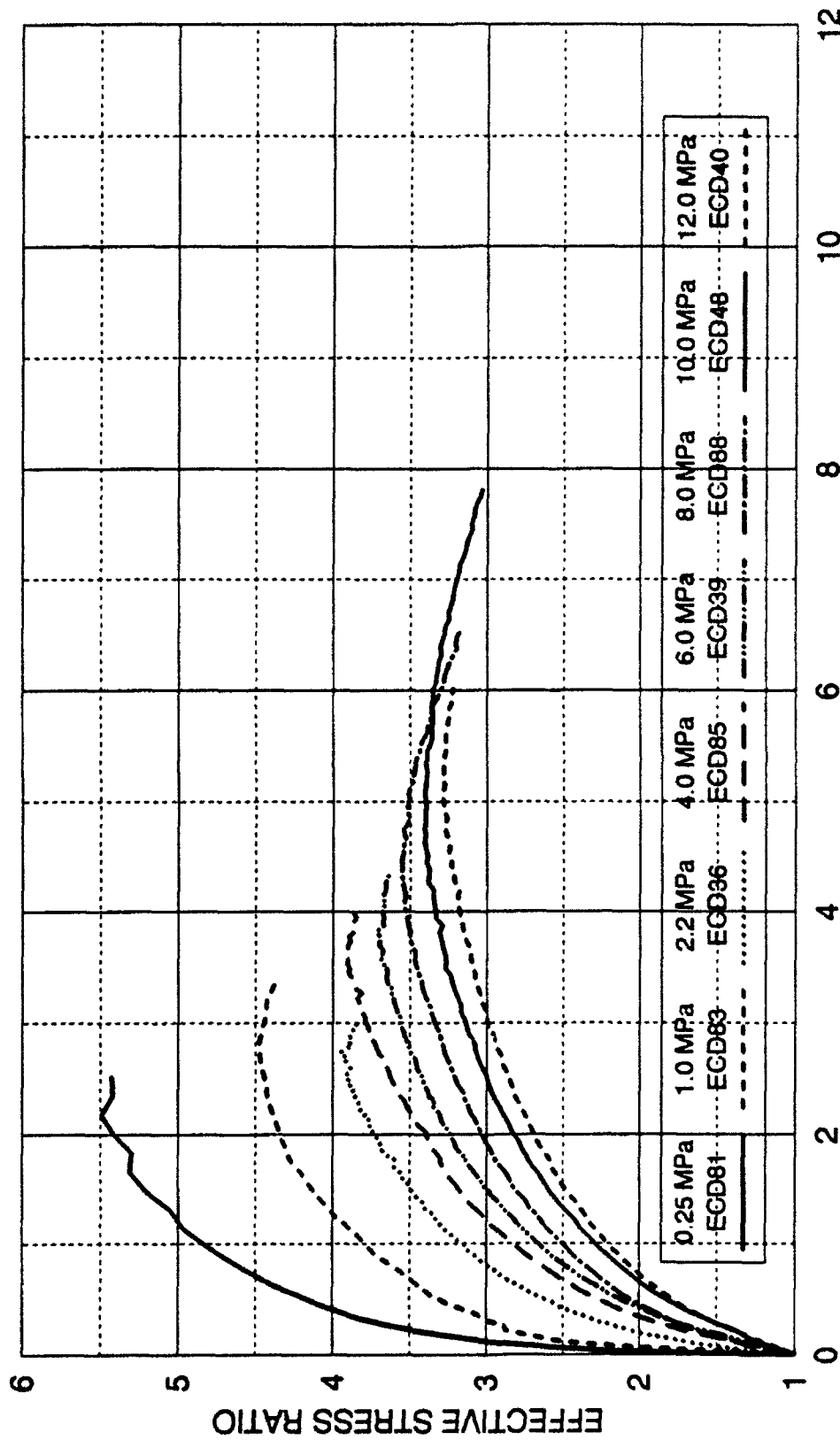


FIGURE 5-1 EFFECTIVE STRESS RATIO 2.1 TO 11.5 MPa  
DRAINED TRIAXIAL COMPRESSION  
DENSE CAMBRIA SAND



MAJOR PRINCIPAL STRAIN (%)

FIGURE 5-22 EFFECTIVE STRESS RATIO 0.25 TO 12.0 MPa  
DRAINED TRIAXIAL EXTENSION  
DENSE CAMBRIA SAND

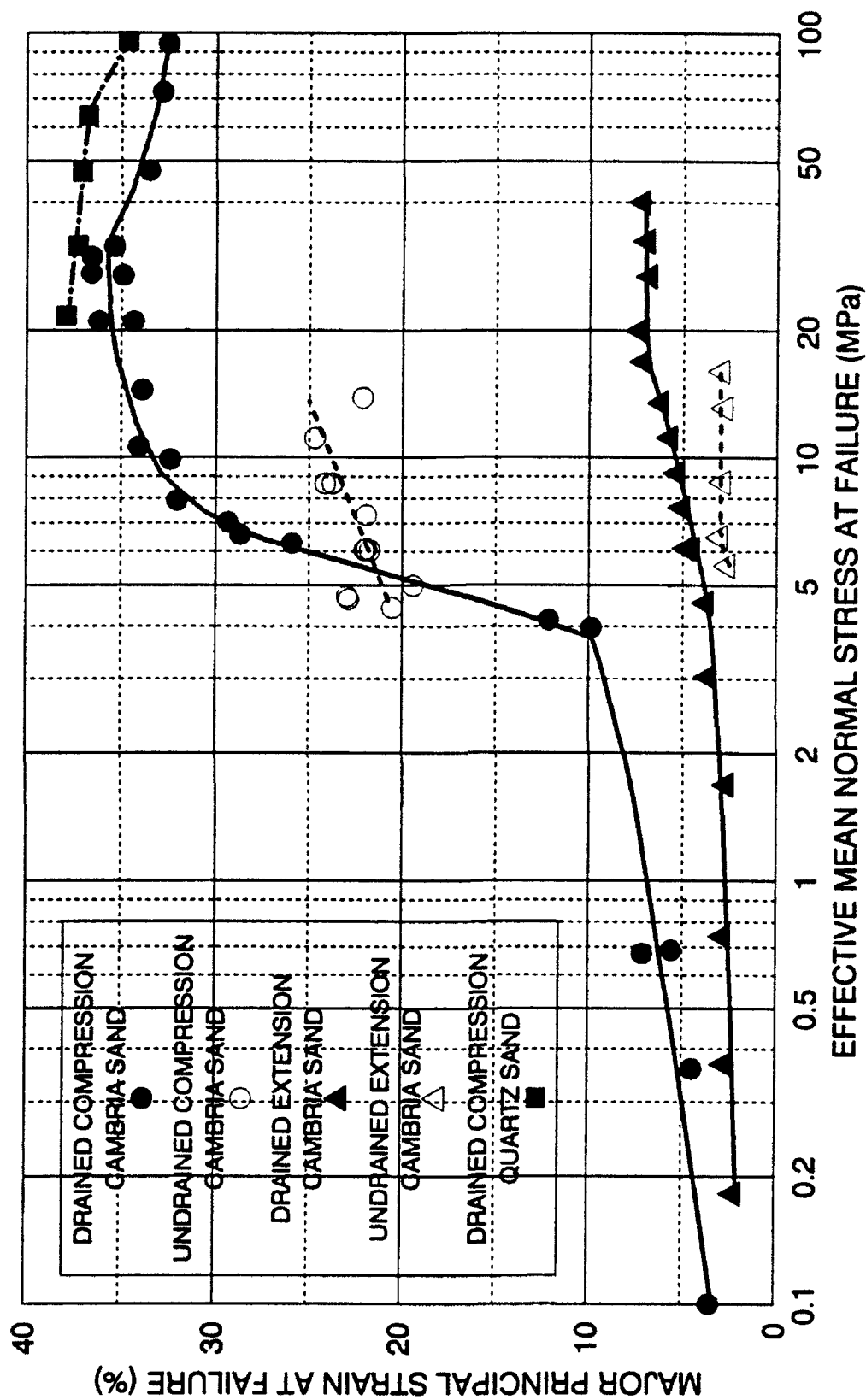


FIGURE 5-32 MAJOR PRINCIPAL STRAIN AT FAILURE  
DRAINED & UNDRAINED COMPRESSION & EXTENSION  
DENSE GAMBRIA SAND AND DENSE QUARTZ SAND

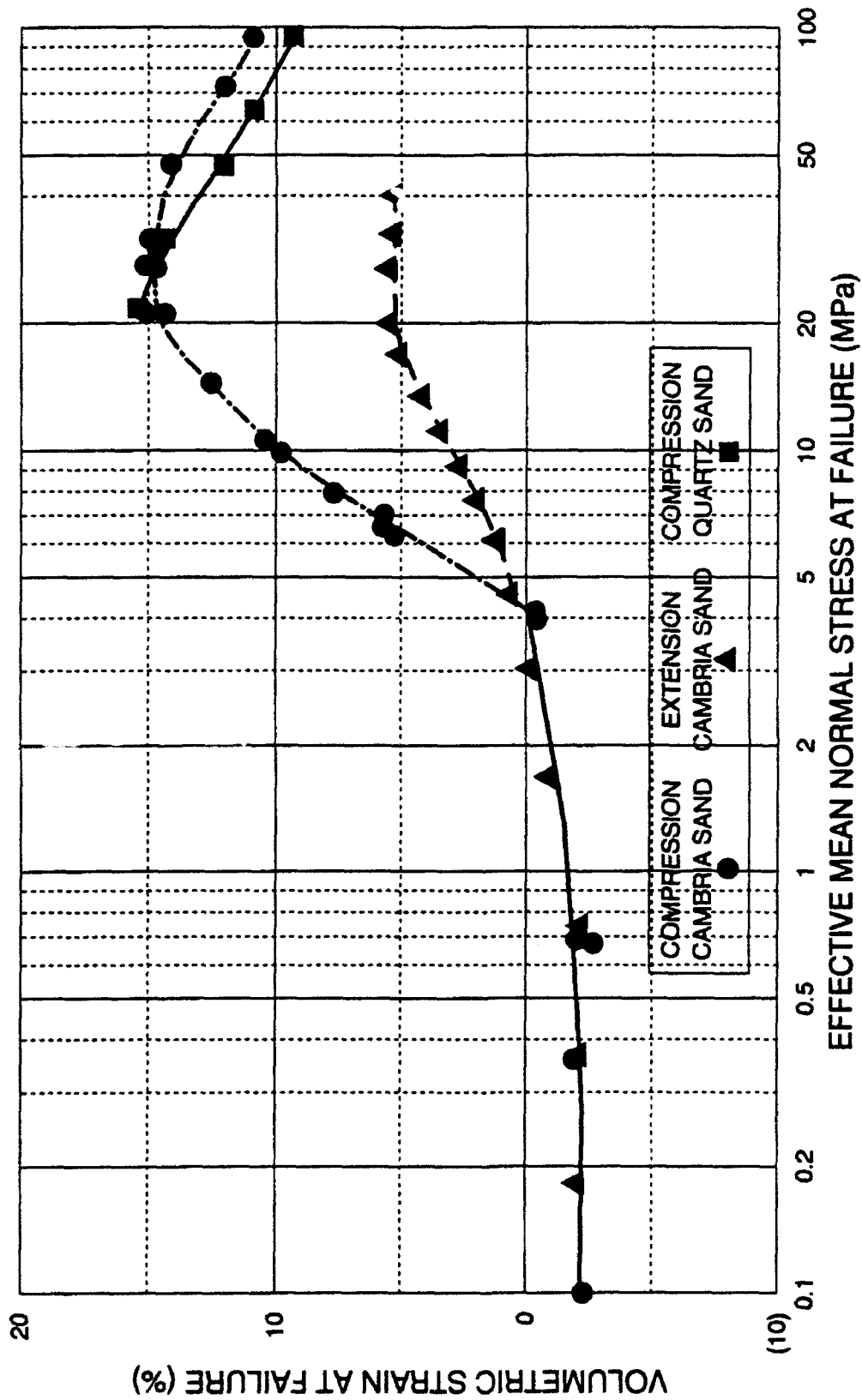


FIGURE 5-34 VOLUMETRIC STRAIN AT FAILURE  
DRAINED COMPRESSION AND EXTENSION  
DENSE CAMBRIA SAND AND DENSE QUARTZ SAND

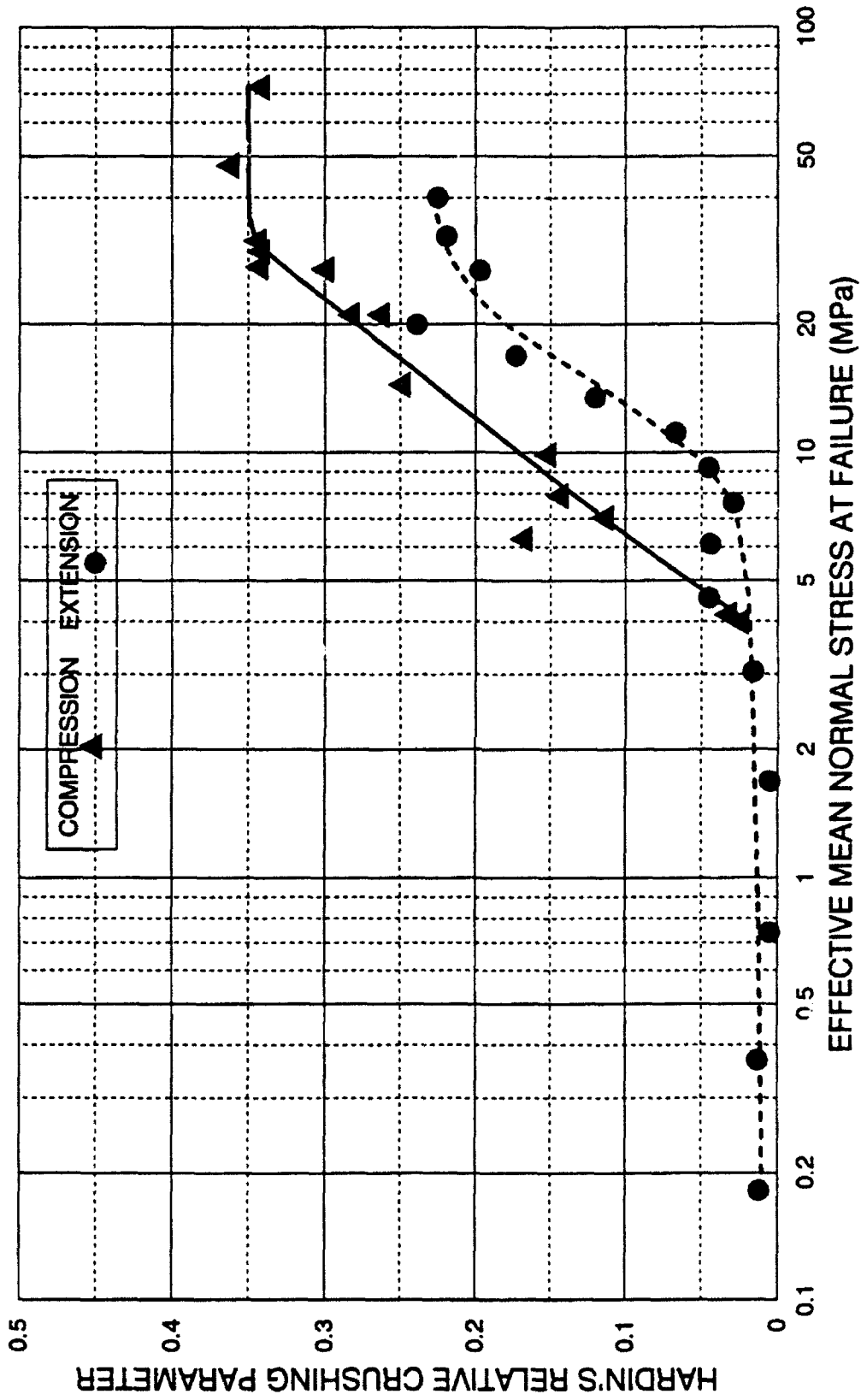


FIGURE 5-33 HARDIN'S RELATIVE CRUSHING  
DRAINED TRIAXIAL COMPRESSION AND EXTENSION  
DENSE CAMBRIA SAND

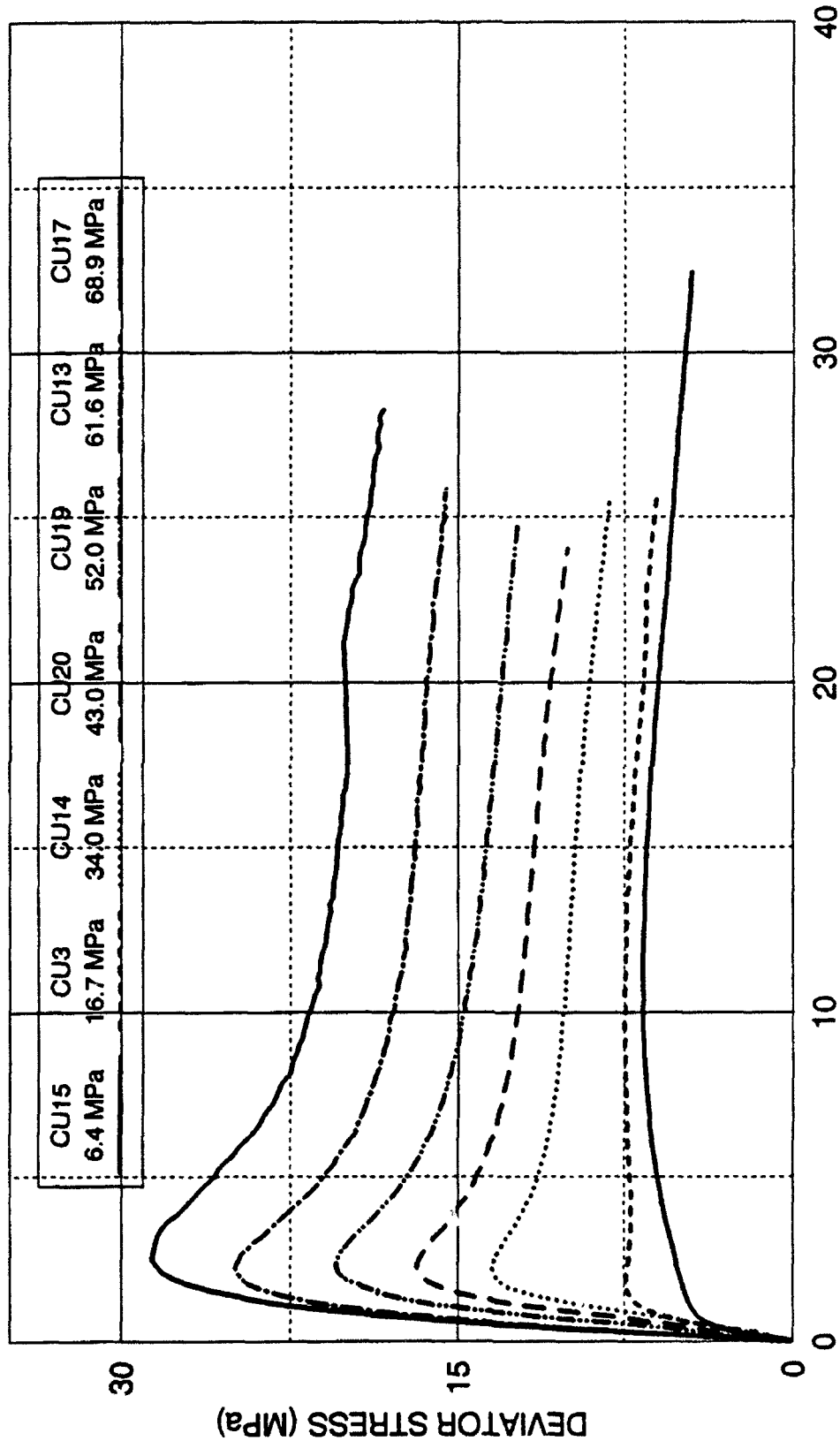
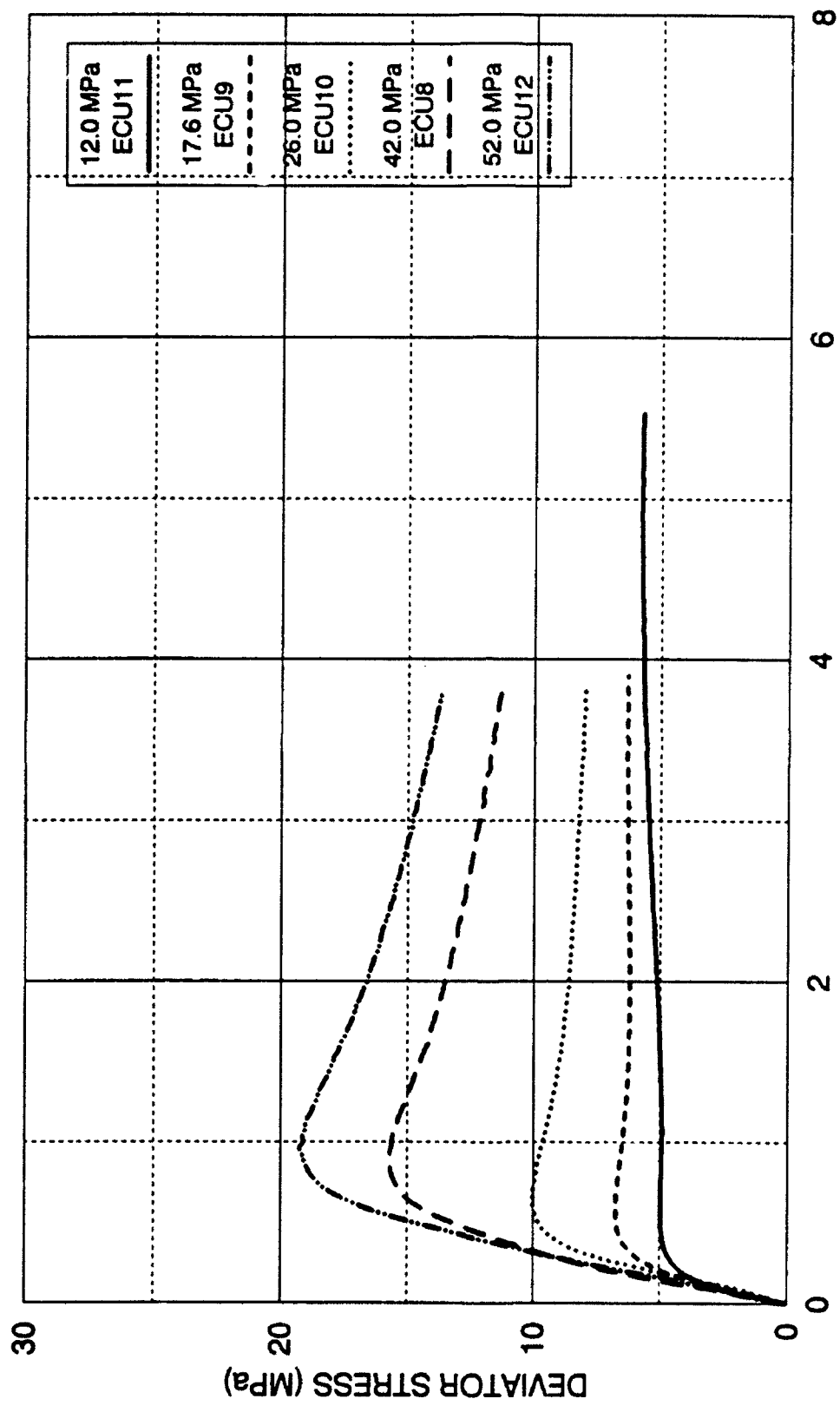


FIGURE 5-12 DEVIATOR STRESS 6.4 TO 68.9 MPa  
UNDRAINED TRIAXIAL COMPRESSION  
DENSE CAMBRIA SAND



MAJOR PRINCIPAL STRAIN (%)

FIGURE 5-29 DEVIATOR STRESS 12.0 TO 52.0 MPa

UNDRAINED TRIAXIAL EXTENSION

DENSE CAMBRIA SAND

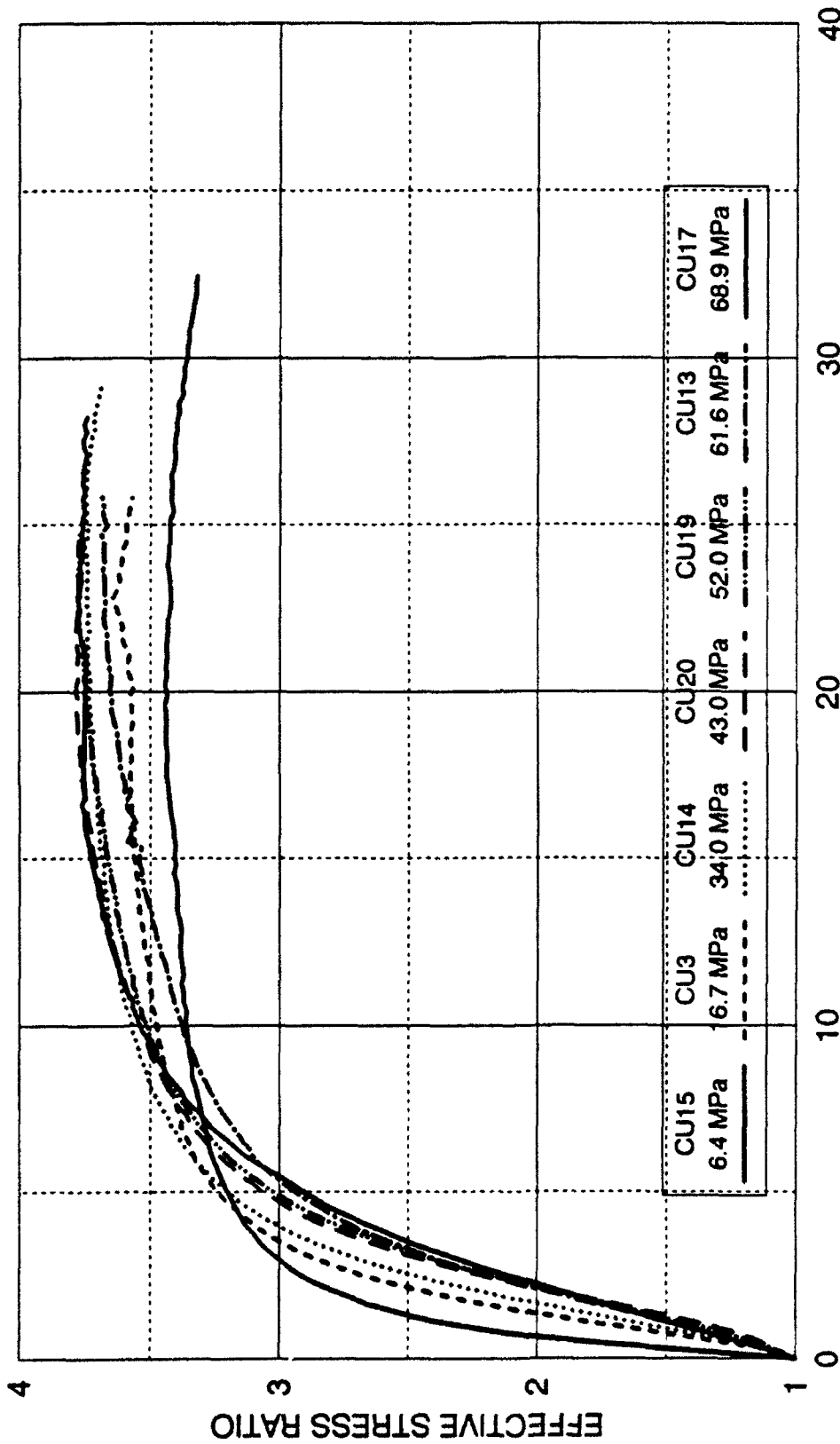
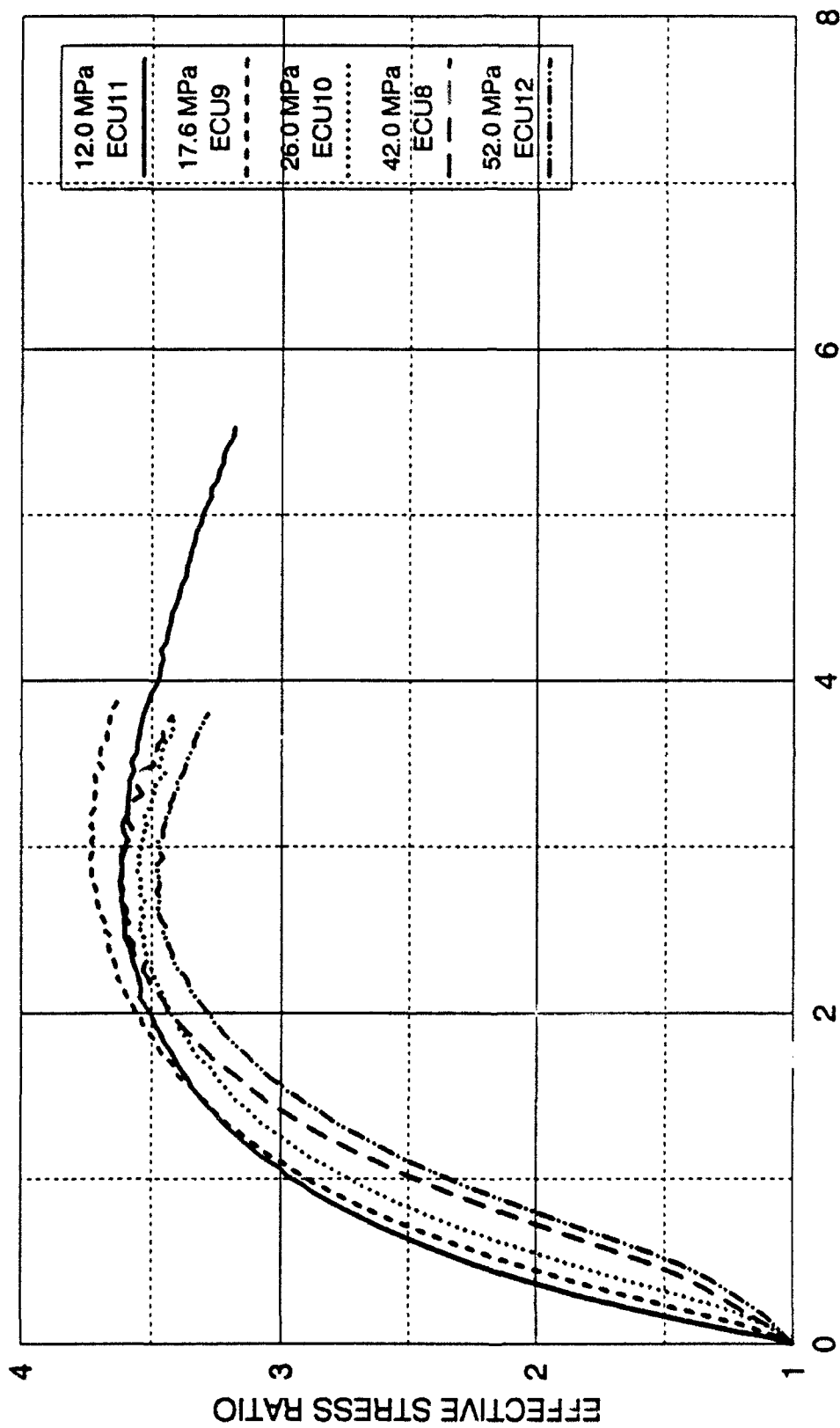


FIGURE 5-11 EFFECTIVE STRESS RATIO 6.4 TO 68.9 MPa  
UNDRAINED TRIAXIAL COMPRESSION  
DENSE CAMBRIA SAND



MAJOR PRINCIPAL STRAIN (%)  
 FIGURE 5-28 EFFECTIVE STRESS RATIO 12.0 TO 52.0 MPa  
 UNDRAINED TRIAXIAL EXTENSION  
 DENSE CAMBRIA SAND

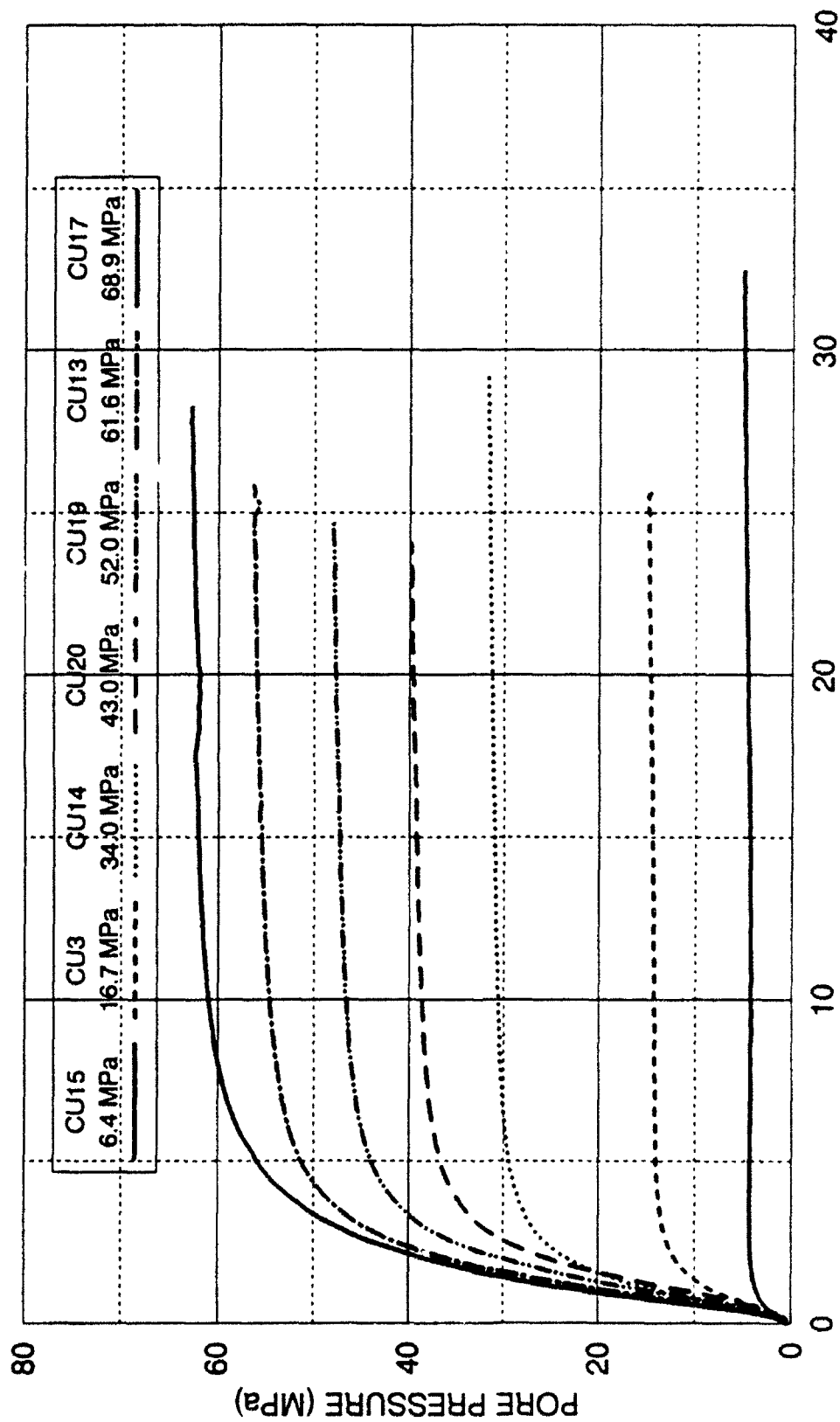
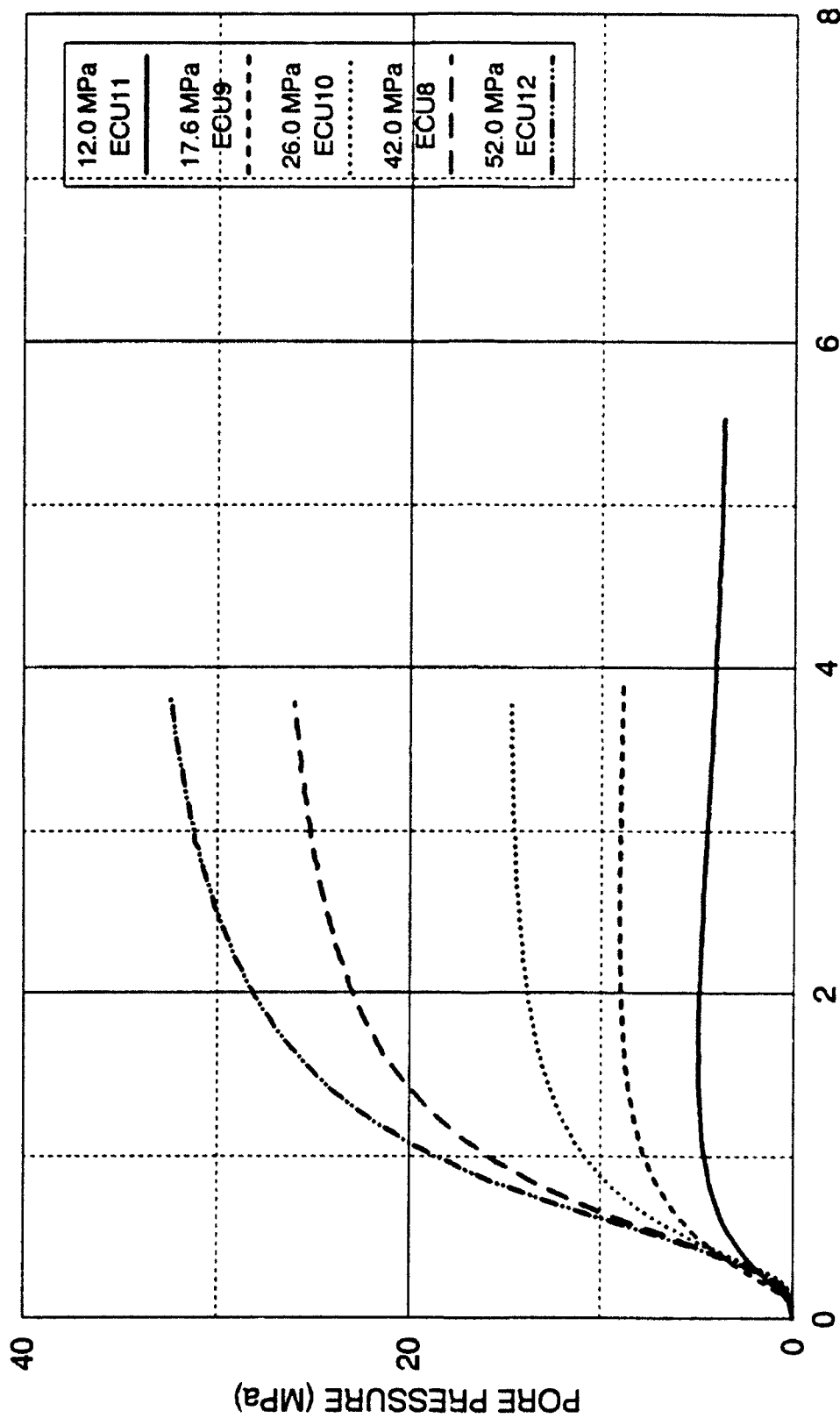


FIGURE 5-13 PORE PRESSURE 6.4 TO 68.9 MPa  
UNDRAINED TRIAXIAL COMPRESSION  
DENSE CAMBRIA SAND



MAJOR PRINCIPAL STRAIN (%)  
FIGURE 5-30 PORE PRESSURE 12.0 TO 52.0 MPa  
UNDRAINED TRIAXIAL EXTENSION  
DENSE CAMBRIA SAND

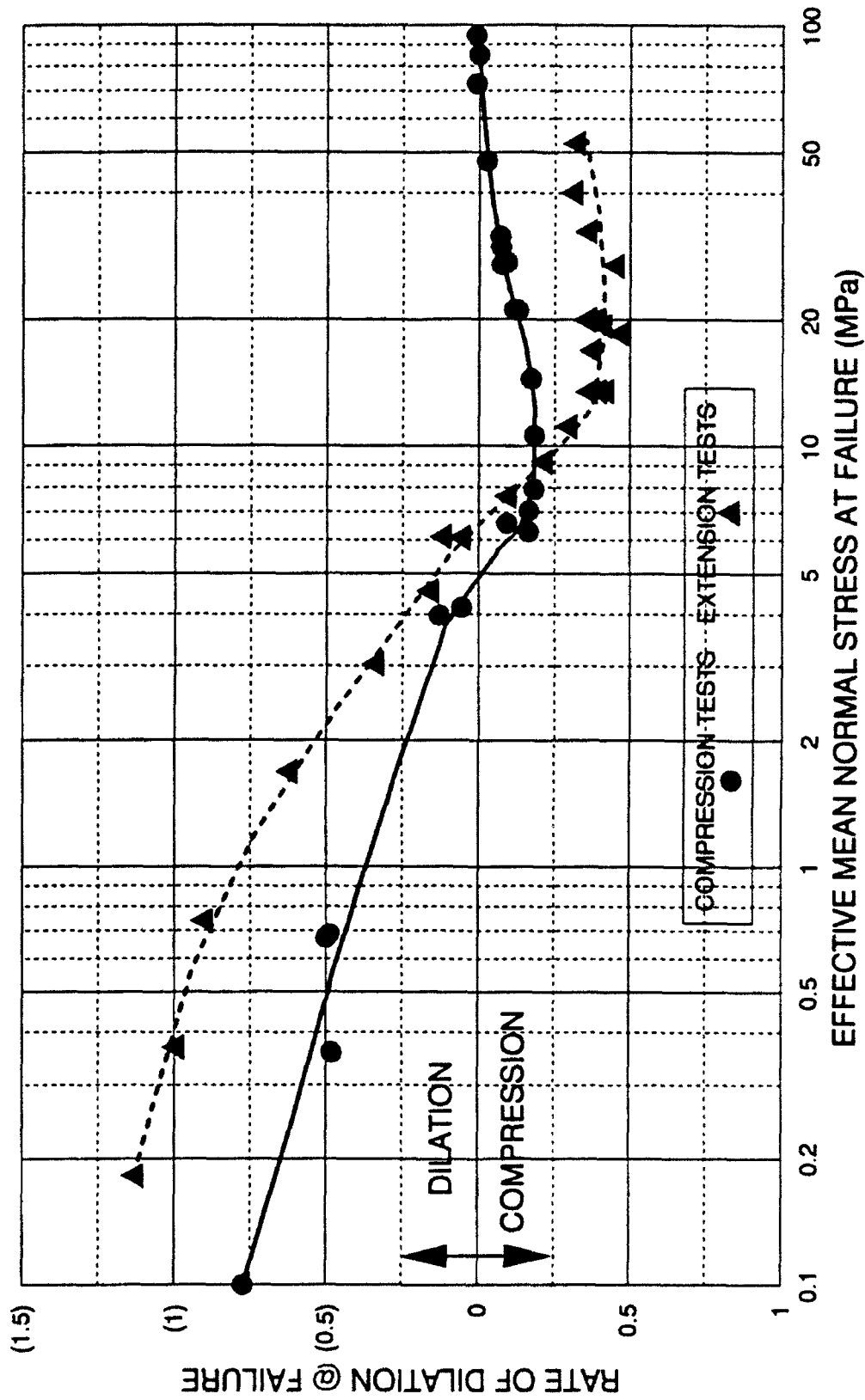


FIGURE 5-35 RATE OF DILATION  
DRAINED TRIAXIAL COMPRESSION AND EXTENSION  
DENSE CAMBRIA SAND

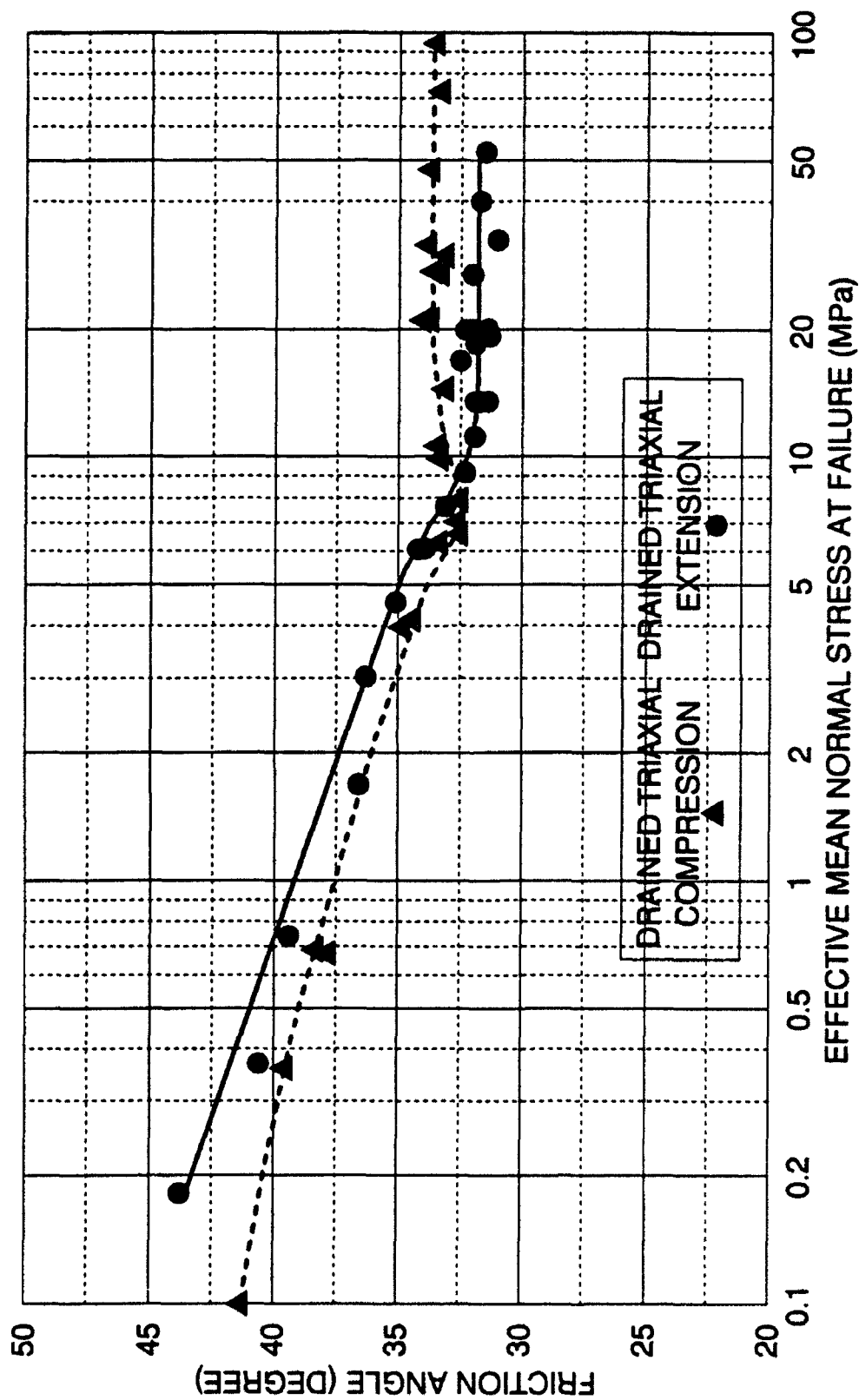


FIGURE 5-36 MOHR-COULOMB SECANT FRICTION ANGLES  
DRAINED TRIAXIAL COMPRESSION & EXTENSION  
DENSE CAMBRIA SAND

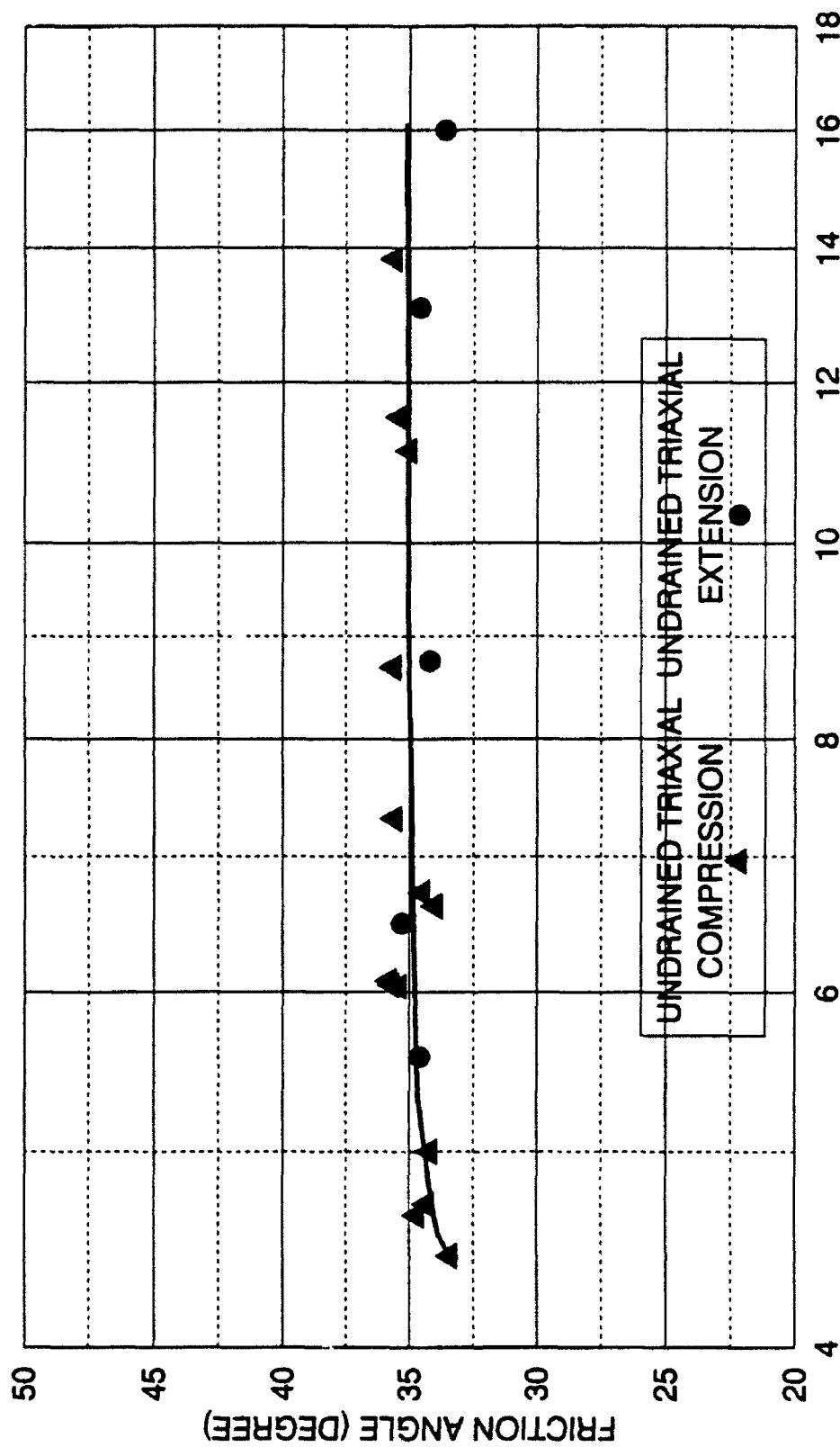
particle crushing is not as extensive, the rate of dilation at failure is observed to reach a maximum level (most compressive behavior), and the friction angle reaches a constant minimum value.

At high pressures the undrained friction angles in compression and extension are generally constant and of equal value, but at a higher value than obtained in the drained tests (Figure 5-37). This is the result of the sand being subjected to high stress regions, as was shown on the effective stress path (Figure 5-14).

#### Instability of Soils at High Pressures (Chapter 6)

Undrained tests in both triaxial compression and extension were used to establish the boundaries of the instability and the temporary instability regions for dense Cambria sand (Figures 6-5 and 6-6). Instability for stress states inside the instability region was demonstrated by special tests (Figure 6-7 and 6-15). In these tests specimens were sheared under drained conditions into the instability region. The specimens were then rendered undrained and placed under stress control, and it was attempted to hold the deviator stress constant. All test specimens became unstable with increasing pore pressures, and eventually reached effective stress failure. These special tests were performed in both triaxial compression and extension.

The location of the instability line at high pressures was determined from experiments (Figure 6-12 and 6-20). Special tests were performed which brought the test specimens to stress states well outside the instability region under drained conditions. The specimens were then rendered undrained and the deviator stress was held constant. Volumetric soil creep at high pressures caused the pore pressures to increase, and this resulted in the effective stress path moving horizontally toward the instability line. When the instability line was crossed, the specimens became unstable, and eventually reached failure.



EFFECTIVE MEAN NORMAL STRESS AT FAILURE (MPa)

FIGURE 5-37 MOHR-COULOMB SECANT FRICTION ANGLES

UNDRAINED TRIAXIAL COMPRESSION & EXTENSION

DENSE CAMBRIA SAND

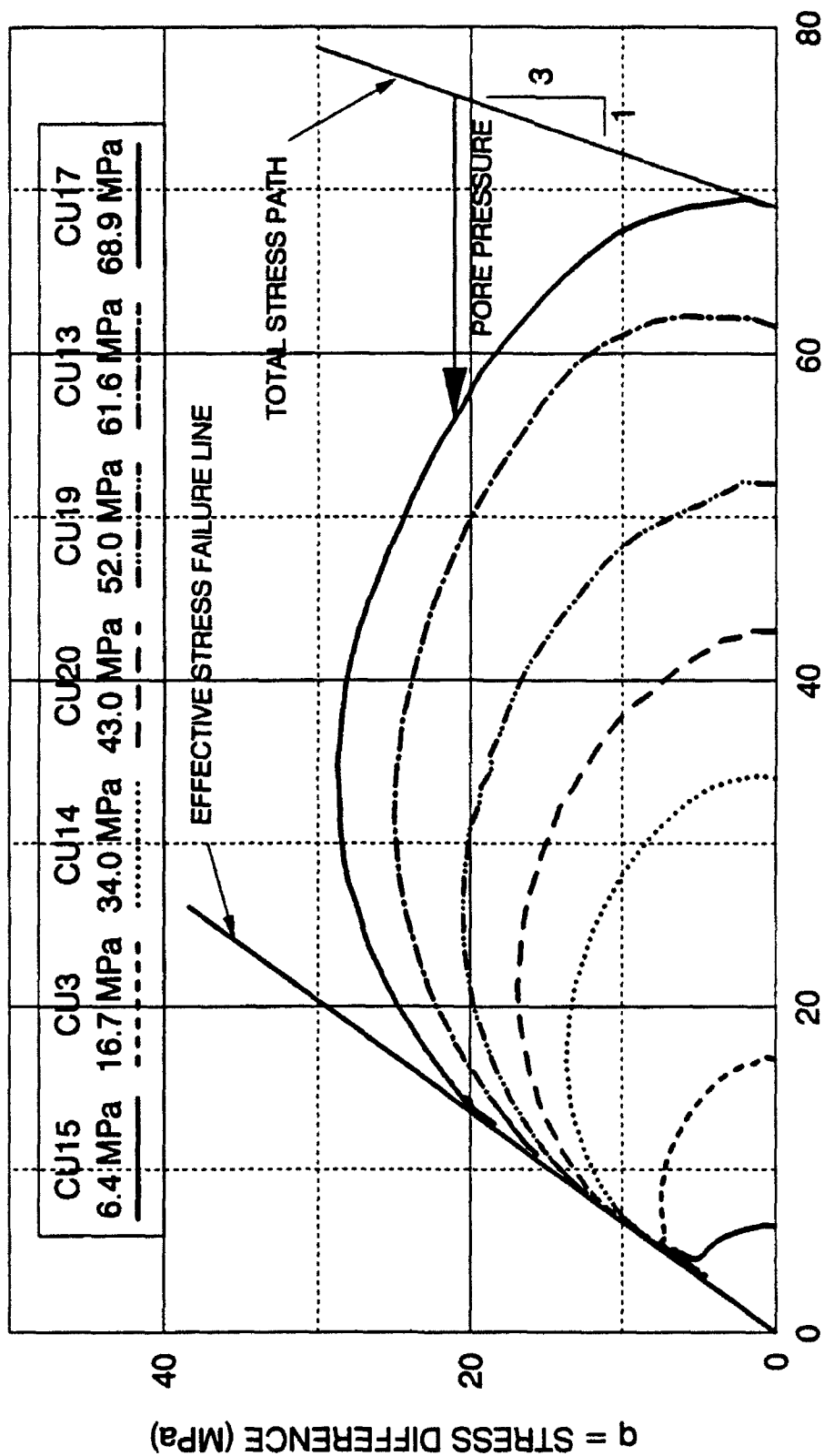


FIGURE 5-14 EFFECTIVE STRESS PATH - CAMBRIDGE  $p'-q$   
UNDRAINED TRIAXIAL COMPRESSION  
DENSE CAMBRIA SAND

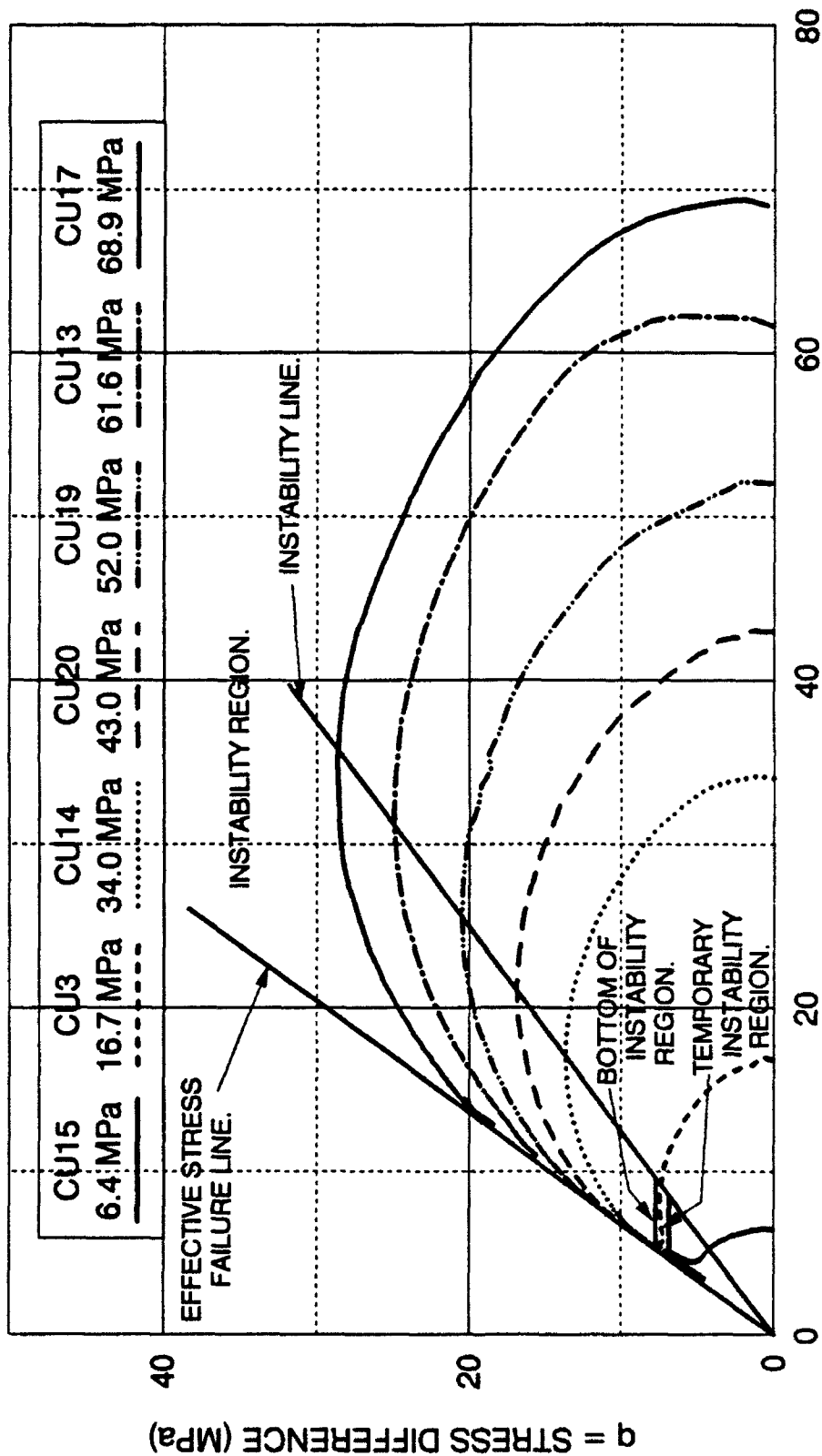
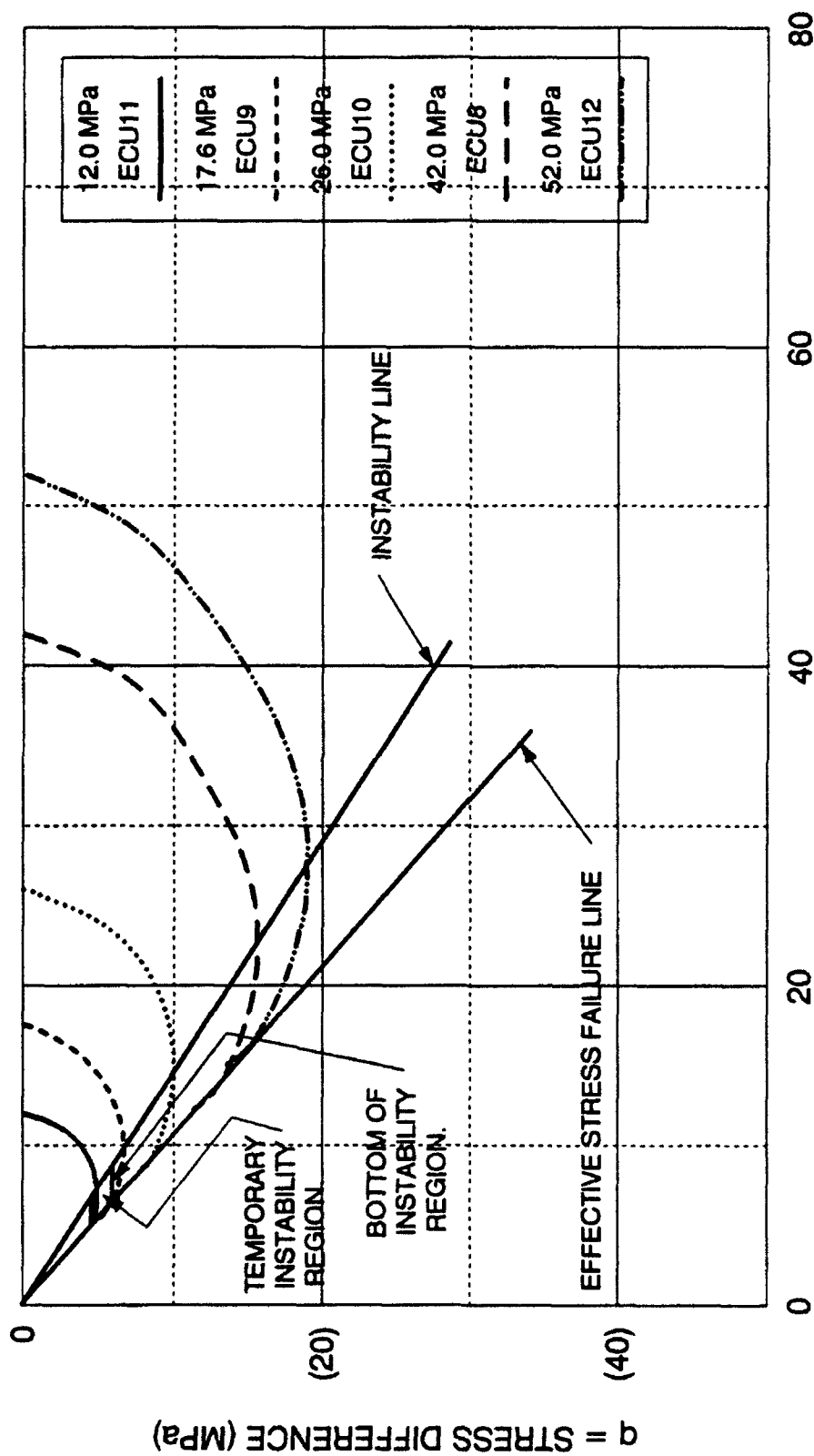
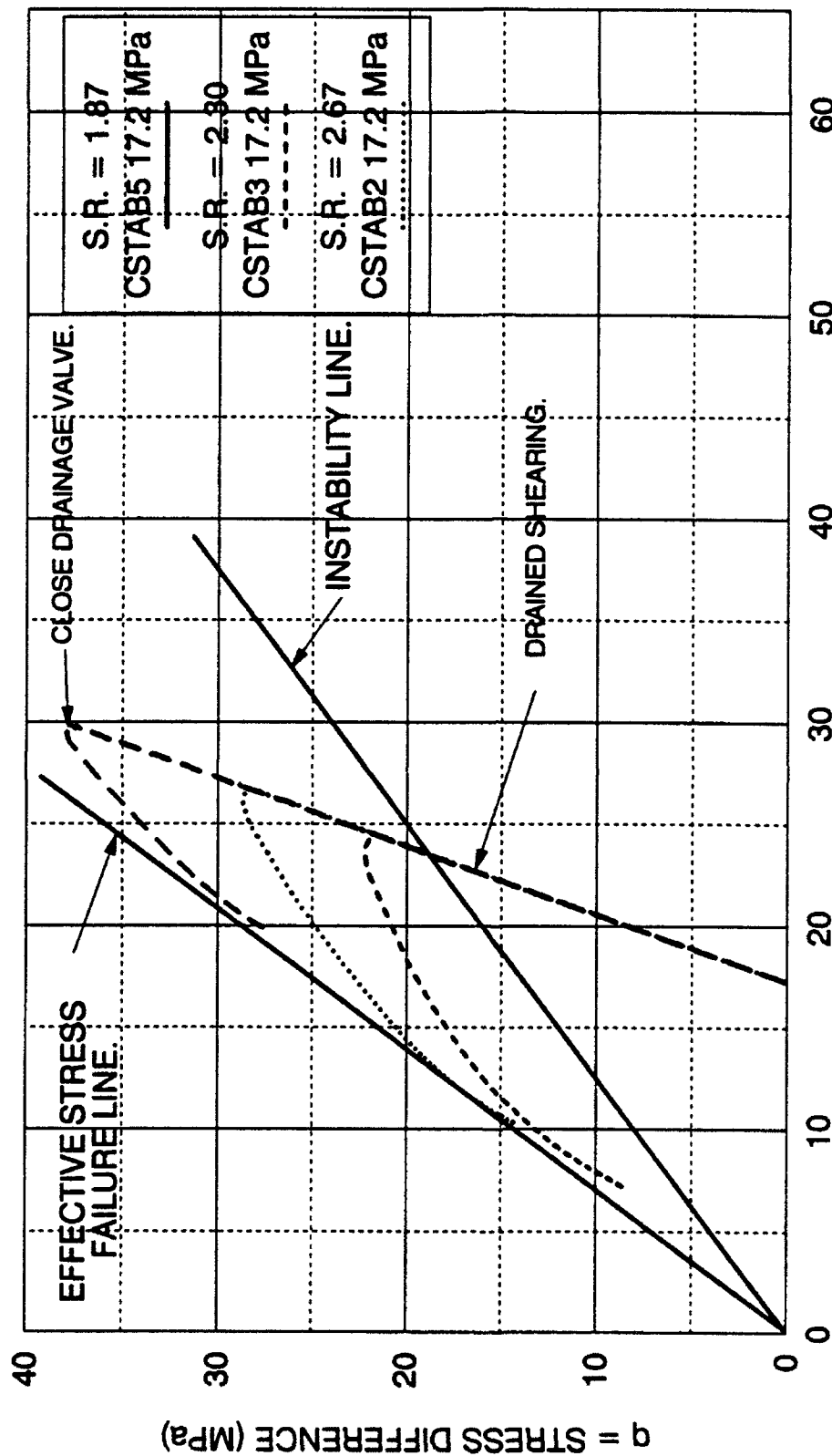


FIGURE 6-5 INSTABILITY AND TEMPORARY INSTABILITY REGION, CAMBRIDGE  $p'-q$   
UNDRAINED TRIAXIAL COMPRESSION  
DENSE CAMBRIA SAND



$p' = \text{EFFECTIVE MEAN NORMAL STRESS (MPa)}$   
 FIGURE 6-6 INSTABILITY AND TEMPORARY INSTABILITY REGIONS, CAMBRIDGE  $p'$ - $q$   
 UNDRAINED TRIAXIAL EXTENSION  
 DENSE CAMBRIA SAND

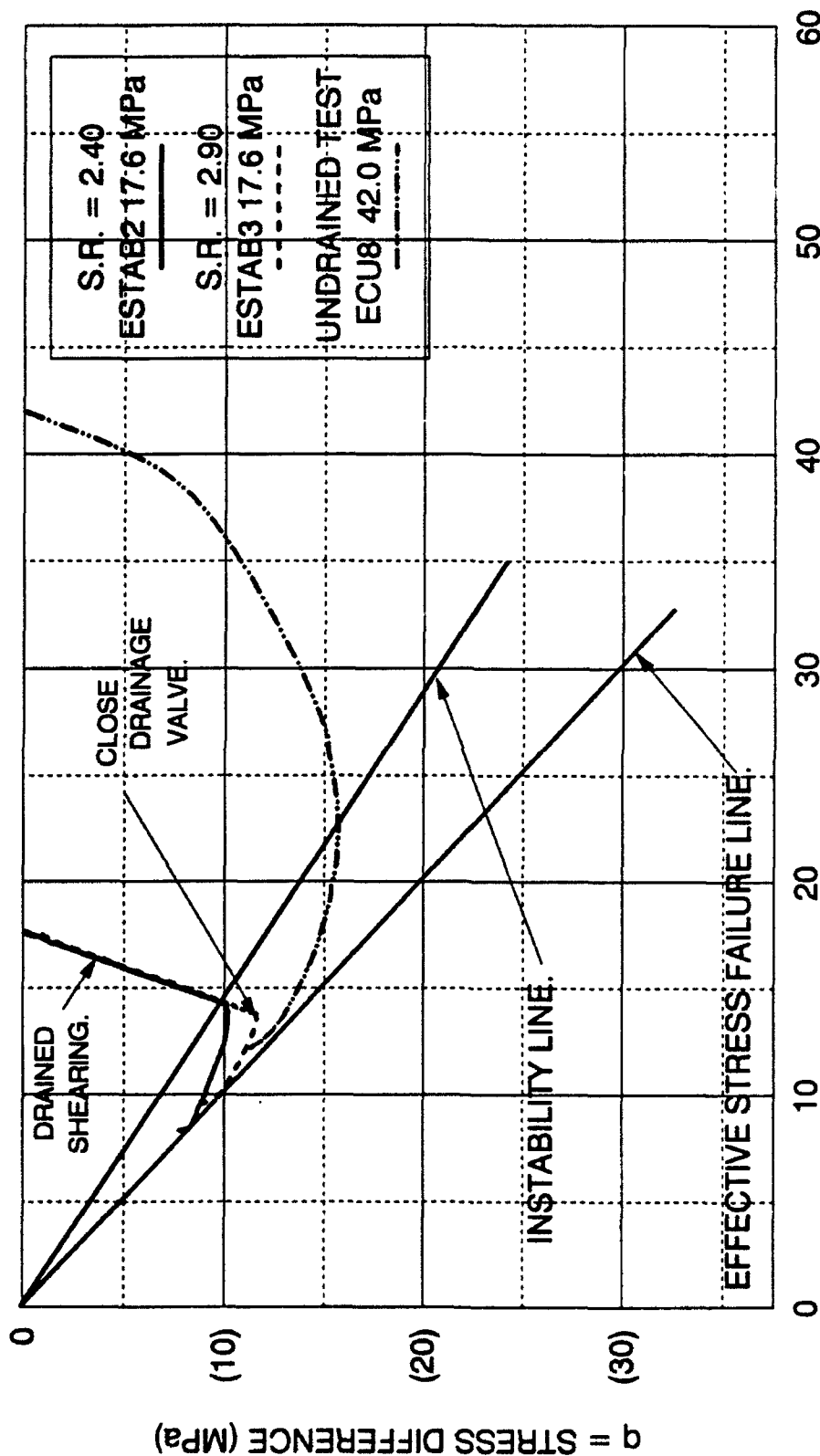


**p' = EFFECTIVE MEAN NORMAL STRESS (MPa)**

**FIGURE 6-7 INSTABILITY TESTS INSIDE INSTABILITY REGION, CAMBRIDGE p'-q**

**DRAINED-UNDRAINED STABILITY COMPRESSION TESTS**

**DENSE CAMBRIA SAND**

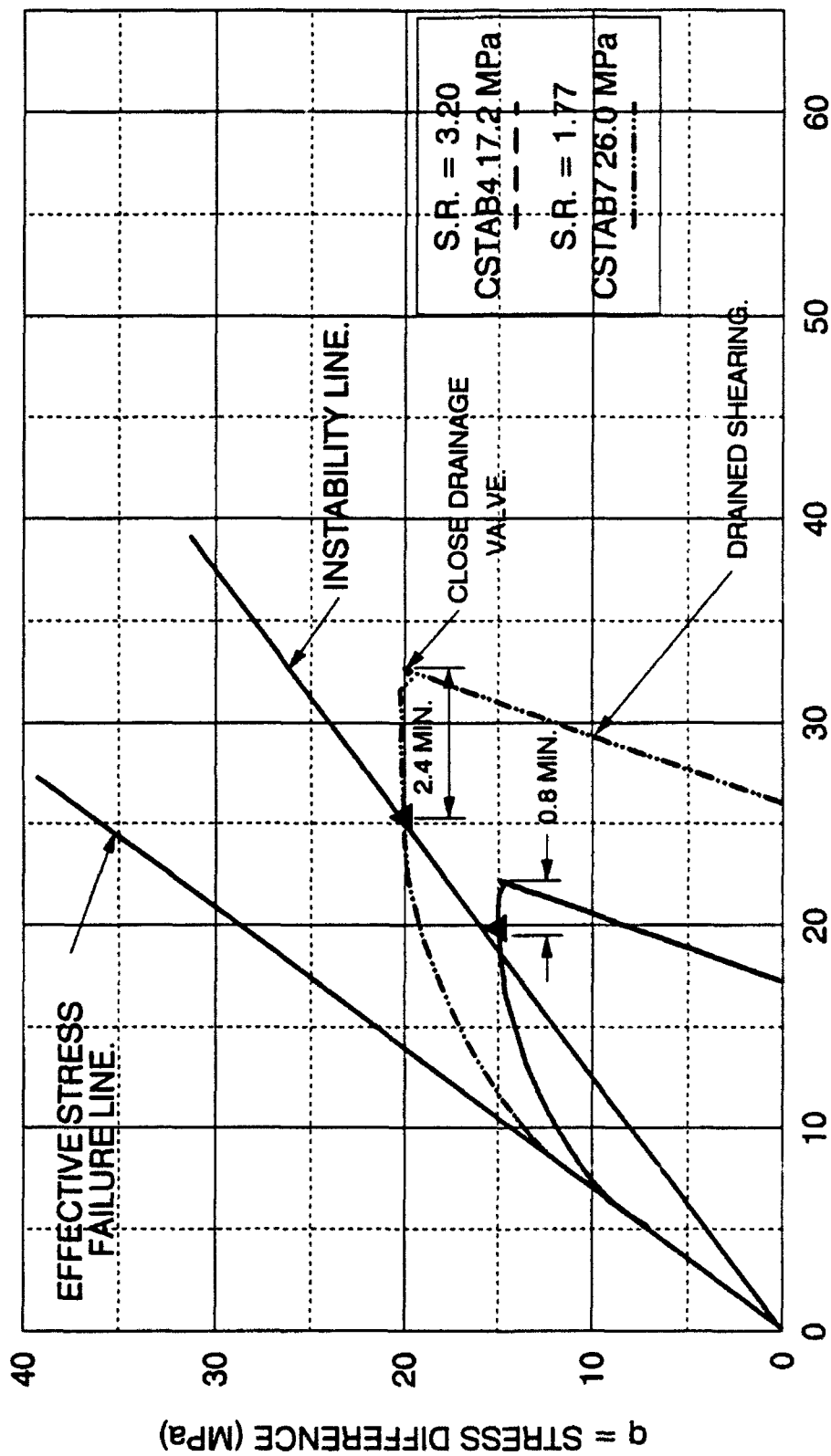


p' = EFFECTIVE MEAN NORMAL STRESS (MPa)

FIGURE 6-15 INSTABILITY TESTS WITHIN INSTABILITY REGION, CAMBRIDGE p'-q

DRAINED-UNDRAINED STABILITY EXTENSION TESTS

DENSE CAMBRIA SAND



p' = EFFECTIVE MEAN NORMAL STRESS (MPa)

FIGURE 6-12 INSTABILITY TESTS CREEPING INTO INSTABILITY REGION, CAMBRIDGE p'-q  
DRAINED-UNDRAINED STABILITY COMPRESSION TESTS

DENSE CAMBRIA SAND

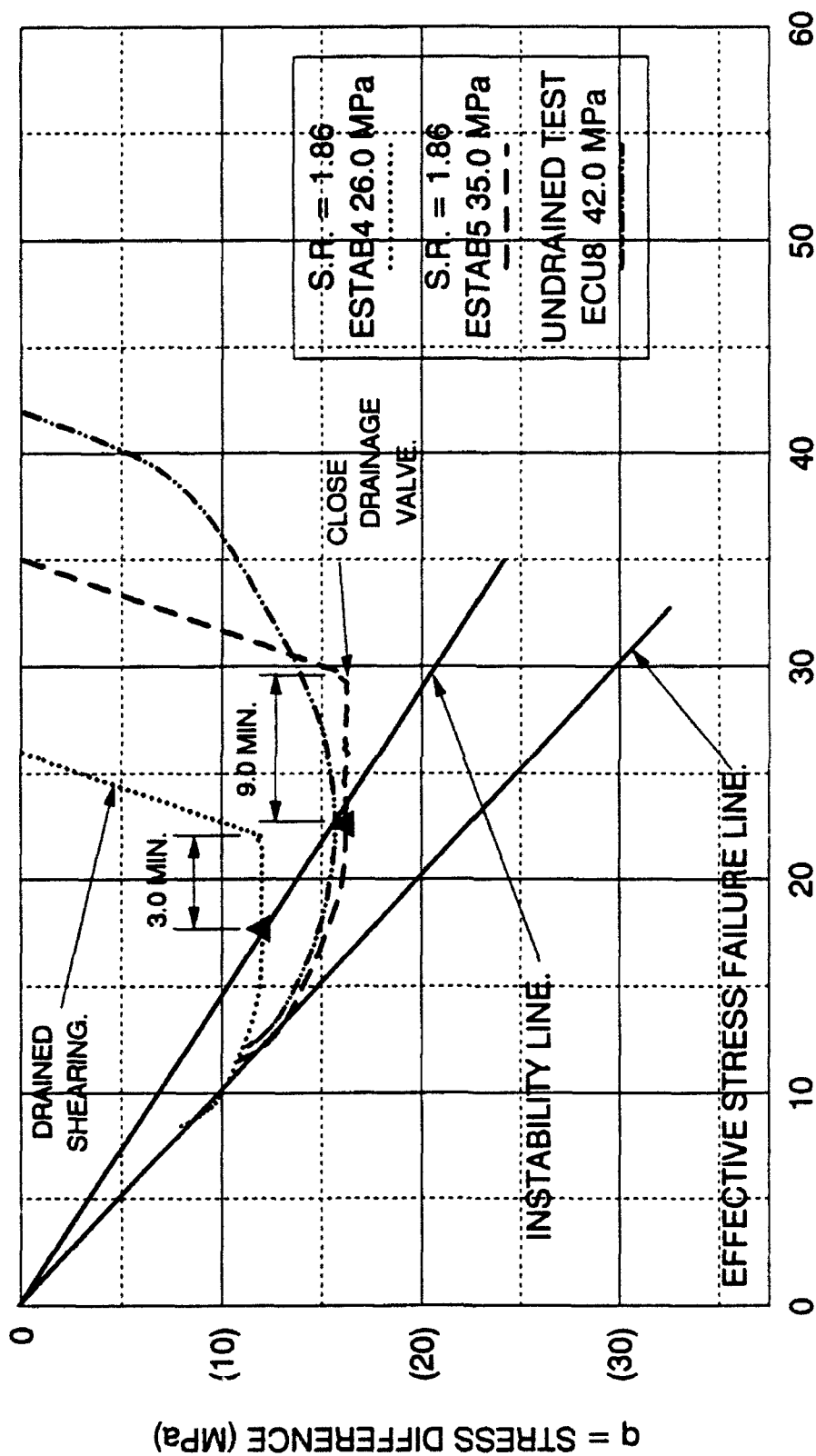


FIGURE 6-20 INSTABILITY TESTS CREEPING INTO INSTABILITY REGION, CAMBRIDGE  $p'$ - $q$   
DRAINED-UNDRAINED STABILITY EXTENSION TESTS  
DENSE CAMBRIA SAND

### B-Values, The Effective Stress Principle, and Strain Rate Effects (Chapter 7)

Values of Skempton's pore pressure parameter  $B$  at high pressures were experimentally determined utilizing special isotropic compression tests (Figures 7-1 and 7-2). The  $B$ -values were found to be substantially below unity and depended on whether the soil was on the virgin consolidation or reloading curve. These results also were reliably predicted using a compressibility equation (Figure 7-4).

The effective stress principle was examined at high pressures by performing undrained triaxial compression tests with three different total stress paths (Figure 7-6). Since the value of  $B$  is much less than unity, the effective stress paths should show effects of the varying total stress paths. However, it was found that the effects of volumetric soil creep overshadowed the potential effects of the changes in total stress path, and no conclusion could be reached regarding the uniqueness of the effective stress path at high pressures.

Since the effect of soil creep was observed to be substantial at high pressures, an investigation of the effect of strain rate on the location of the instability line was undertaken by performing a series of drained and undrained triaxial compression tests at different strain rates. The location of the instability line does not appear to be influenced by effects of strain rate (Figure 7-9). It was demonstrated that the undrained effective stress paths change, but the different maximum deviator stresses still fall on the same instability line. It was determined from drained conditions that increasing strain rate (Table 7.2) increases the deviator stress slightly, decreases the volumetric strains slightly, and increases the axial strains to failure slightly. The mechanism identified as causing strain rate effects at high pressures was the effect of increasing dilatancy (less time for particle crushing) with increasing strain rate. At high strain rates the soil does not have time to undergo as much particle breakage and rearranging as it can experience at lower strain rates. Even though the effects of strain rate was determined to be insignificant for drained tests, the effects on undrained tests was substantial (Table 7.1). It was found that

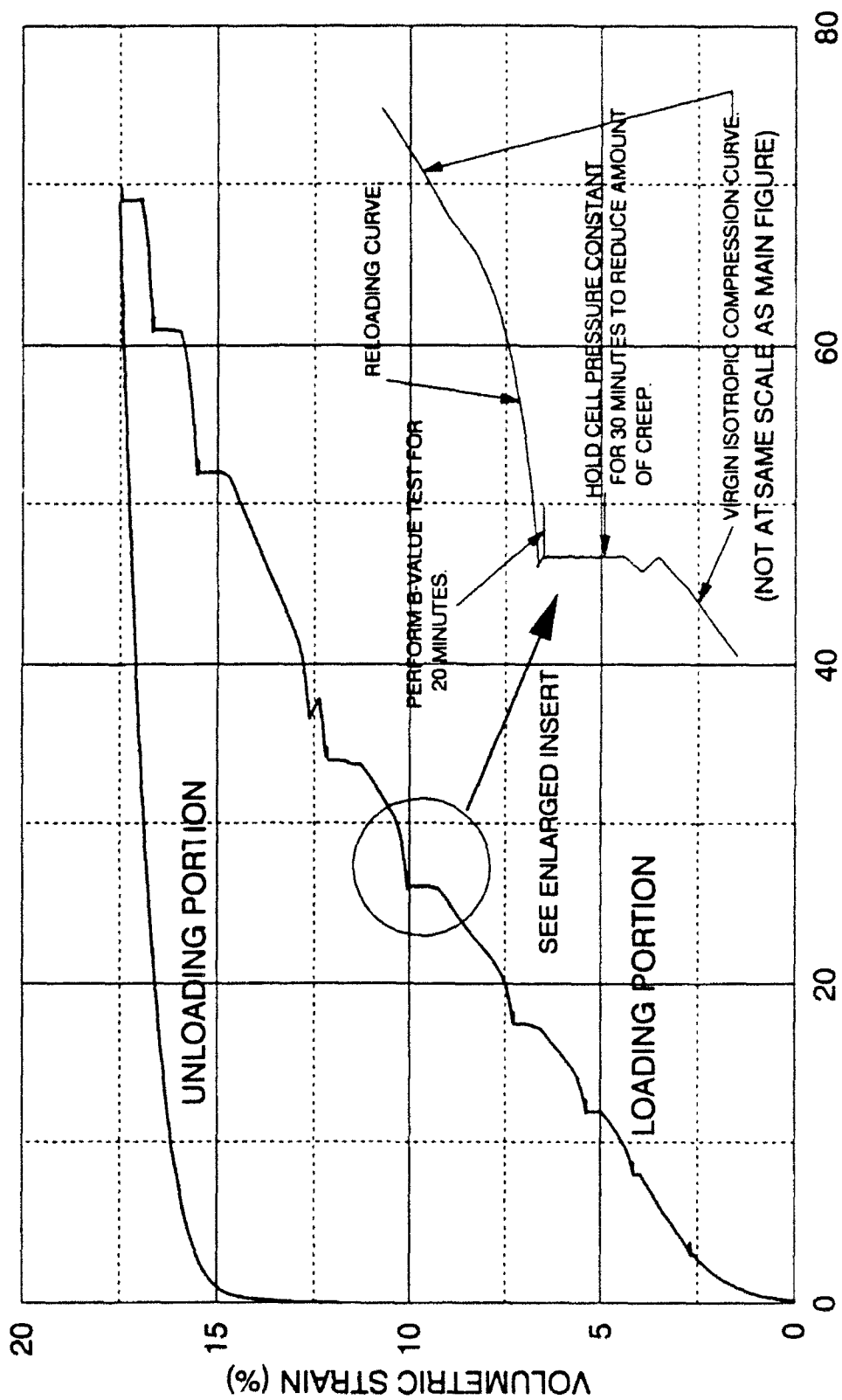


FIGURE 7-1 ISOTROPIC COMPRESSION AND UNLOADING WITH ENLARGED INDIVIDUAL TEST LOCATIONS OF B-VALUE TESTS  
DENSE CAMBRIA SAND

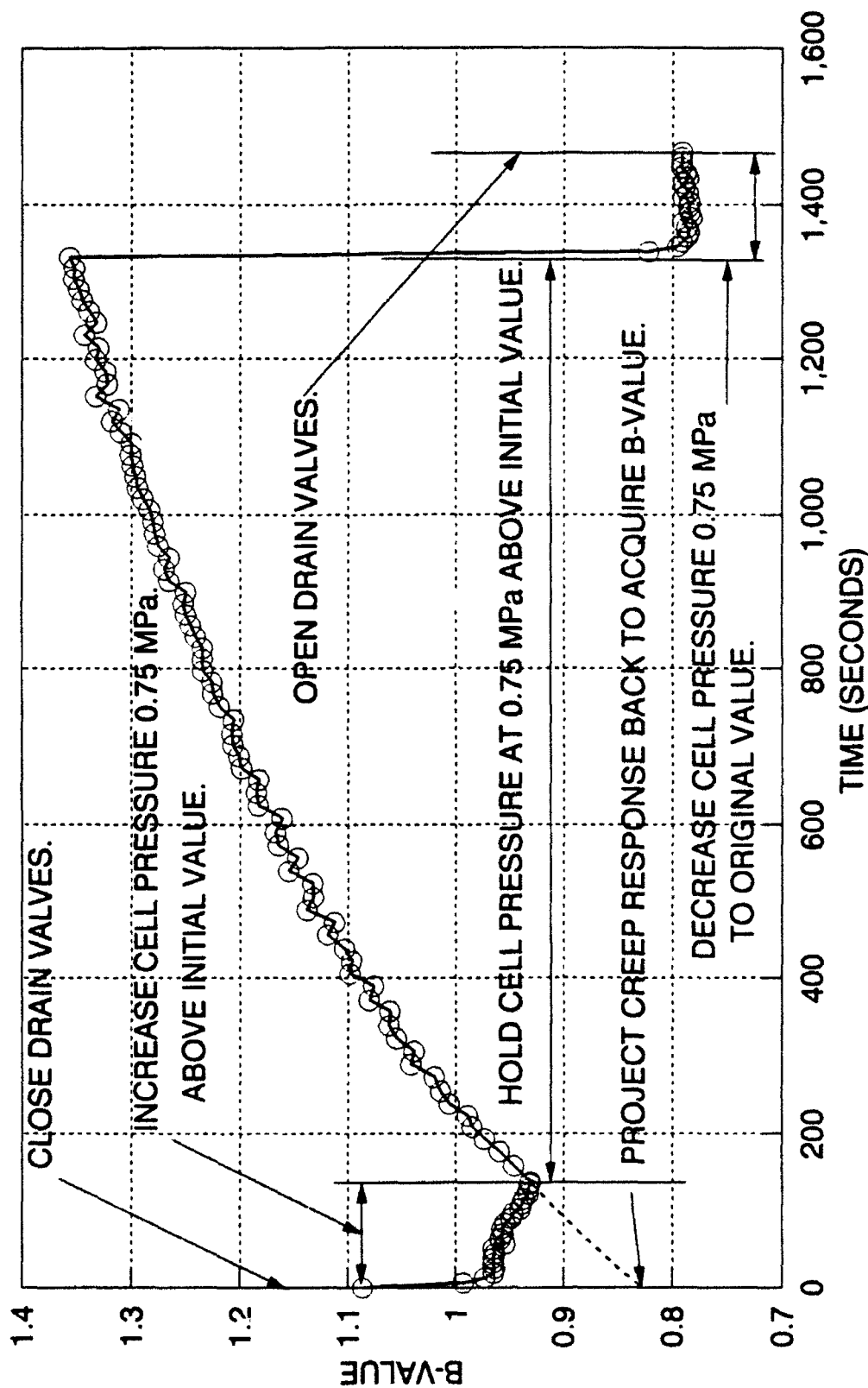


FIGURE 7-2 VARIATION IN B-VALUES DURING INDIVIDUAL B-VALUE TEST  
AT 12.0 MPa EFFECTIVE CONFINING PRESSURE  
DENSE CAMBRIA SAND

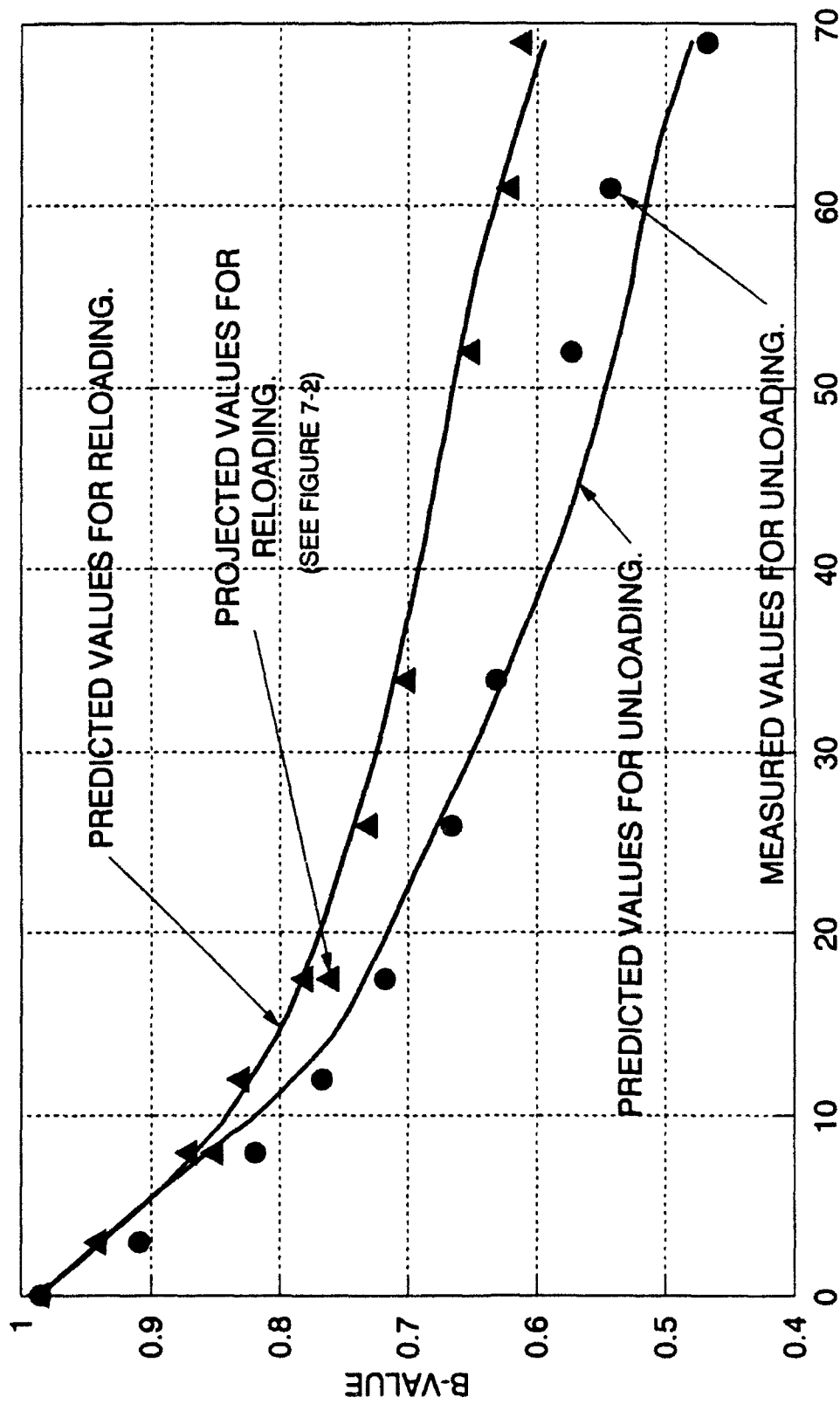


FIGURE 7-4 EXPERIMENTAL & PREDICTED B-VALUES  
FOR RELOADING AND UNLOADING CONDITIONS  
DENSE CAMBRIA SAND

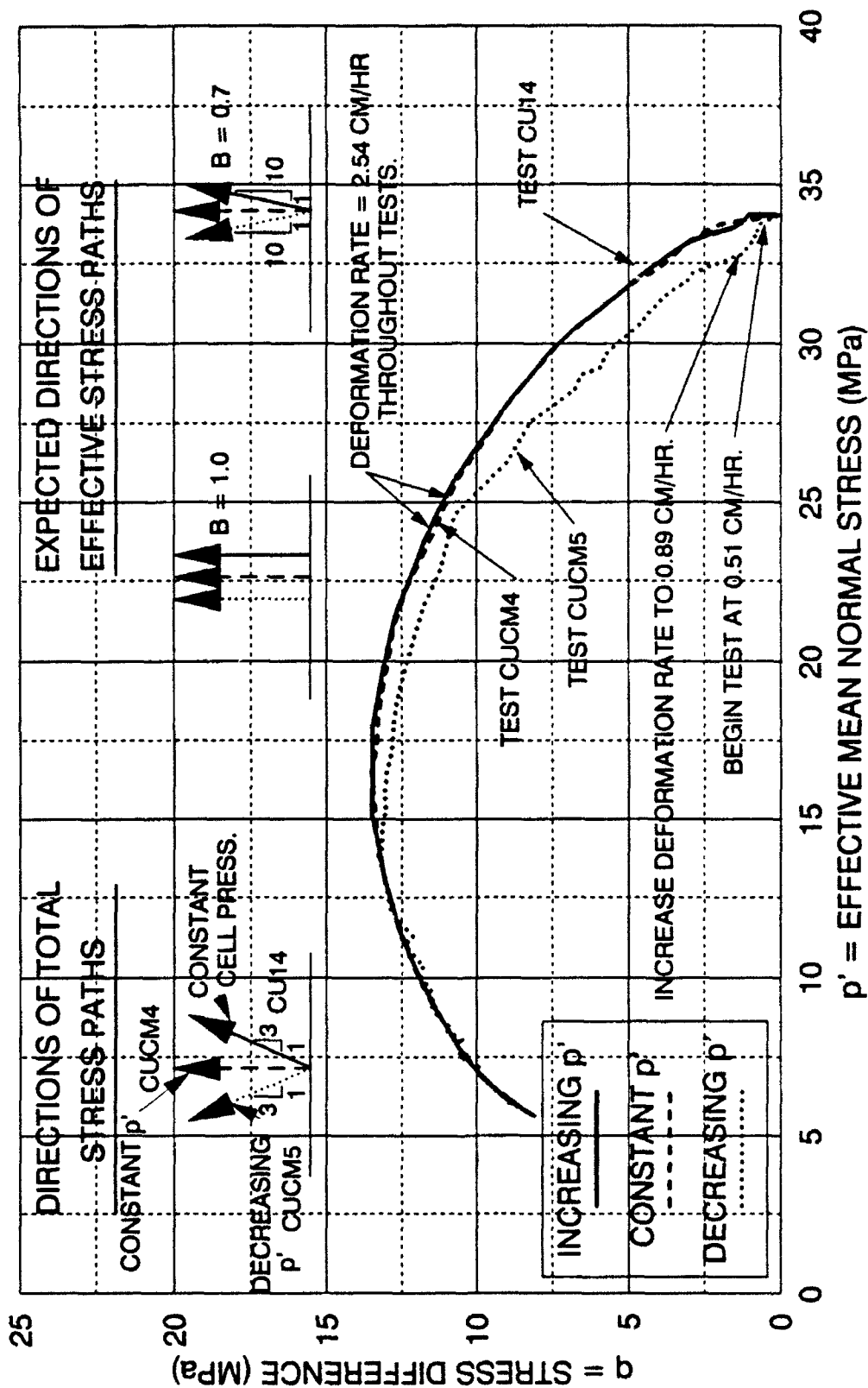
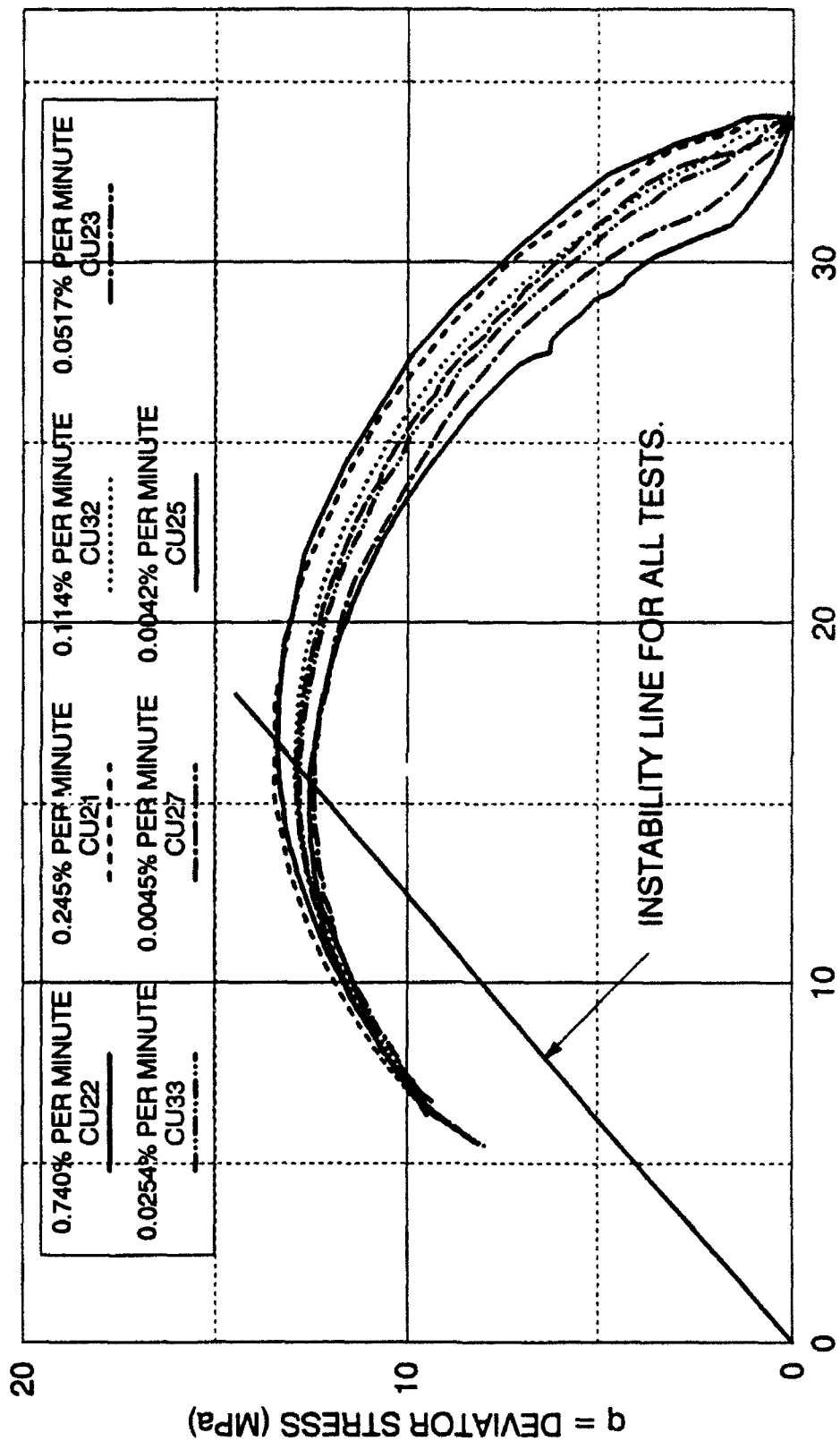


FIGURE 7-6 EFFECTIVE STRESS PATHS, CAMBRIDGE  $p'$ - $q$ , FOR DIFFERENT TOTAL STRESS PATHS, AND DIFFERENT EXPECTED DIRECTIONS AT 34.0 MPa CONFINING PRESSURE  
DENSE CAMBRIA SAND



$p' = \text{EFFECTIVE MEAN NORMAL STRESS (MPa)}$

FIGURE 7-9 EFFECTIVE STRESS PATH, CAMBRIDGE  $p'$ - $q$   
UNDRAINED TRIAXIAL COMPRESSION TESTS AT DIFFERENT STRAIN RATES  
INITIAL EFFECTIVE CONFINING PRESSURE 34.0 MPa

STRAIN RATE (%/MINUTE)	MAXIMUM DEVIATOR STRESS (MPa)	FRICTION ANGLE (DEGREE)	AXIAL STRAIN AT FAILURE (%)	VOLUMETRIC STRAIN AT FAILURE (%)
0.0517% TO 0.74%	42.72 TO 43.40	33.6 TO 33.9	35.1 TO 35.9%	15.3 TO 14.7%
+1.430%	+1.6%	+0.8%	+2.3%	-3.9%

TABLE 7.2 EFFECTS OF STRAIN RATE VARIATIONS IN  
DRAINED COMPRESSION ON DENSE CAMBRIA SAND  
AT 34.0 MPa CONFINING PRESSURE

STRAIN RATE (%/MINUTE)	MAXIMUM DEVIATOR STRESS (MPa)	AXIAL STRAIN AT INSTABILITY LINE	FRICTION ANGLE (DEGREE)	AXIAL STRAIN AT FAILURE (%)	EFFECTIVE CONFINING PRESSURE AT FAILURE (MPa)
0.0042% TO 0.74%	12.56 TO 13.48	1.84 TO 2.38%	36.2 TO 34.5	18.5 TO 28.3%	2.8 TO 3.6 MPa
+17,800%	+7.3%	+29%	-4.7%	+53%	+29%

TABLE 7.1 EFFECTS OF STRAIN RATE VARIATIONS IN  
UNDRAINED TRIAXIAL COMPRESSION TESTS ON DENSE  
CAMBRIA SAND AT 34.0 MPa CONFINING PRESSURE

decreasing strain rates in undrained tests substantially reduces the maximum deviator stress, substantially increases the strain to effective stress failure, substantially increases pore pressures, substantially increases effective stress friction angles, and substantially decreases the effective confining pressures at failure.

#### Particle Breakage at High Pressures (Chapter 8)

Sieve analyses on many sheared specimens of Cambria sand were performed and grain size distributions were evaluated (Figures 8-2 through 8-5). Commonly used empirical particle breakage factors created by Marsal, by Lee and Farhoomand, and by Hardin were calculated based upon these grain size curves. It was found that triaxial compression tests had significantly more particle crushing than triaxial extension tests (Figures 8-6 through 8-9). Undrained tests appear to produce more particle breakage than drained tests, when results are compared on the basis of effective mean normal stress at failure. This was due to effects of stress path, and the effective mean normal stress at failure was not considered to be a good variable on which to base the comparison (Figure 8-10) of crushing. Void ratio at failure provided a better variable for comparison, since the drained and undrained tests appeared to be on the same lines (Figures 8-11 through 8-14). However, the extension and compression tests still appeared on different lines.

Total input energy was calculated at the end of the test and it was determined to be a unifying variable, with results of particle breakage parameters from drained and undrained triaxial compression and extension tests all appearing on a unique line (Figures 8-15 through 8-18).

Thin sections of sheared specimens were obtained and examined under a light polarizing microscope (Figures 8-19 and 8-20). Photographs of the thin-sections indicate that the mechanism of compaction was different in Cambria sand and in quartz sand. The Cambria sand,

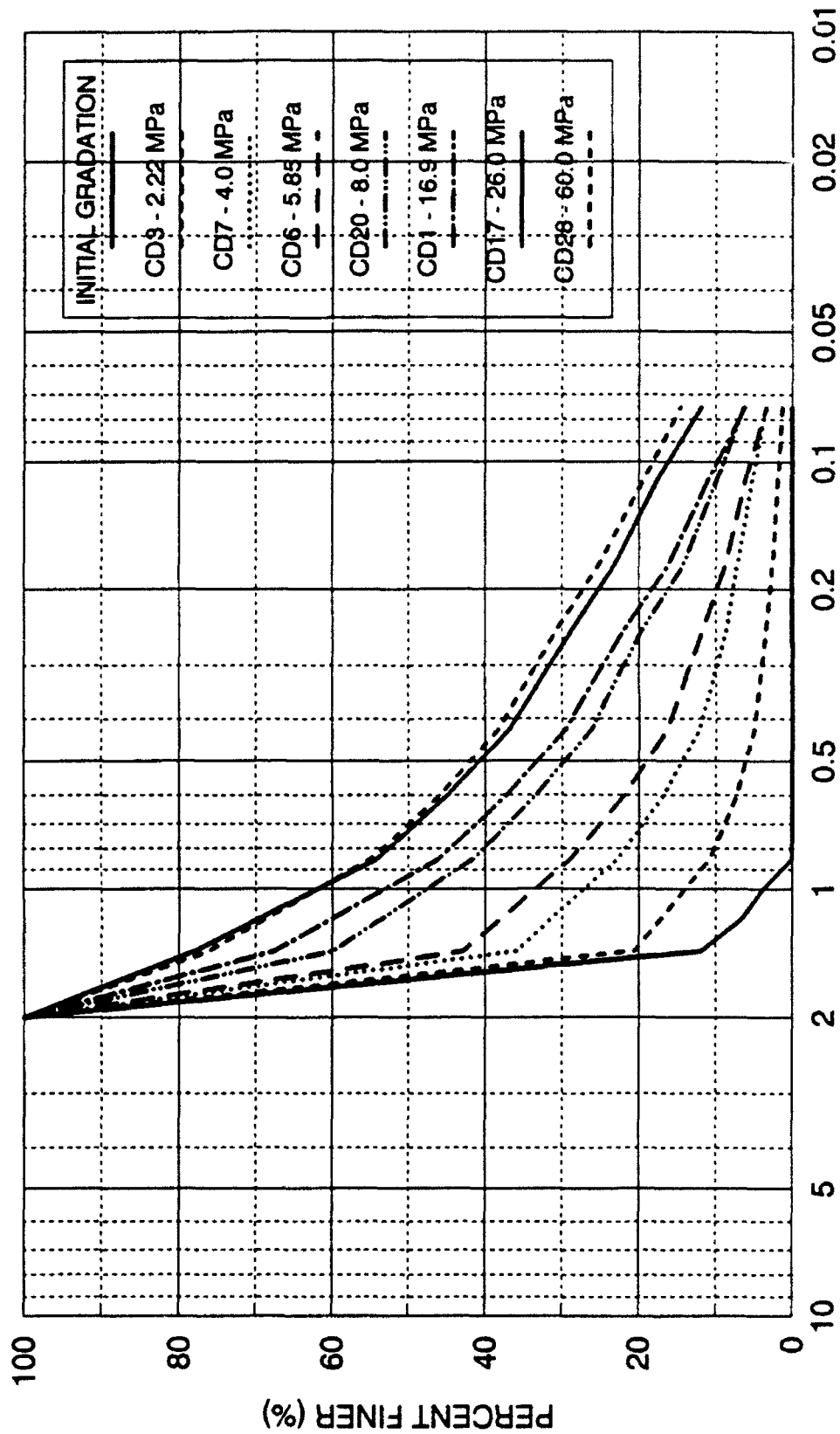


FIGURE 8-2 GRAIN SIZE DISTRIBUTION CURVES  
DRAINED TRIAXIAL COMPRESSION TESTS  
DENSE CAMBRIA SAND

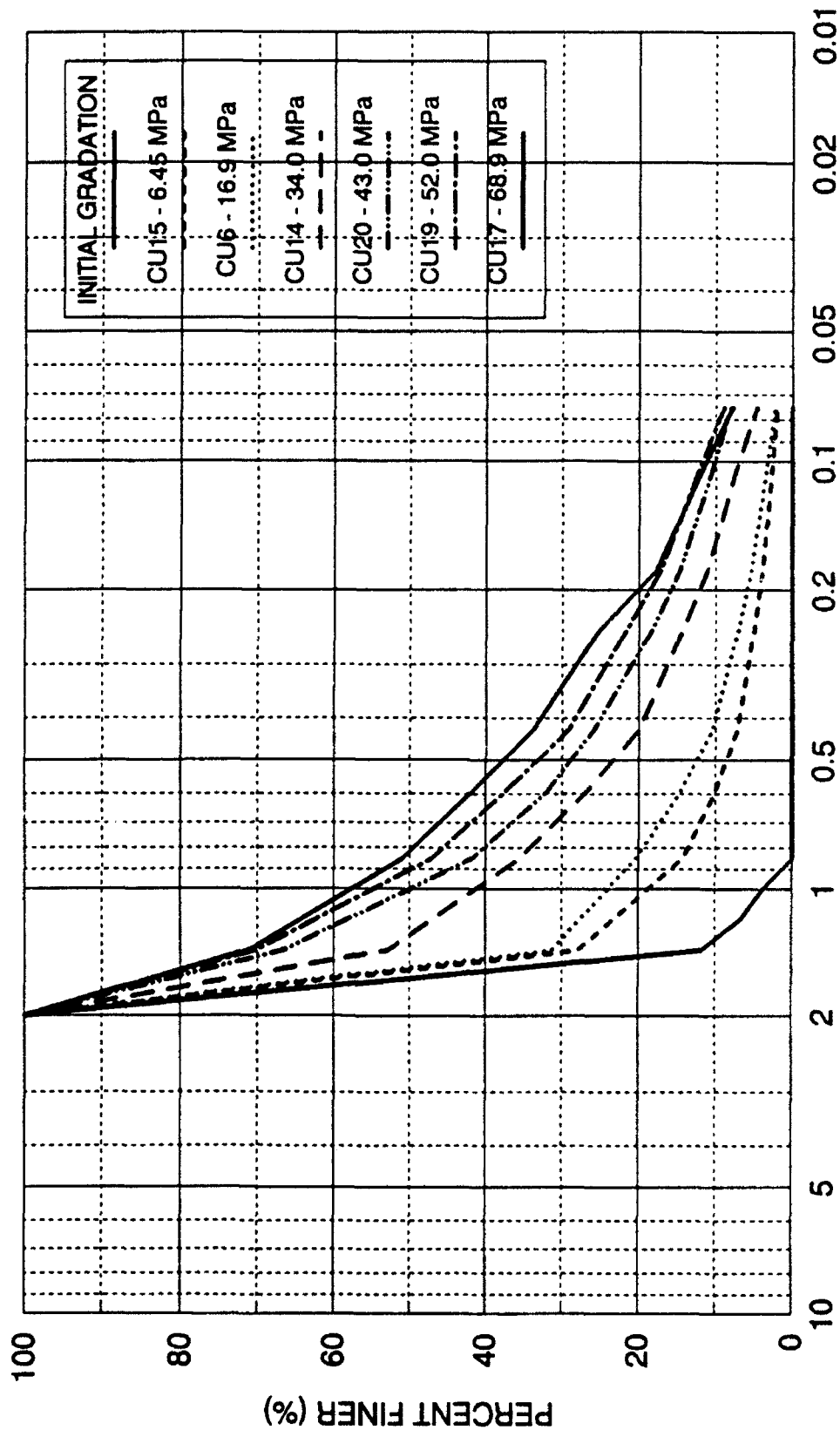


FIGURE 8-3 GRAIN SIZE DISTRIBUTION CURVES  
UNDRAINED TRIAXIAL COMPRESSION TESTS  
DENSE CAMBRIA SAND

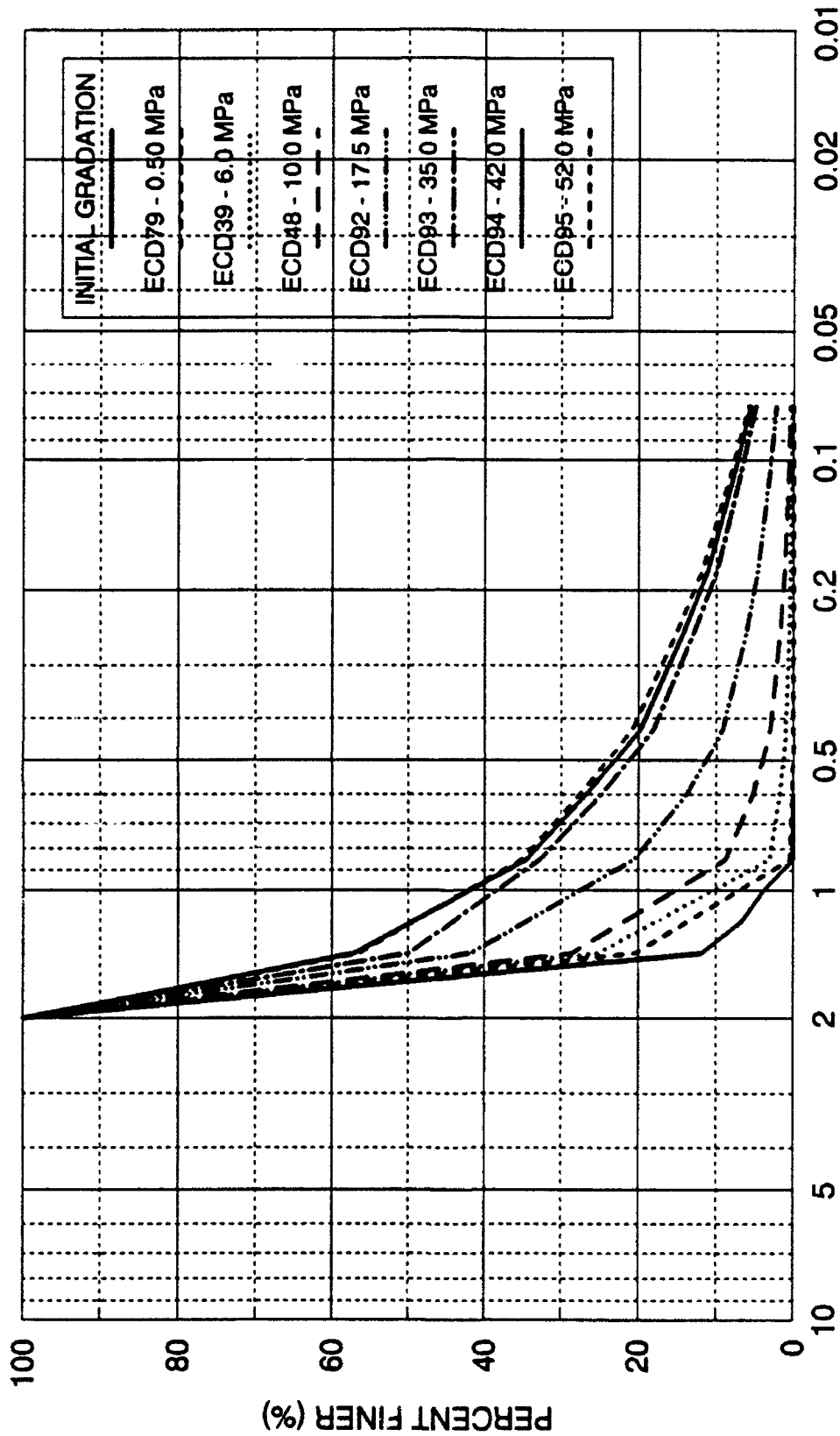


FIGURE 8-4 GRAIN SIZE DISTRIBUTION CURVES  
DRAINED TRIAXIAL EXTENSION TESTS  
DENSE CAMBRIA SAND

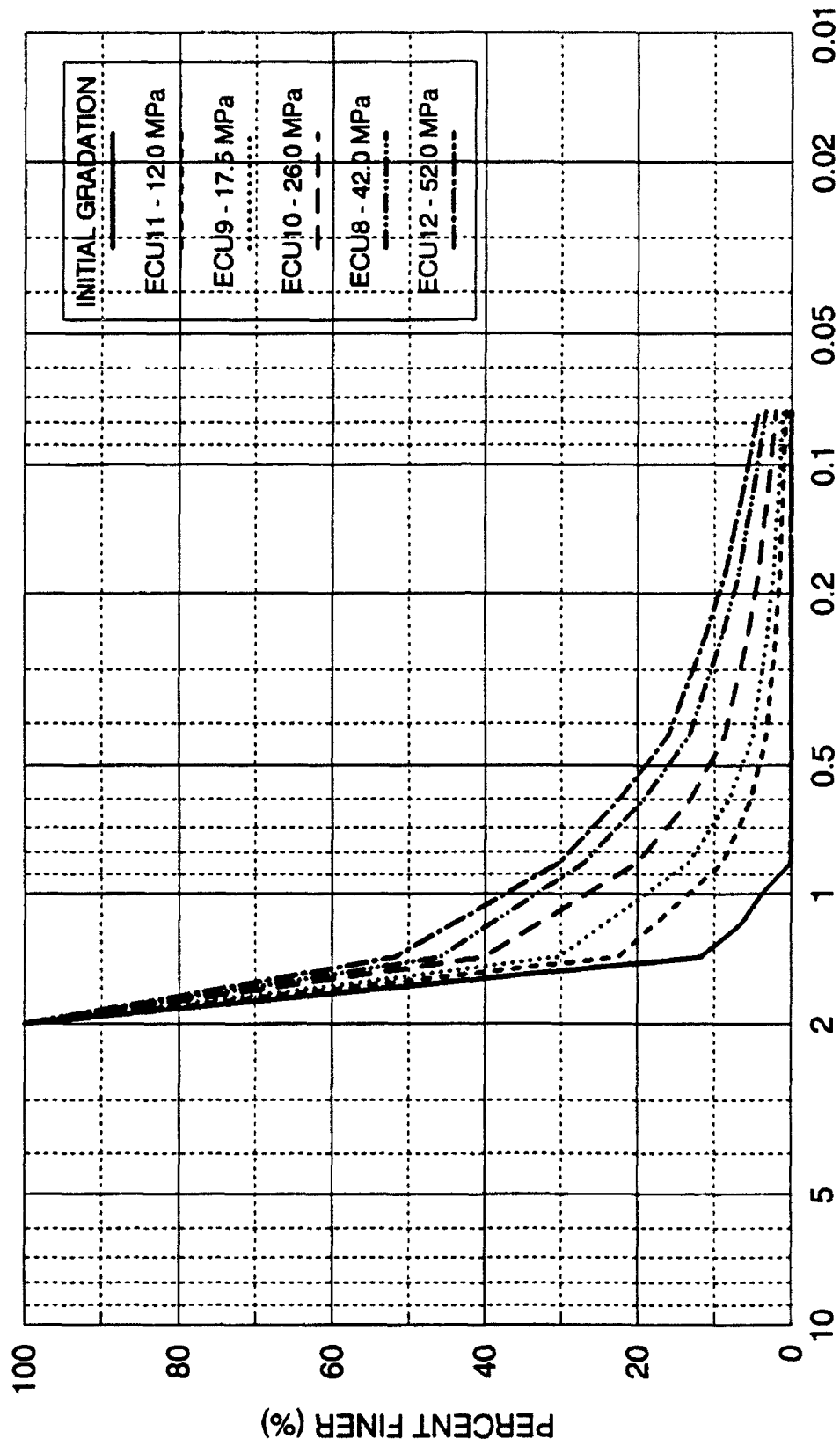


FIGURE 8-5 GRAIN SIZE DISTRIBUTION CURVES  
UNDRAINED TRIAXIAL EXTENSION TESTS  
DENSE CAMBRIA SAND

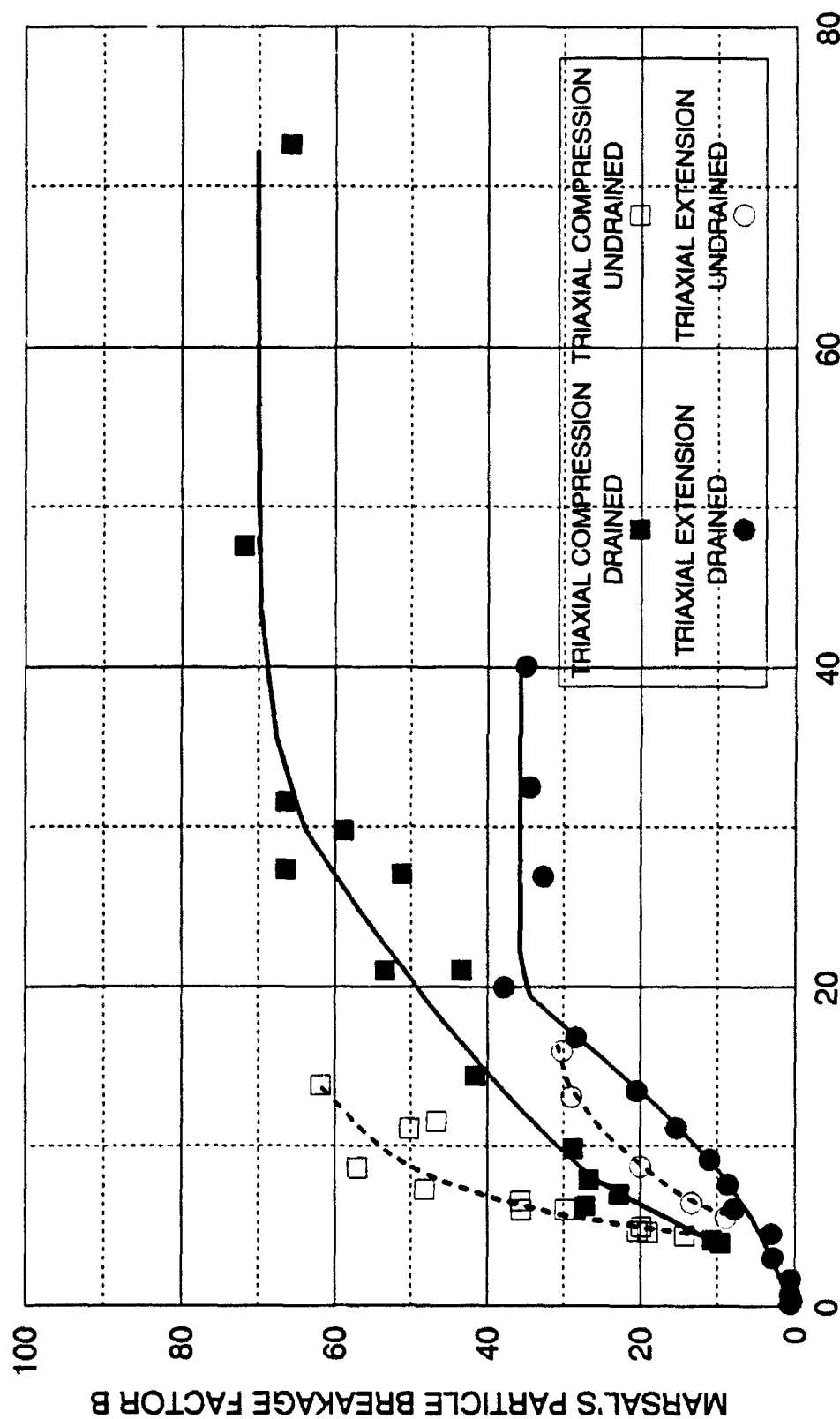
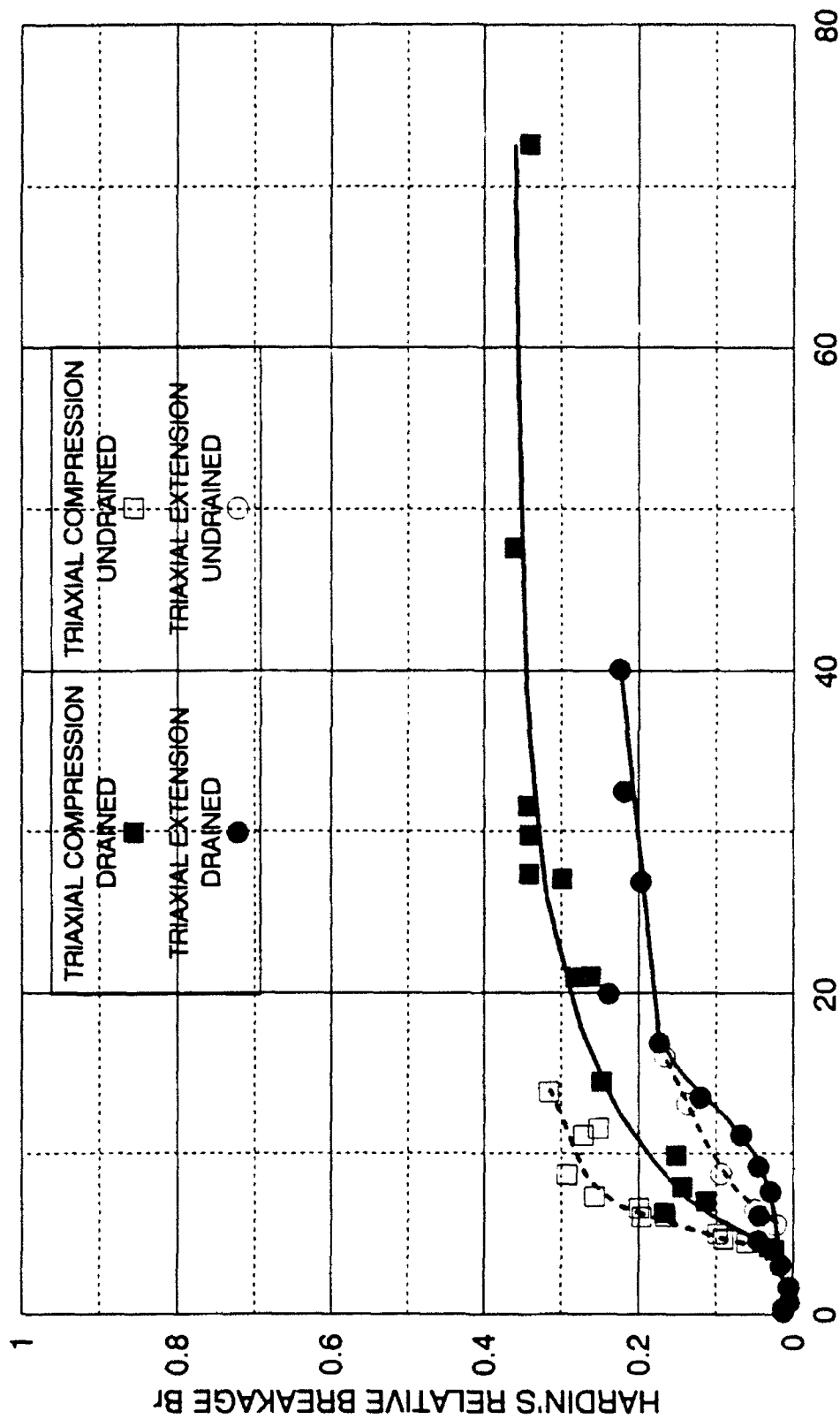
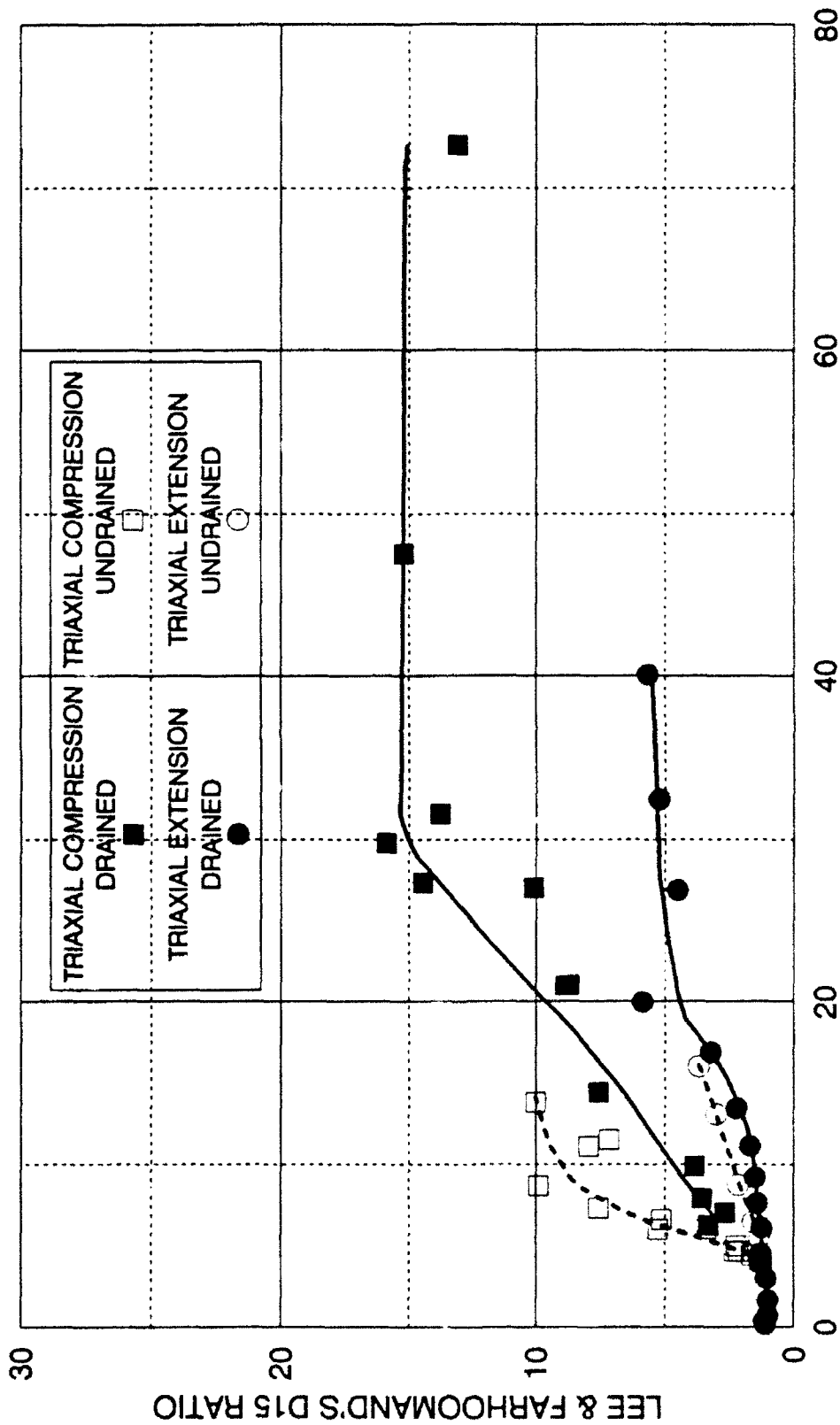
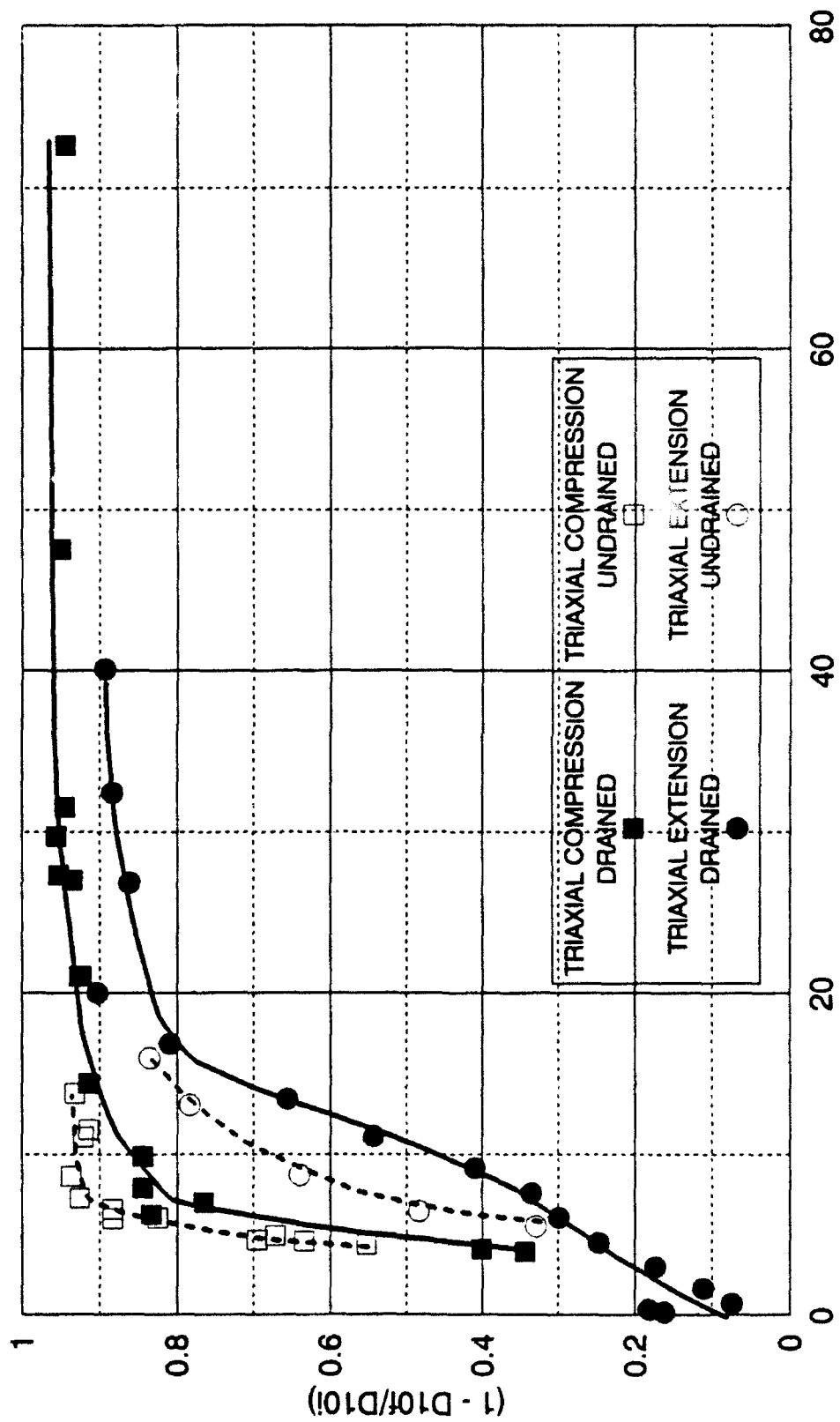


FIGURE 8-6 MARSAL'S PARTICLE BREAKAGE FACTOR B RELATED TO  $p'$   
DRAINED AND UNDRAINED TRIAXIAL COMPRESSION AND EXTENSION TESTS  
DENSE CAMBRIA SAND



$p' = \text{MEAN NORMAL STRESS AT FAILURE (MPa)}$   
 FIGURE 8-7 HARDIN'S RELATIVE BREAKAGE  $B_r$  RELATED TO  $p'$   
 DRAINED AND UNDRAINED TRIAXIAL COMPRESSION AND EXTENSION TESTS  
 DENSE CAMBRIA SAND





$p' = \text{MEAN NORMAL STRESS AT FAILURE (MPa)}$

FIGURE 8-9  $B_{10} = (1 - D_{10f}/D_{10i})$  RELATED TO  $p'$

DRAINED AND UNDRAINED TRIAXIAL COMPRESSION AND EXTENSION TESTS

DENSE CAMBRIA SAND

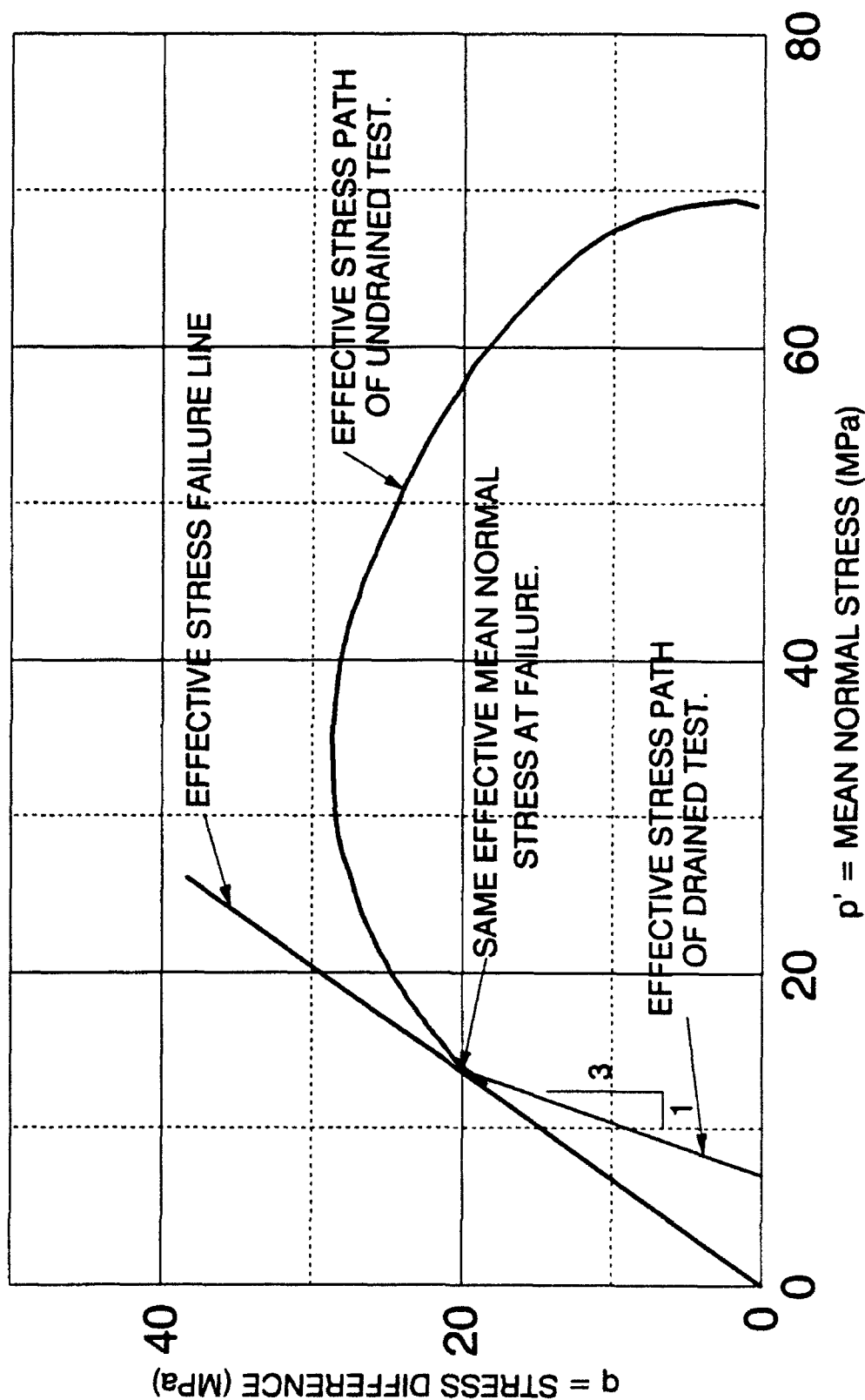
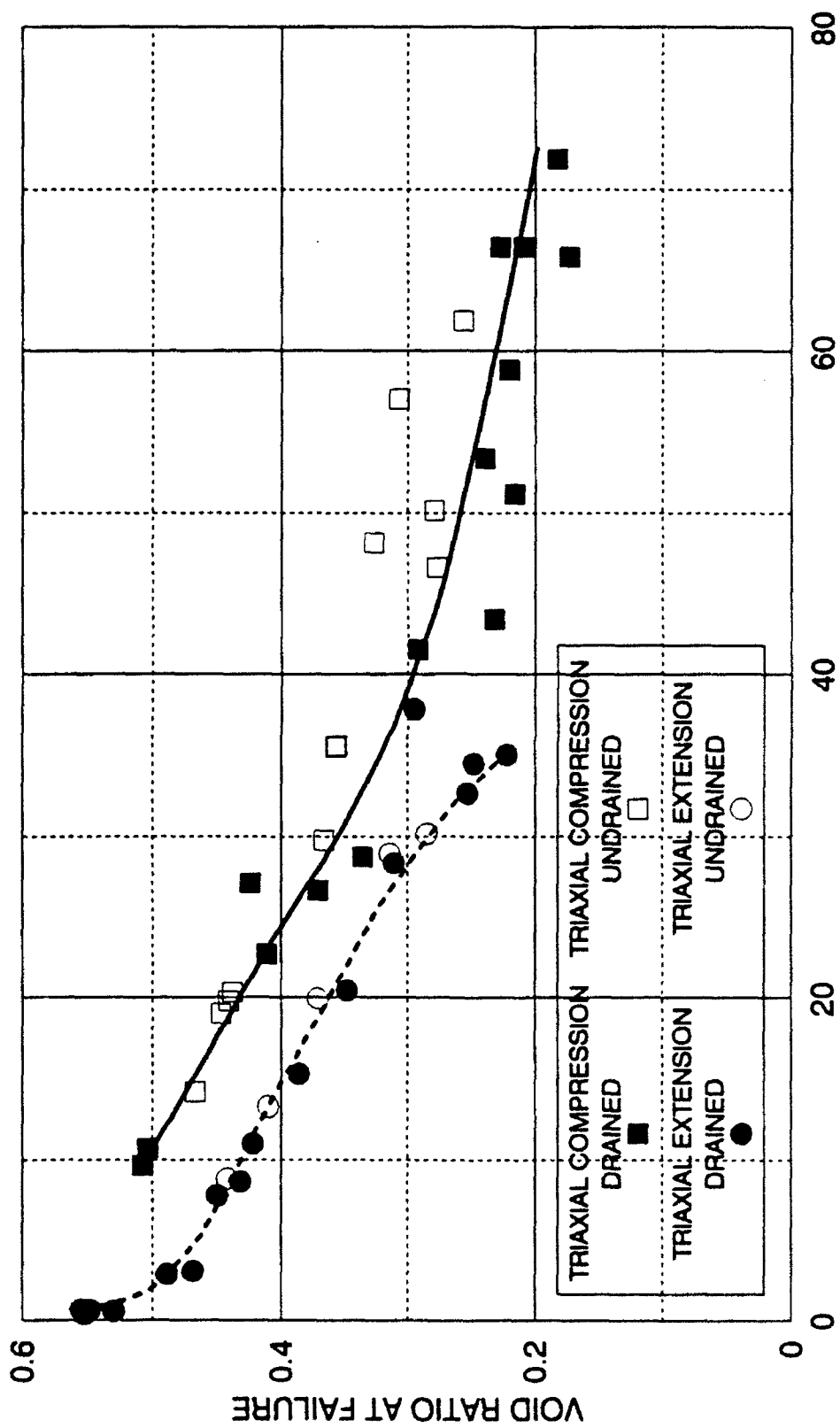
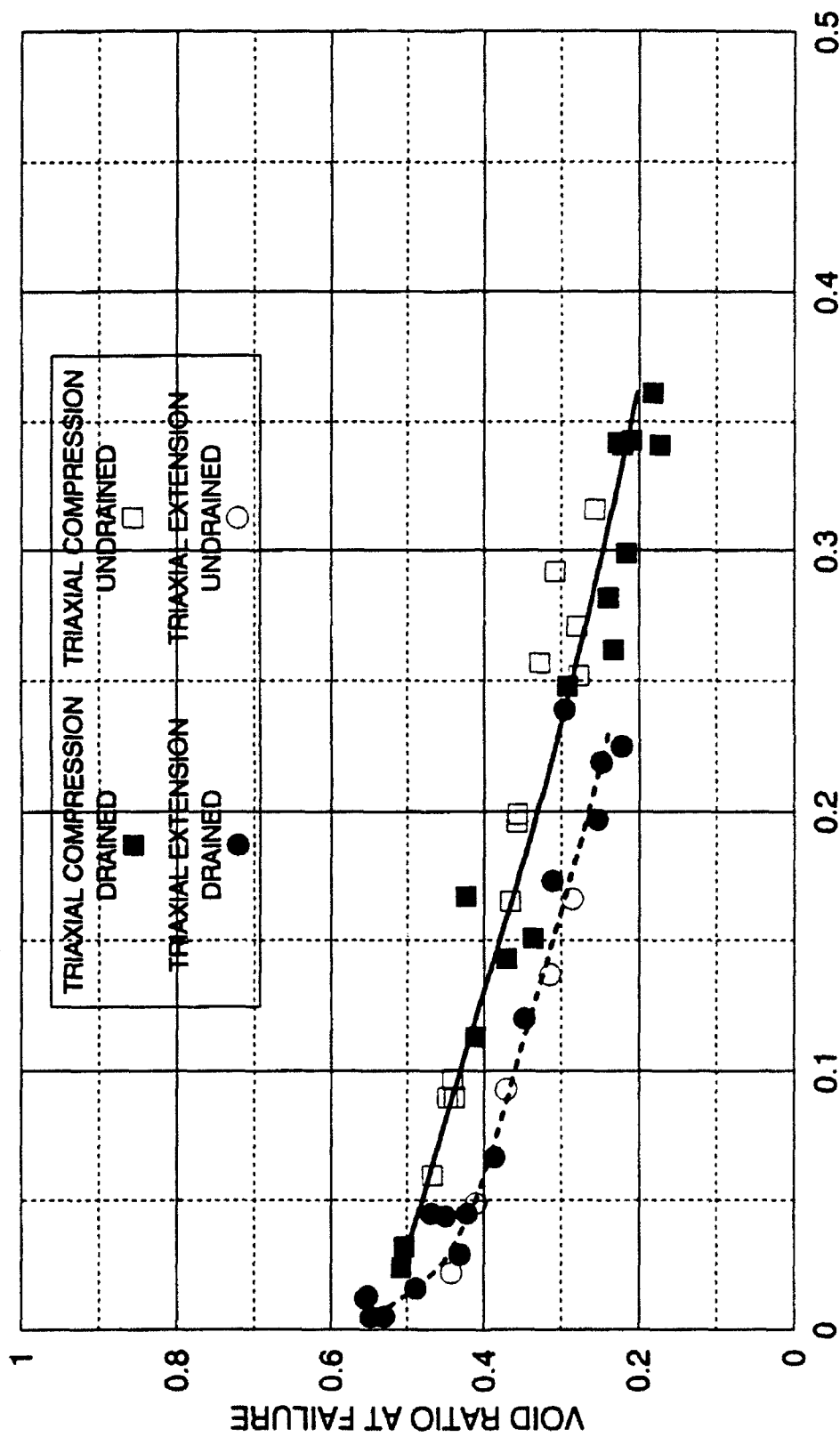


FIGURE 8-10 EFFECT OF STRESS PATH ON PARTICLE BREAKAGE  
BETWEEN DRAINED AND UNDRAINED TESTS  
DENSE CAMBRIA SAND

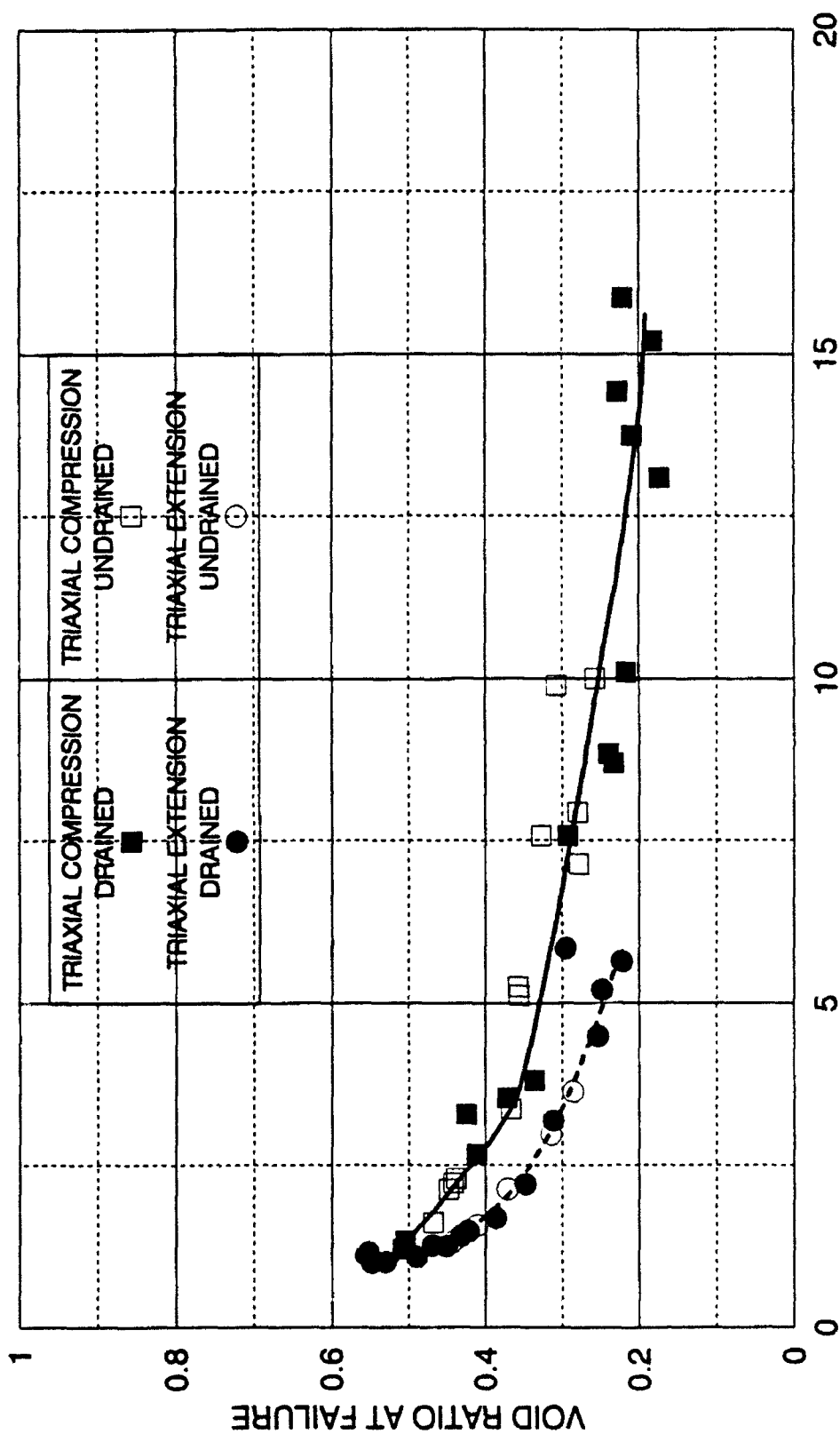


MARSAL'S PARTICLE BREAKAGE FACTOR B  
 FIGURE 8-11 MARSAL'S PARTICLE BREAKAGE FACTOR B RELATED TO VOID RATIO  
 DRAINED AND UNDRAINED TRIAXIAL COMPRESSION AND EXTENSION TESTS  
 DENSE CAMBRIA SAND



HARDIN'S RELATIVE BREAKAGE  $B_r$

FIGURE 8-12 HARDIN'S RELATIVE BREAKAGE FACTOR  $B_r$  RELATED TO VOID RATIO  
DRAINED AND UNDRAINED TRIAXIAL COMPRESSION AND EXTENSION TESTS  
DENSE CAMBRIA SAND



LEE & FARHOOMAND'S D15 RATIO  
 DRAINED AND UNDRAINED TRIAXIAL COMPRESSION AND EXTENSION TESTS  
 DENSE CAMBRIA SAND

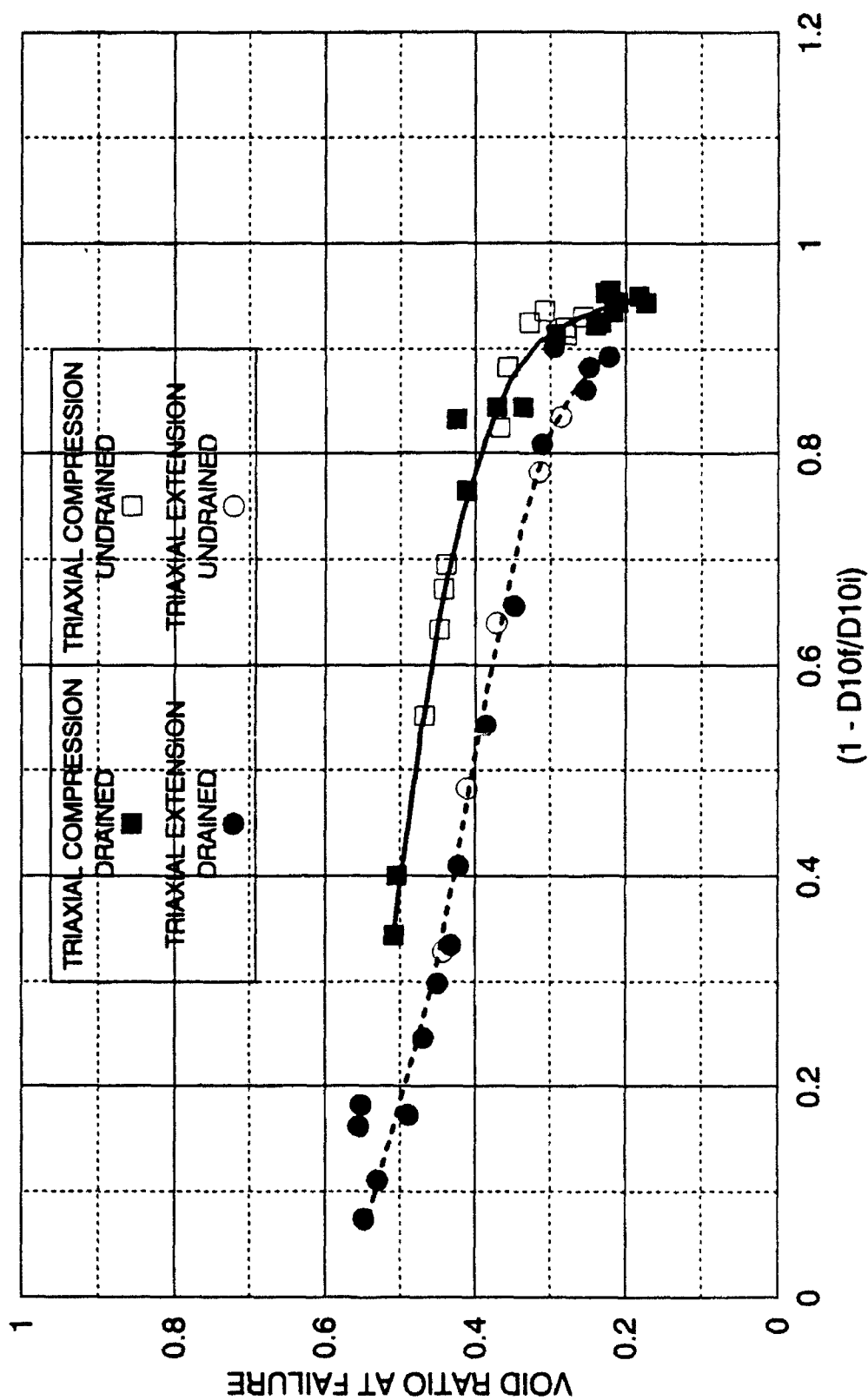


FIGURE 8-14  $B10 = (1 - D10f/D10i)$  FACTOR RELATED TO VOID RATIO  
DRAINED AND UNDRAINED TRIAXIAL COMPRESSION AND EXTENSION TESTS  
DENSE CAMBRIA SAND

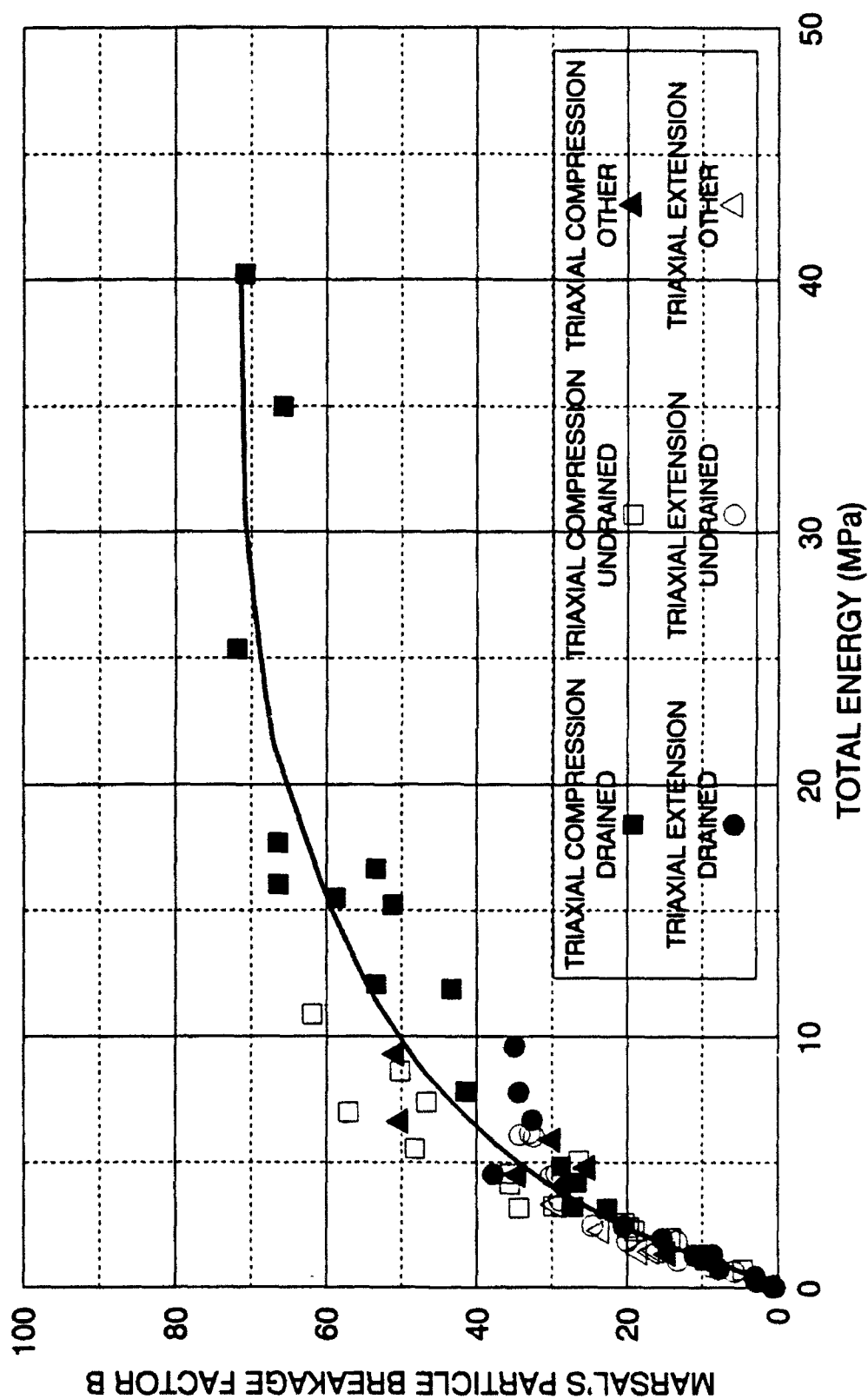


FIGURE 8-15 MARSAL'S PARTICLE BREAKAGE FACTOR B RELATED TO ENERGY  
DRAINED AND UNDRAINED TRIAXIAL COMPRESSION AND EXTENSION TESTS  
DENSE CAMBRIA SAND

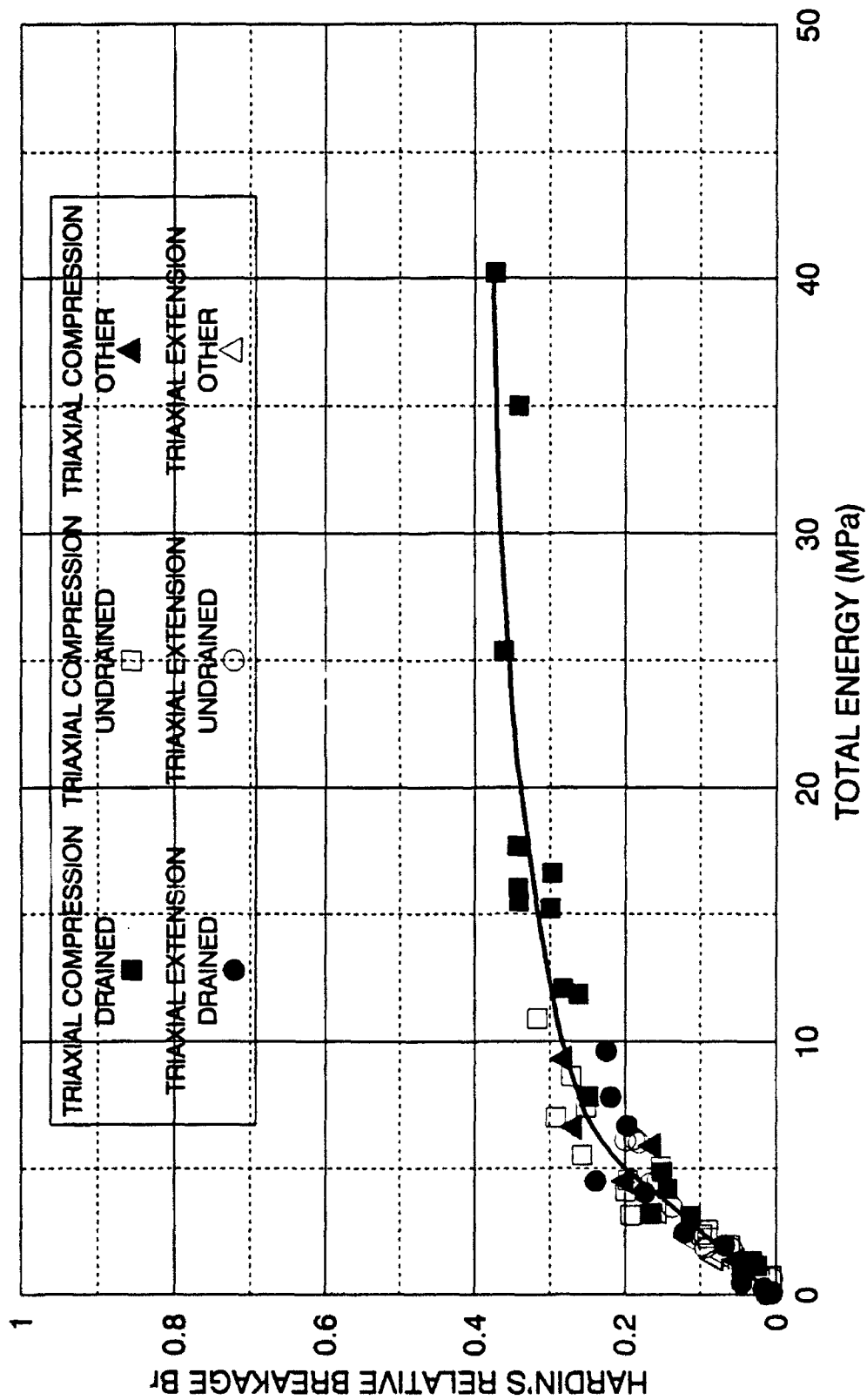


FIGURE 8-16 HARDIN'S RELATIVE BREAKAGE  $B_r$  RELATED TO ENERGY  
DRAINED AND UNDRAINED TRIAXIAL COMPRESSION AND EXTENSION TESTS  
DENSE CAMBRIA SAND

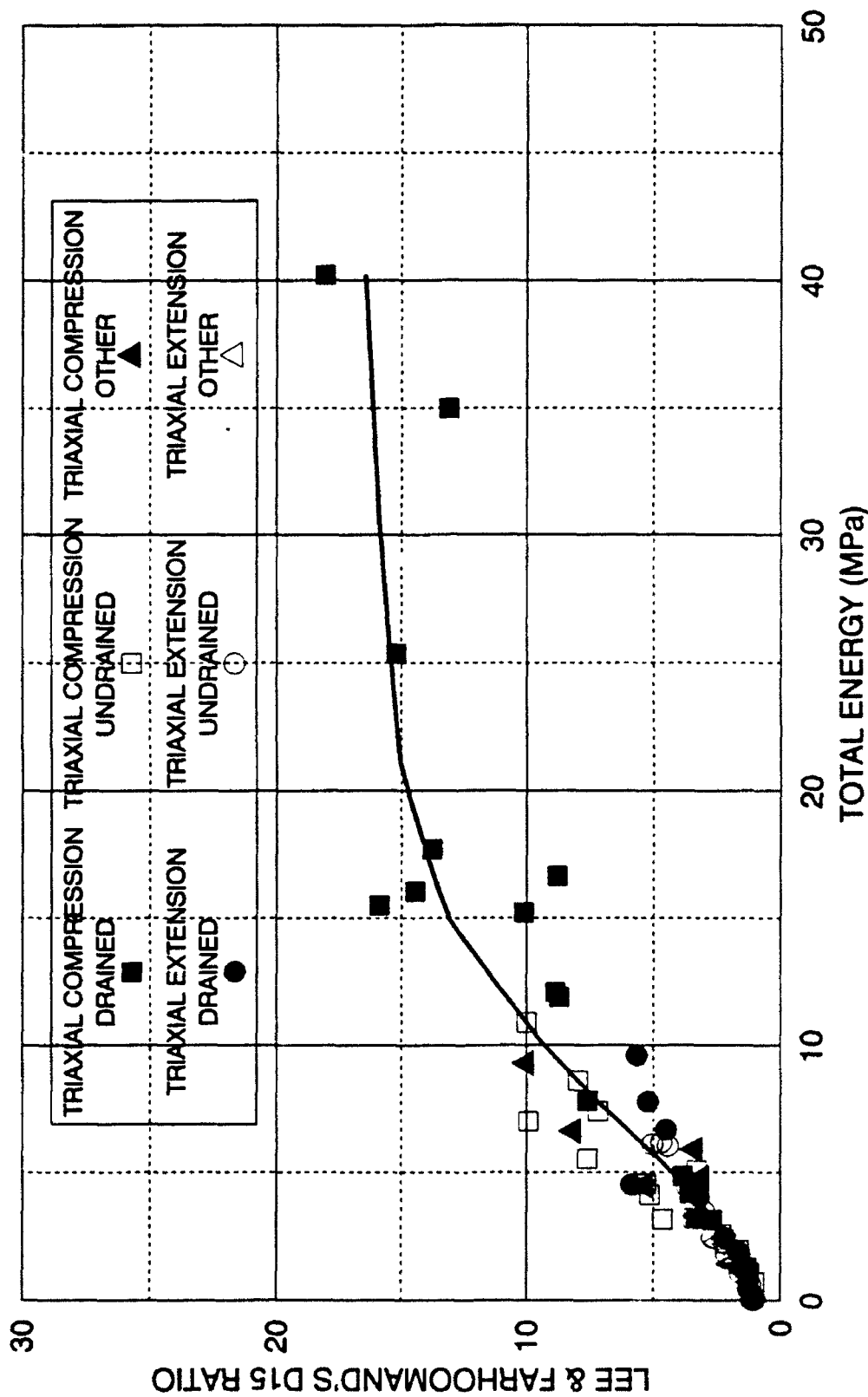


FIGURE 8-17 LEE & FARHOOMAND'S D15 RATIO BREAKAGE FACTOR, RELATED TO ENERGY  
DRAINED AND UNDRAINED TRIAXIAL COMPRESSION AND EXTENSION TESTS  
DENSE CAMBRIA SAND

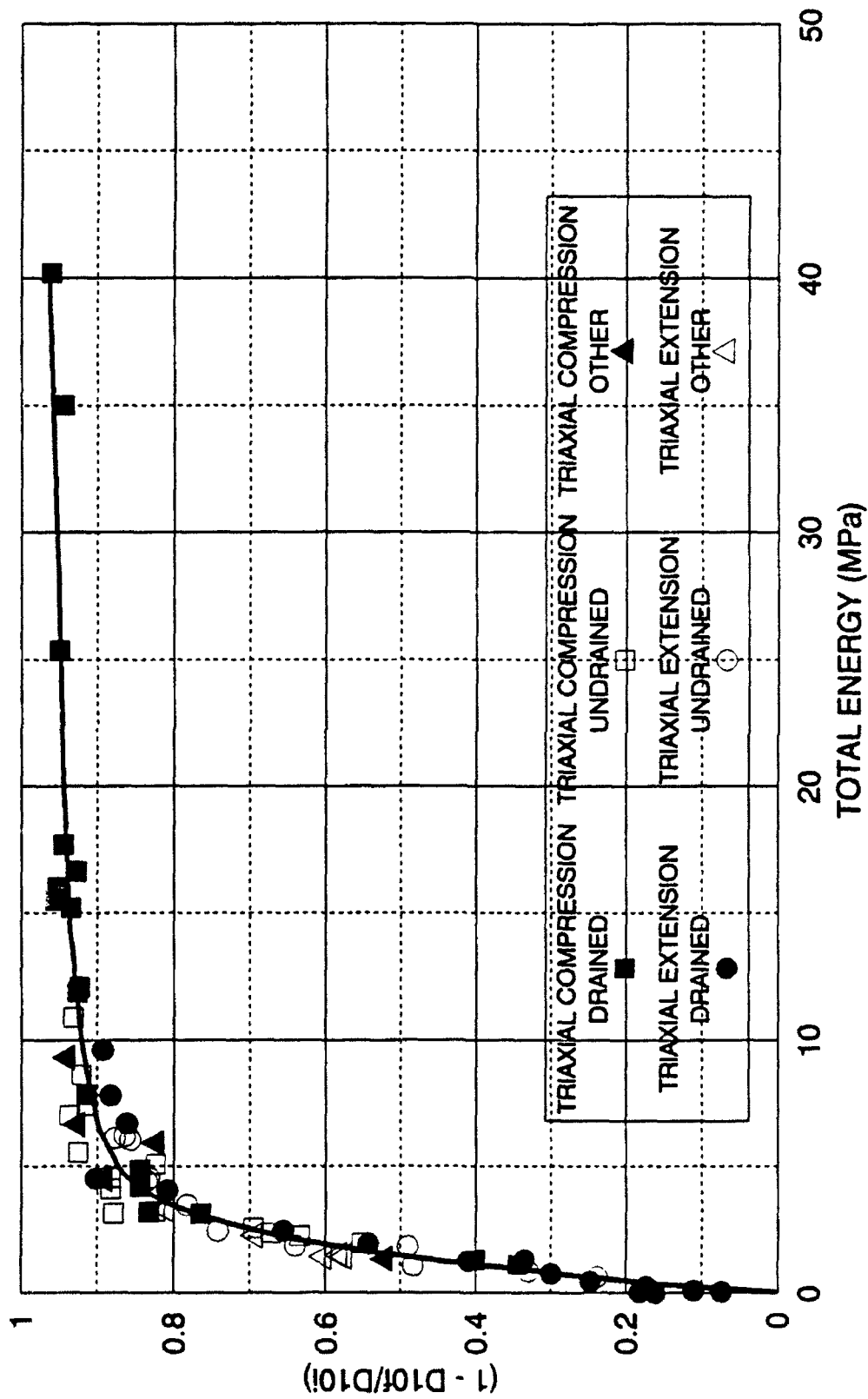


FIGURE 8-18  $B_{10} = (1 - D10f/D10i)$  BREAKAGE FACTOR RELATED TO ENERGY  
DRAINED AND UNDRAINED TRIAXIAL COMPRESSION AND EXTENSION TESTS  
DENSE CAMBRIA SAND

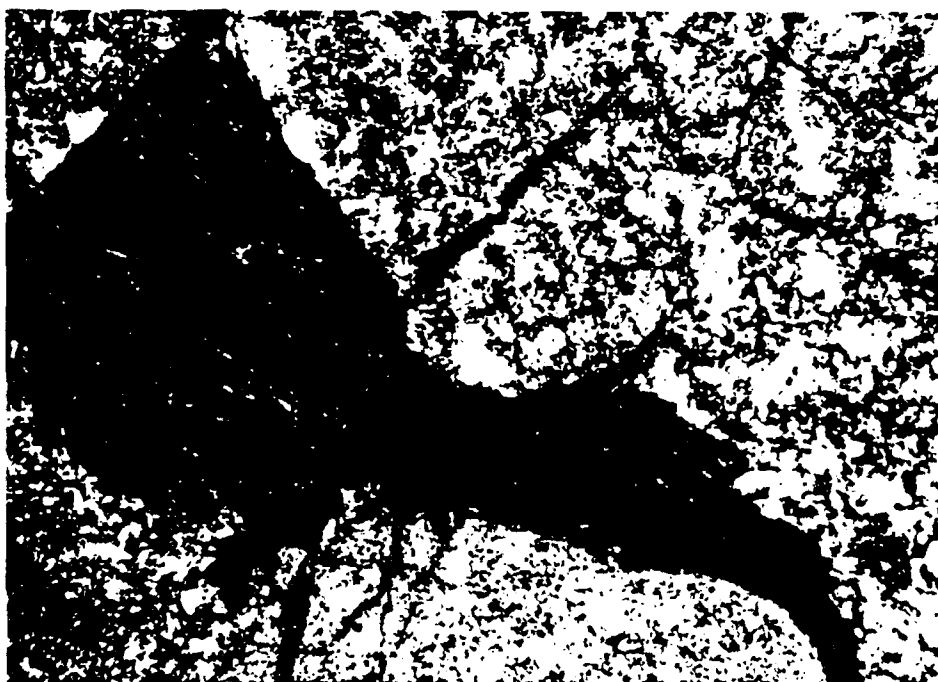
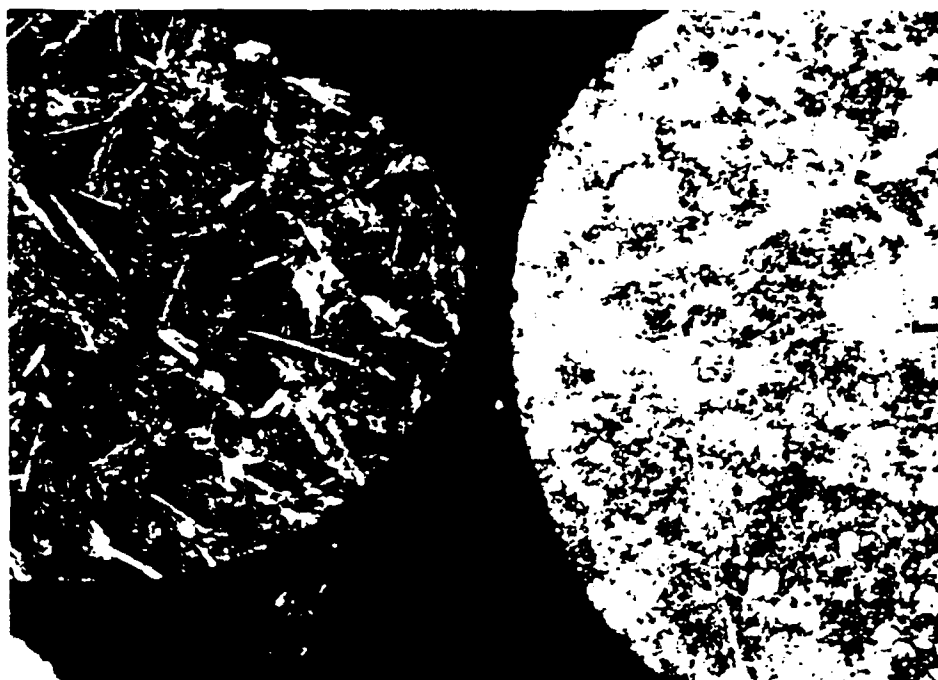


Figure 8-19 Photographs of Thin Sections of Cambria Sand  
before and after Shearing.

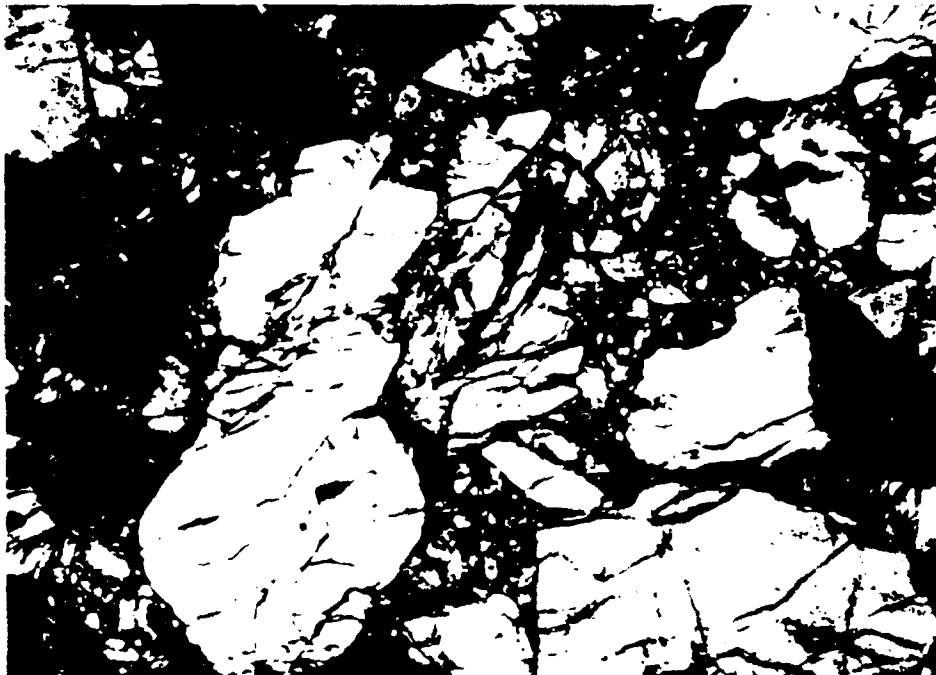


Figure 8-20 Photographs of Thin Sections of Quartz Sand  
before and after Shearing.

which is composed of grains of different hardnesses, experienced softer grains squeezing plastically between the harder grains. The quartz sand, whose grains are of more uniform hardness, experienced grain fracturing and rearranging. However, either can be treated using the total energy input as a unifying parameter.

A new particle breakage factor  $B_{10}$  was proposed, which facilitates the prediction of permeability based upon Hazen's permeability equation. When correlated with total input energy (Figure 8-21), this new breakage factor, which is based on the  $D_{10}$  particle grain size, was designed to be easily represented by a hyperbolic curve fit through its crushing curve. With this new particle breakage factor, it is possible to predict permeability based upon input energy into the soil. This proposed method is potentially useful in prediction of variations in permeability in earth dams or other geotechnical structures in which particle crushing occurs. Using a hyperbolic curve fit, it is also possible to predict some types of grain size distributions (Figure 8-23) after shearing and crushing.

Extension tests that exhibited strain localization were analyzed for total input energy and particle breakage factors were estimated from grain size distribution curves to ascertain the effect of strain localization on particle crushing. The input energy computations were made on the basis of stresses and strains calculated assuming uniform strain conditions. It was determined that tests exhibiting strain localization had lower values of particle breakage than uniform strain tests (Figures 8-24 through 8-27).

#### One-Dimensional Compression Tests and Elastic Parameters (Chapter 9)

A high pressure one-dimensional compression testing apparatus was designed and fabricated (Figure 9-1 through 9-3) to test soil up to 900 MPa axial stress magnitudes. The soil containment cell was instrumented with strain gages to infer internal lateral normal soil stresses.

High pressure one-dimensional compression tests on Cambria sand, quartz sand, and

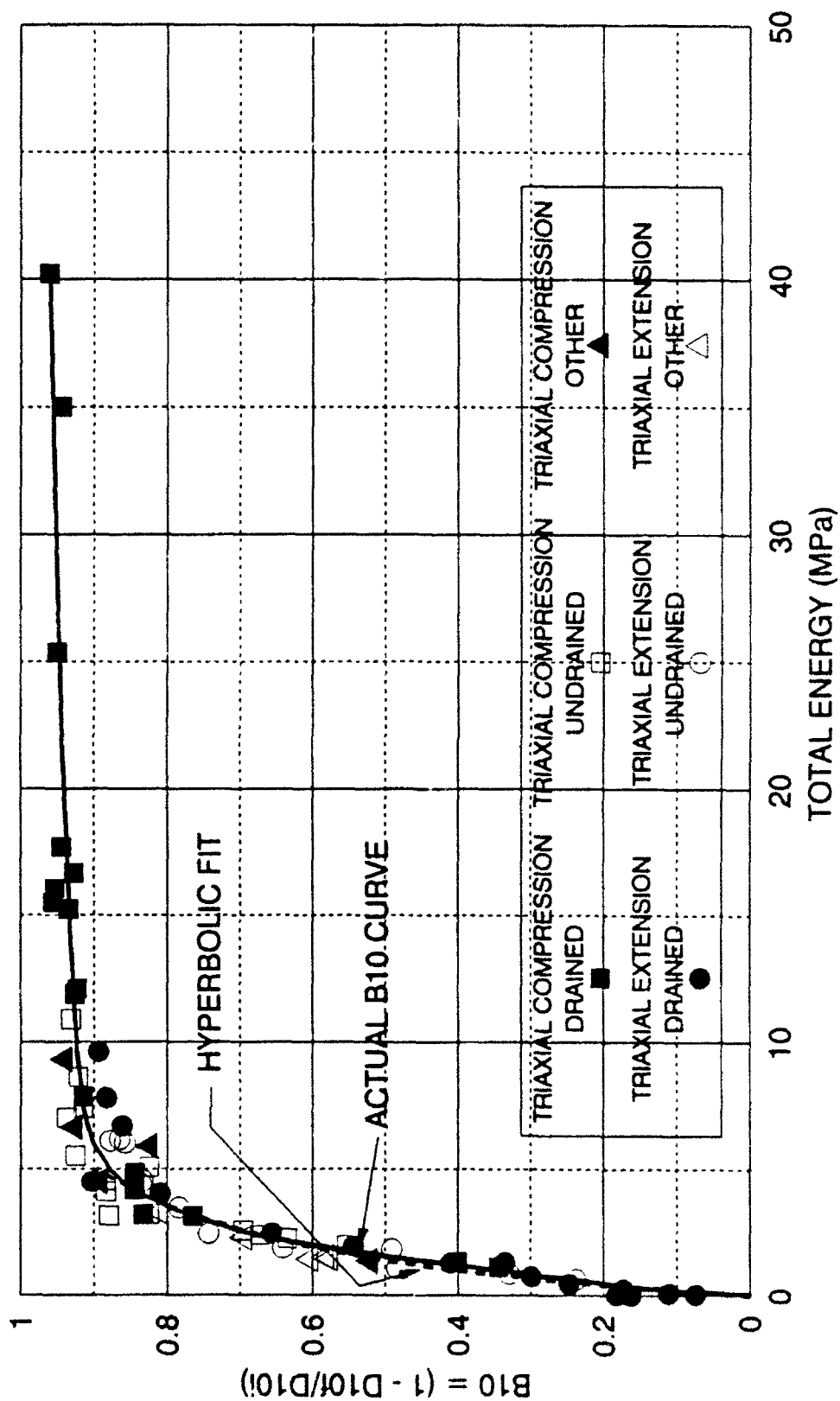


FIGURE 8-21 ACTUAL B10 CRUSHING CURVE WITH HYPERBOLIC FIT  
DRAINED AND UNDRAINED TRIAXIAL COMPRESSION AND EXTENSION TESTS  
DENSE CAMBRIA SAND

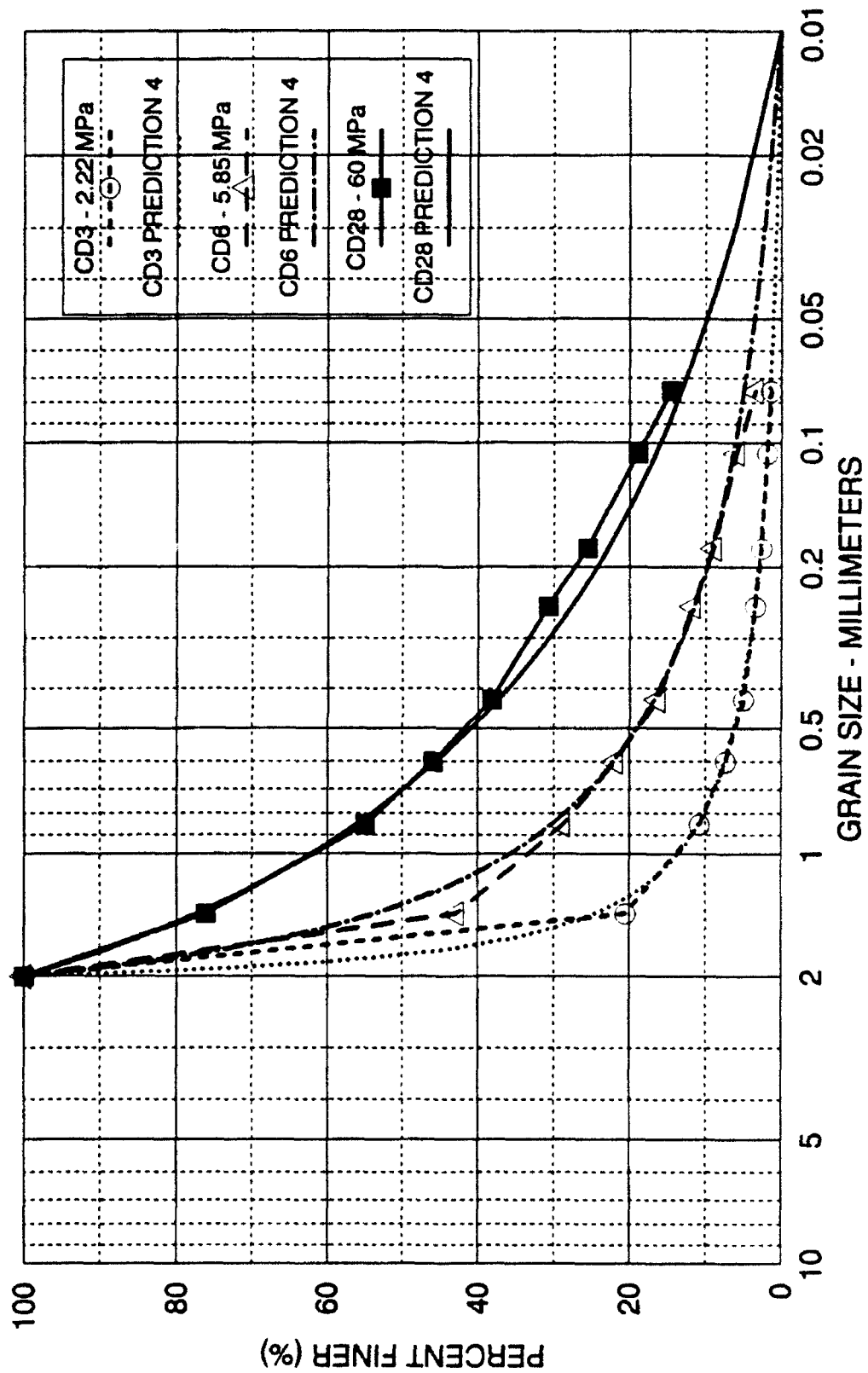


FIGURE 8-23 GRAIN SIZE CURVES AND HYPERBOLIC MODELLED PREDICTIONS  
FOR SOME DRAINED TRIAXIAL COMPRESSION TESTS  
DENSE CAMBRIA SAND

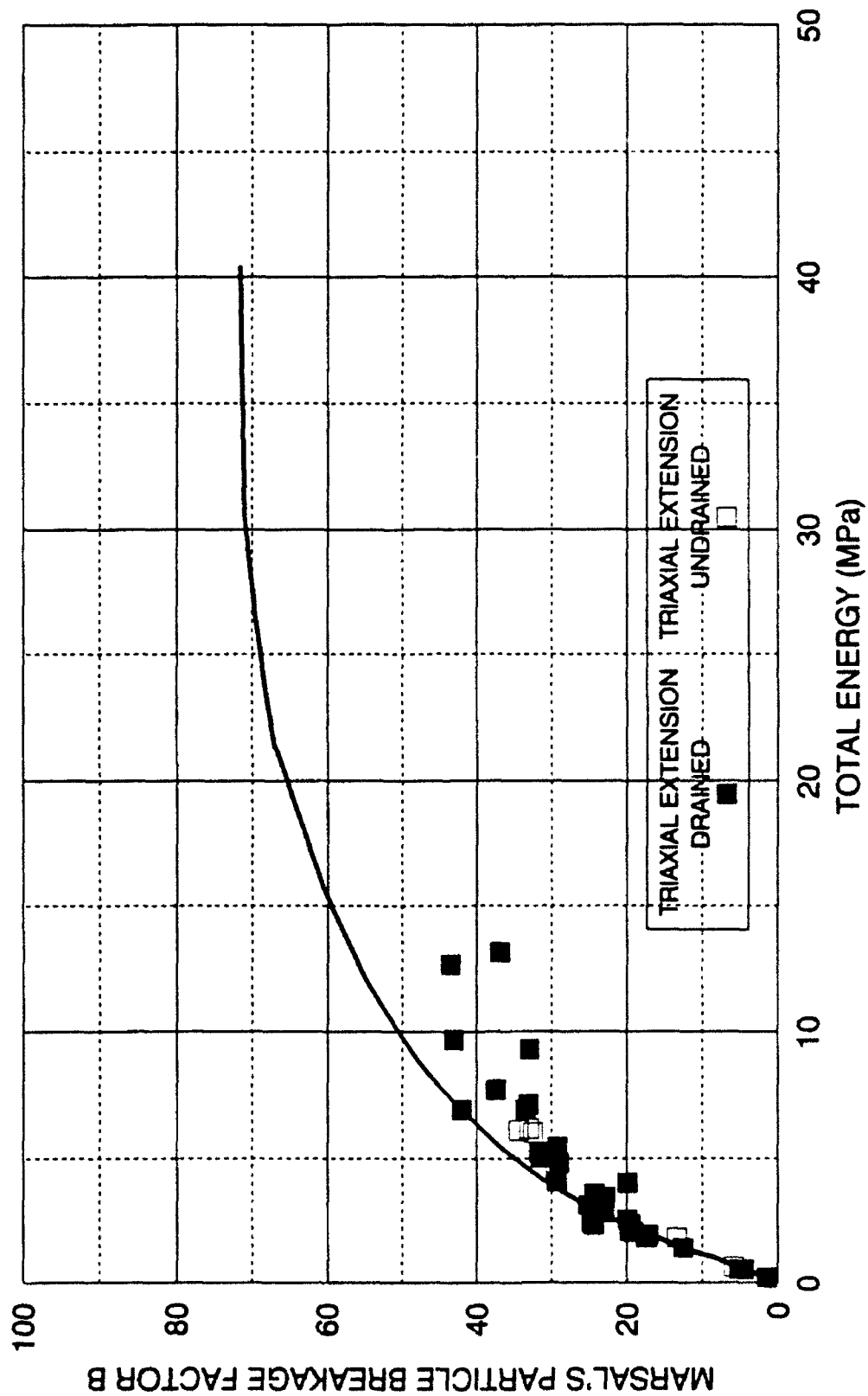


FIGURE 8-24 MARSAL'S BREAKAGE FACTOR B  
EFFECT OF STRAIN LOCALIZATION ON CRUSHING CURVE  
EXTENSION TESTS ON DENSE CAMBRIA SAND

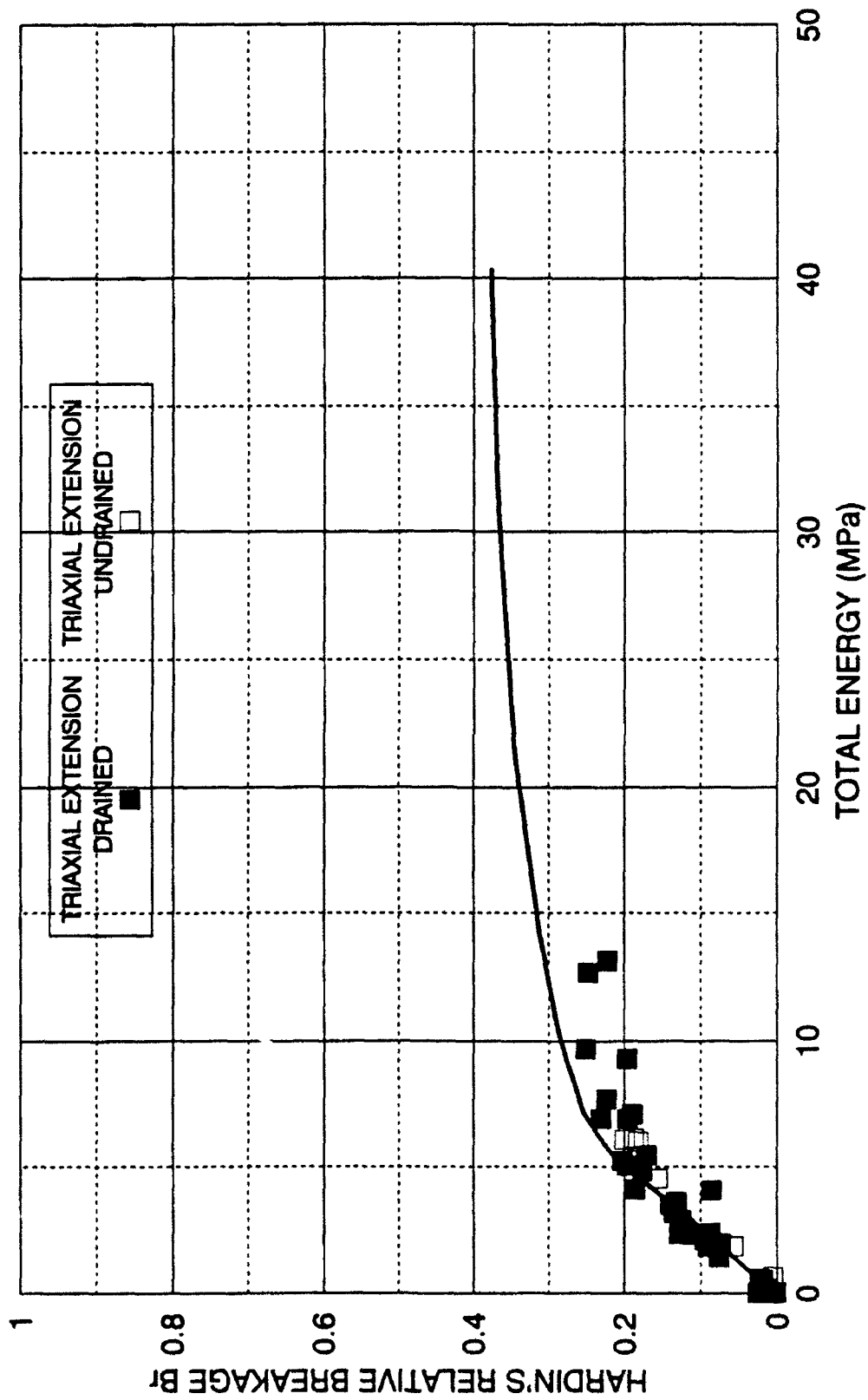


FIGURE 8-25 HARDIN'S RELATIVE BREAKAGE FACTOR  $B_r$   
EFFECT OF STRAIN LOCALIZATION ON CRUSHING CURVE  
EXTENSION TESTS ON DENSE CAMBRIA SAND

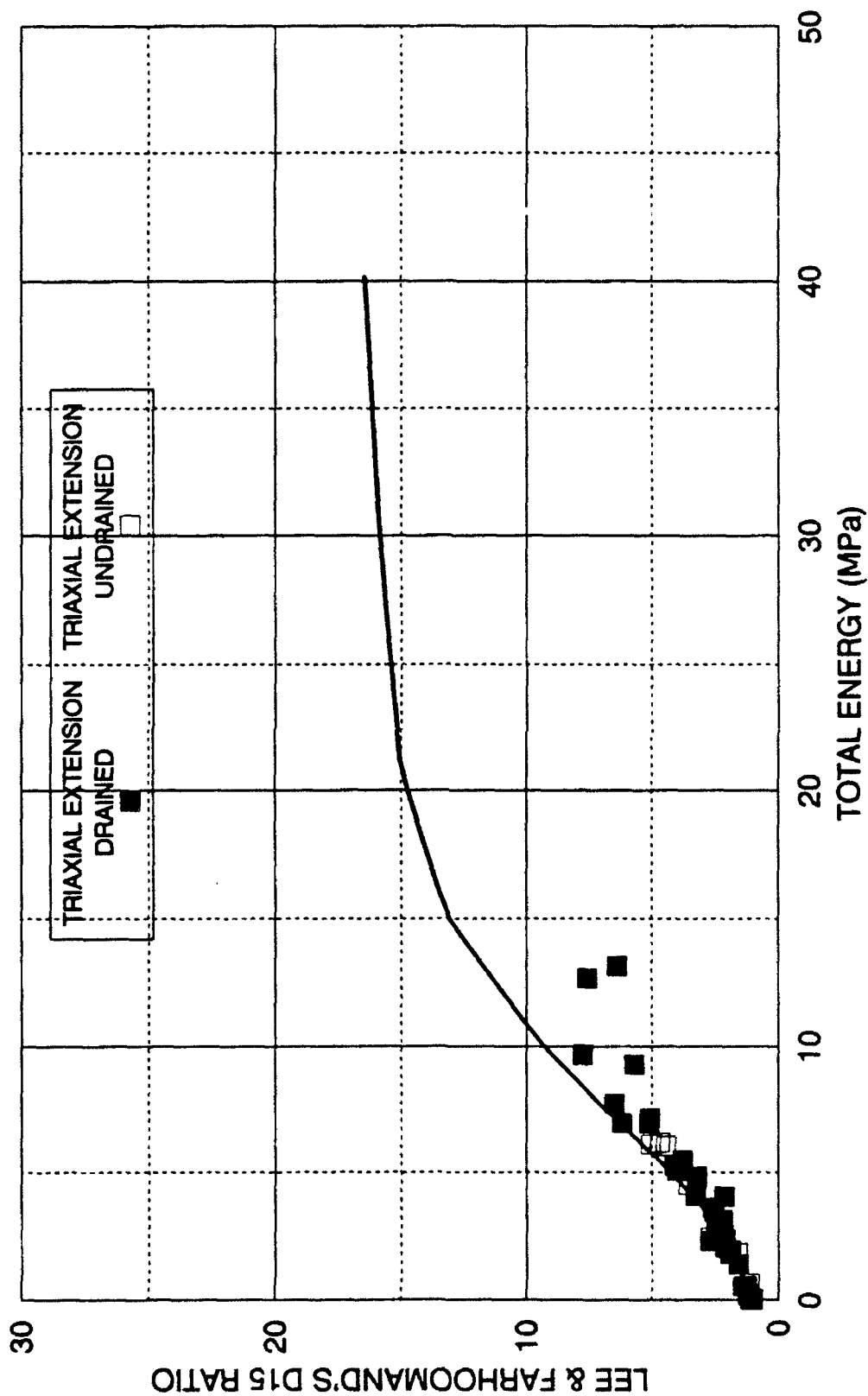


FIGURE 8-26 LEE & FARHOUMAND'S D15 RATIO BREAKAGE FACTOR  
EFFECT OF STRAIN LOCALIZATION ON CRUSHING CURVE  
EXTENSION TESTS ON DENSE CAMBRIA SAND

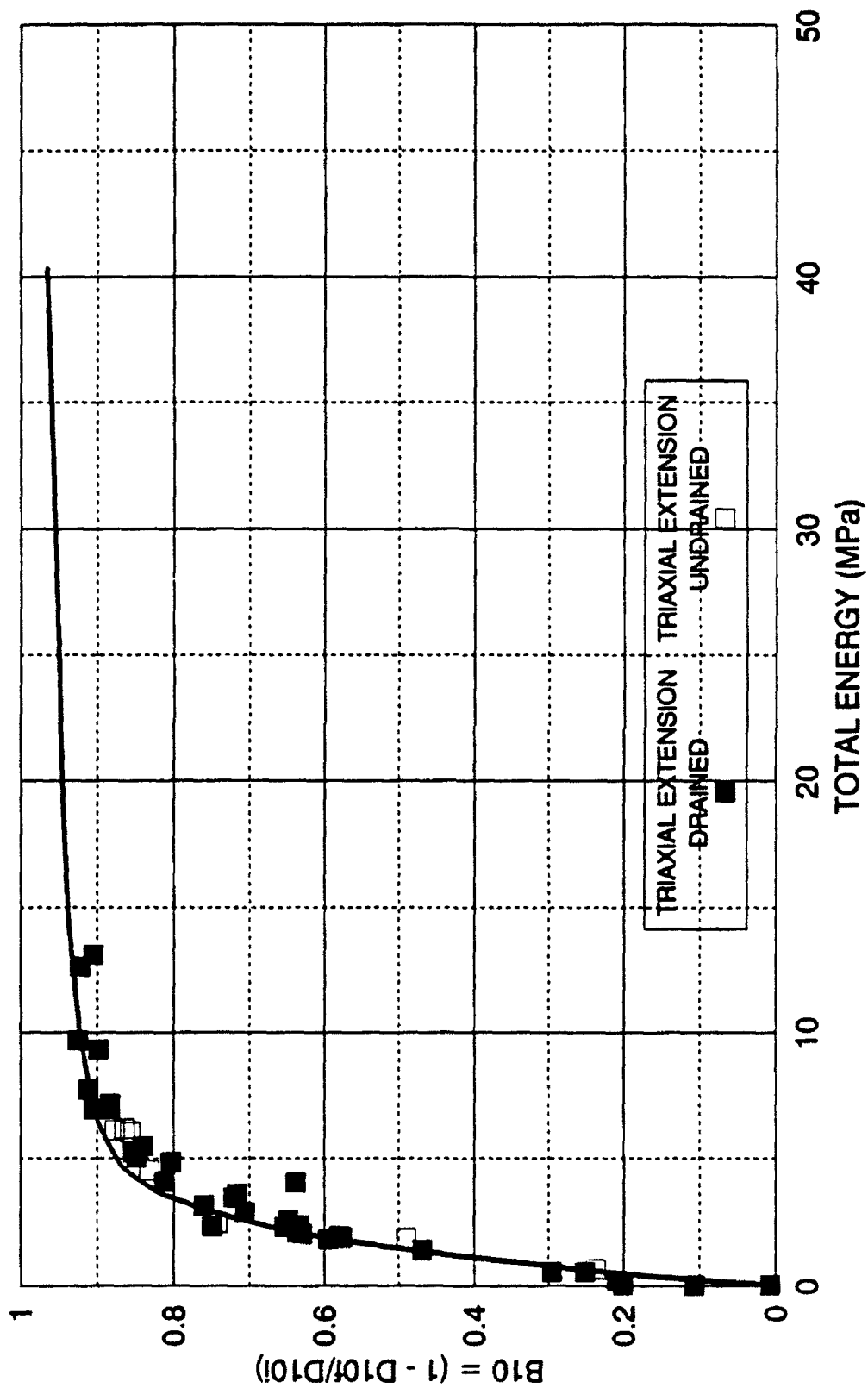
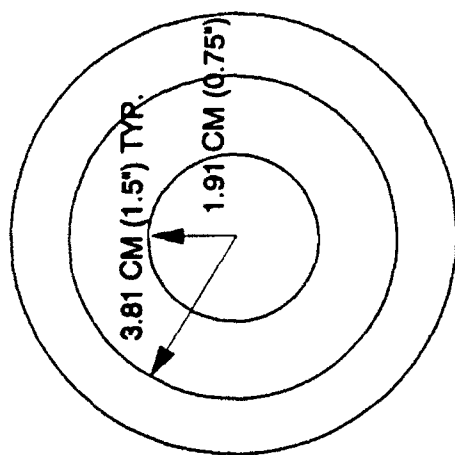
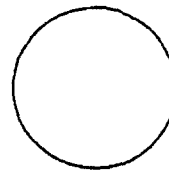


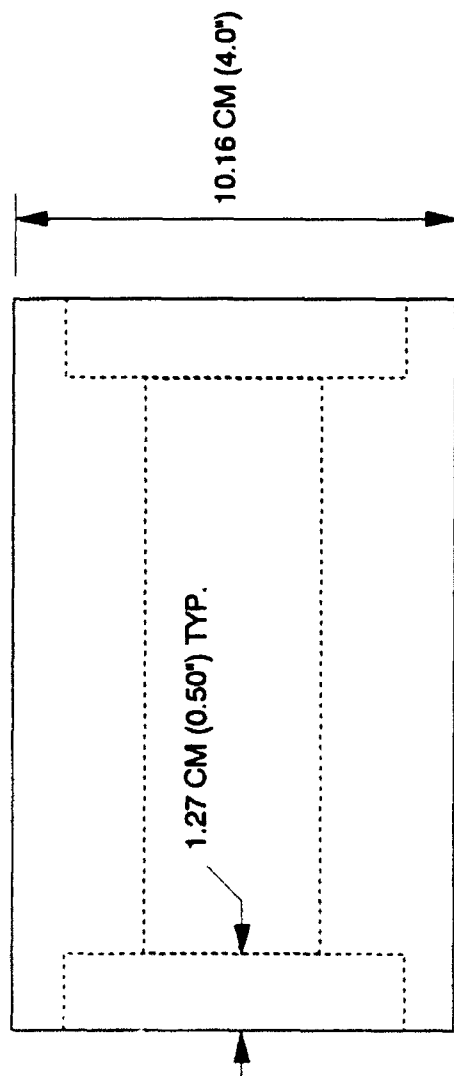
FIGURE 8-27 B10 BREAKAGE FACTOR  
EFFECT OF STRAIN LOCALIZATION ON CRUSHING CURVE  
EXTENSION TESTS ON DENSE CAMBRIA SAND



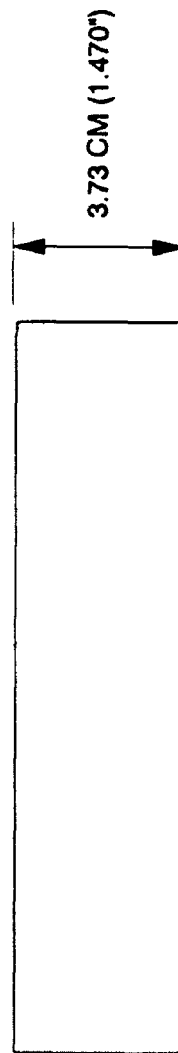
END VIEW



END VIEW



CELL



PISTON

FIGURE 9-1 SOIL CONTAINMENT CELL  
ONE-DIMENSIONAL COMPRESSION TESTS

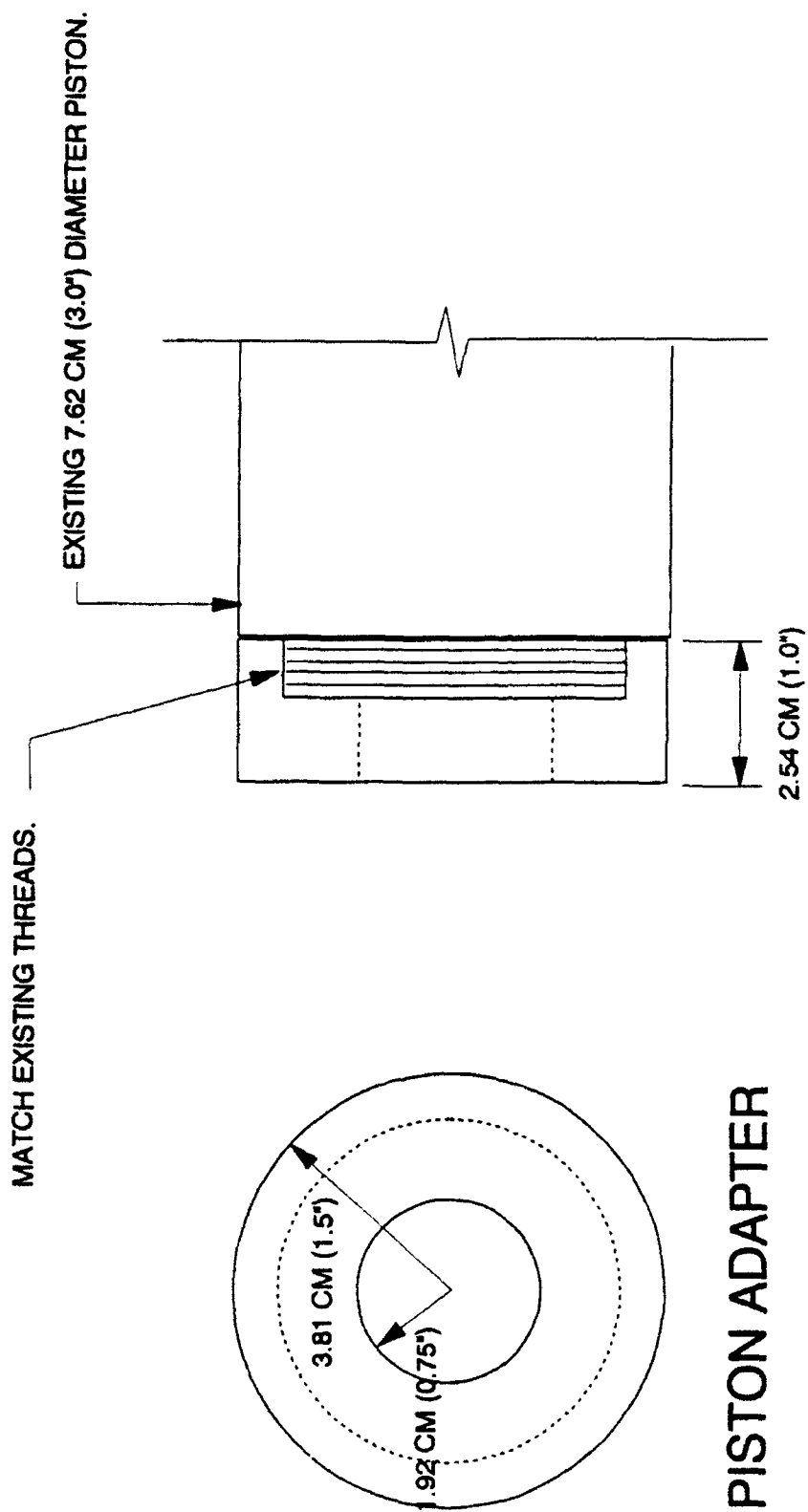
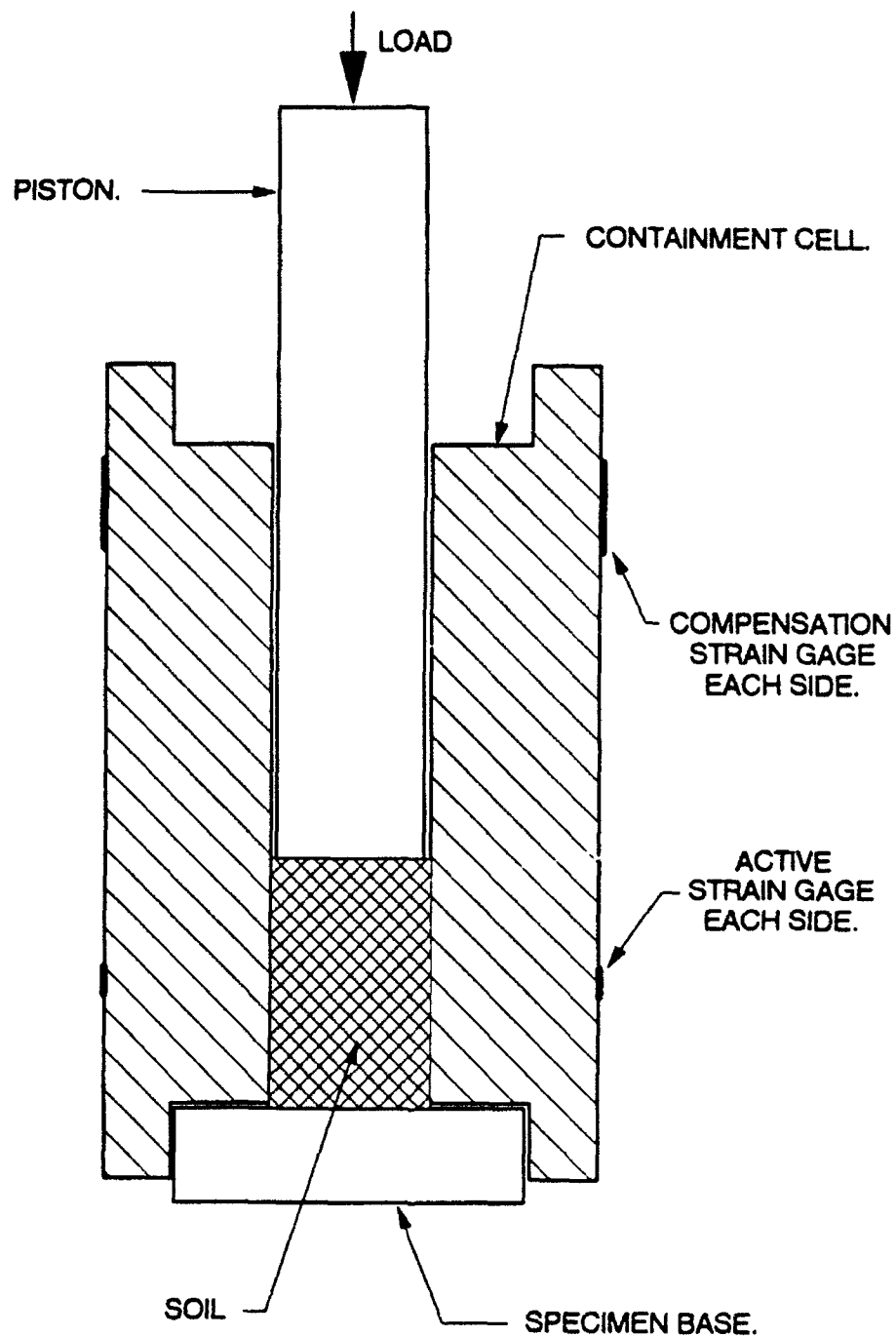


FIGURE 9-2 PISTON ADAPTER  
ONE-DIMENSIONAL COMPRESSION TESTS



### ONE-DIMENSIONAL TEST

NOT TO SCALE

FIGURE 9-3 ONE-DIMENSIONAL COMPRESSION TESTING SYSTEM  
ASSEMBLED APPARATUS, STRAIN GAGE LOCATIONS, AND SPECIMEN

Sacramento River sand were performed at different initial densities. Full-friction and reduced-friction tests were performed and friction was found to have only minor effects on the overall soil behavior. The effect of initial void ratio was seen to disappear at high stress magnitudes with initially loose sand eventually reaching the same density as initially dense sand (Figures 8 and 9-9).

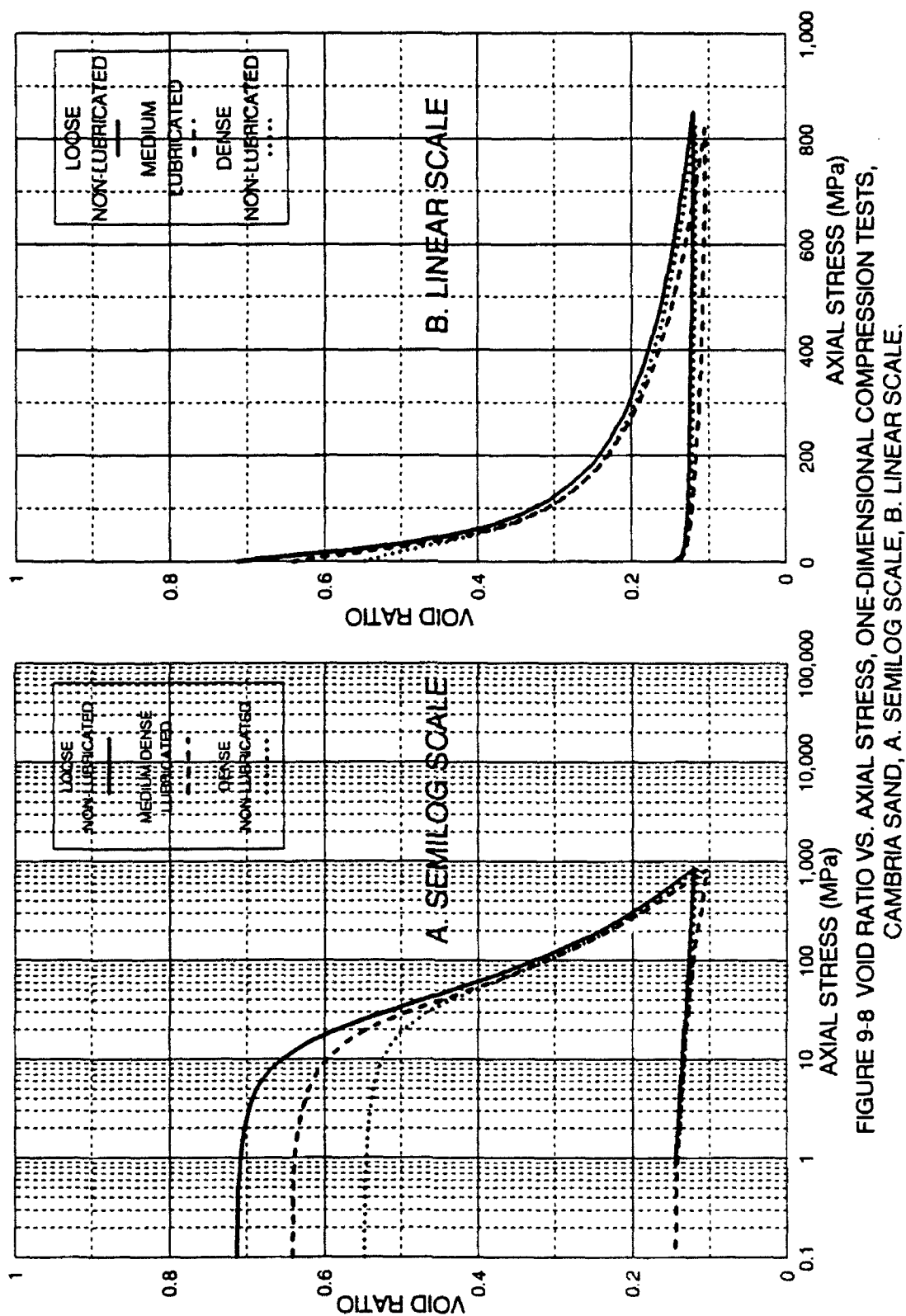
Thin sections were made from sheared specimens from the one-dimensional compression tests, after the specimens were extruded from the soil containment cell. The photographs of the thin sections appeared very similar to those made from high pressure triaxial compression tests (Figures 9-11 and 9-12).

An elastic numerical analysis was performed so that measured strains on the soil containment cell could be converted into appropriate values of internal lateral normal soil stresses. Thus  $K_0$  could be estimated at high pressures. It was found that  $K_0$  decreased from low pressures to constant values at high pressures that ranged between 0.37 and 0.40 for the three sands tested (Figures 9-14 through 9-16). Jaky's equation for  $K_0$  appears valid at low pressures, but does not appear to be correct at high pressures. As the void ratio decreases under increasing axial stress, the relative positions of  $K_0$  curves from different initial densities indicate that looser soils have lower values of  $K_0$  than denser soils (Figures 9-20 and 9-21).

A special loading-unloading-reloading-unloading drained triaxial compression test was performed at five different confining pressures to obtain the elastic modulus and Poisson's ratio over a wide confining pressure range (Figures 9-26 and 9-27). It was determined that the elastic modulus and Poisson's ratio of Cambria sand increased linearly with the logarithm of confining pressure.

#### General Soil Behavior at High Pressures (Chapter 10)

An attempt was made to correlate high pressure experimental results with commonly used



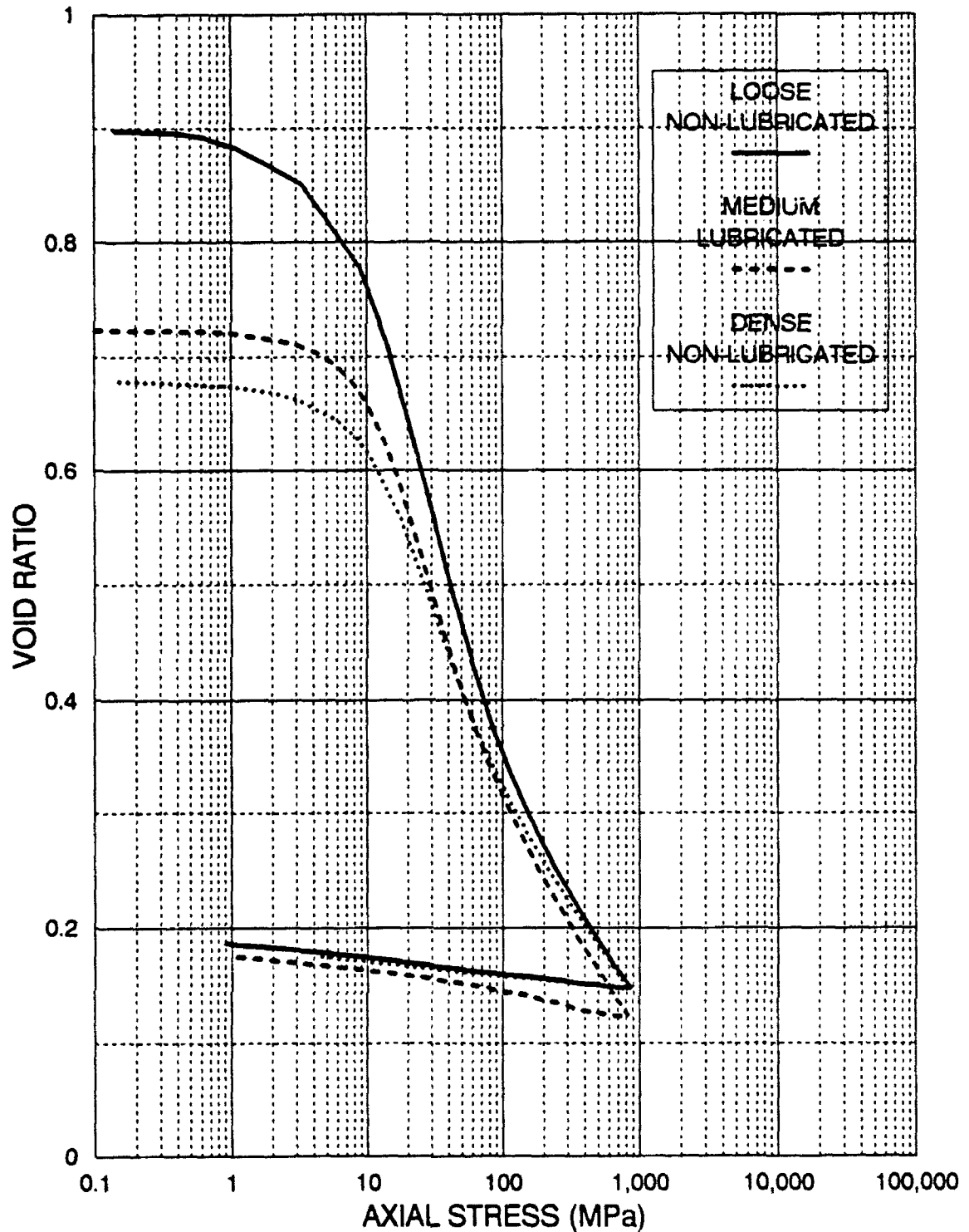


FIGURE 9-9 VOID RATIO VS. STRESS  
ONE-DIMENSIONAL COMPRESSION TEST  
QUARTZ SAND

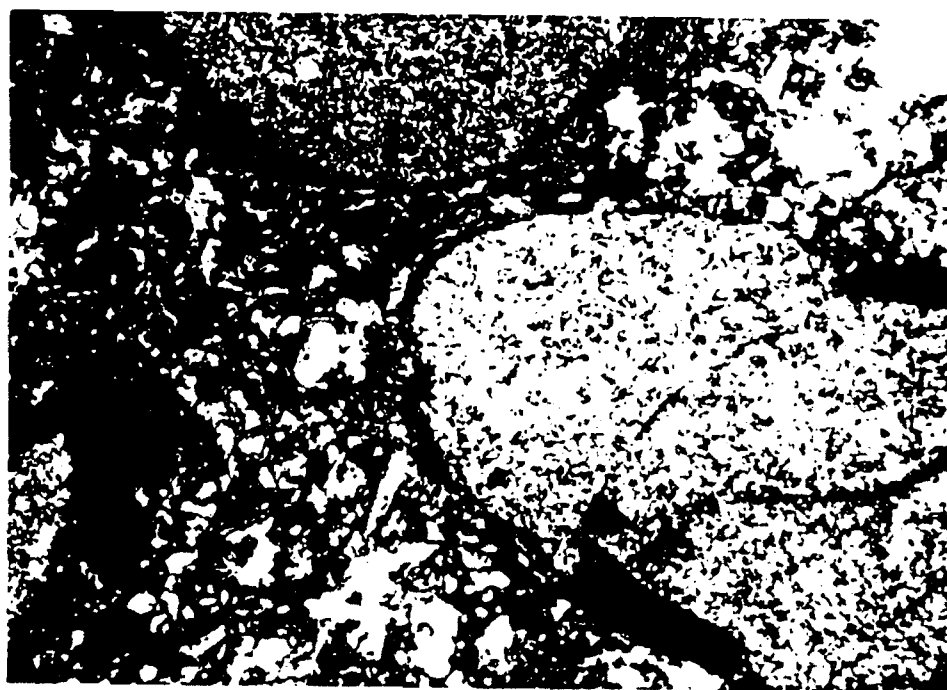
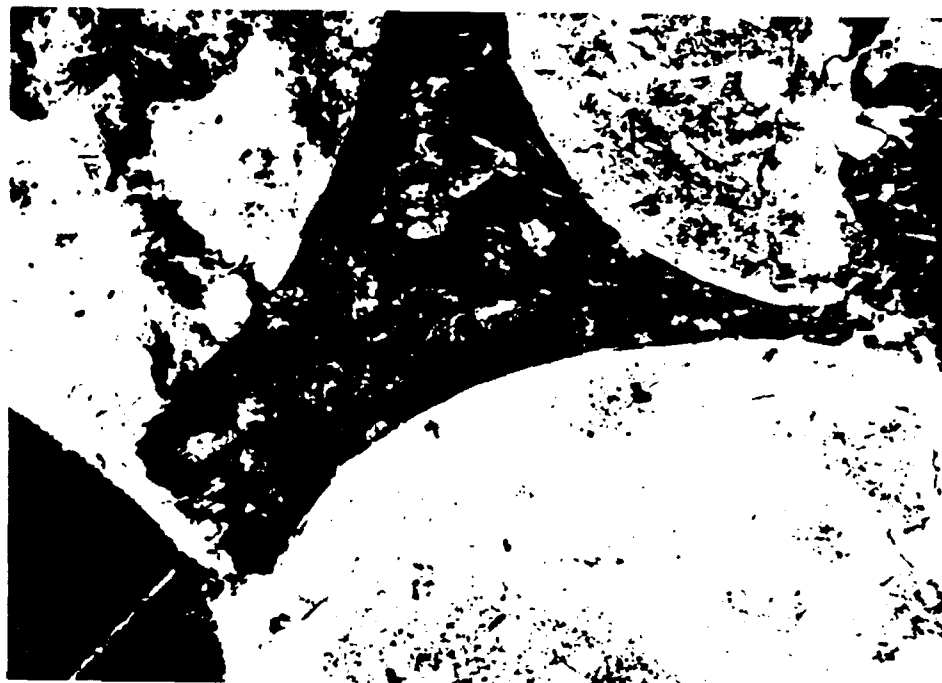


Figure 9-11 Photographs of Thin Section Showing Cambria Sand after Shearing, One-Dimensional Compression Test.

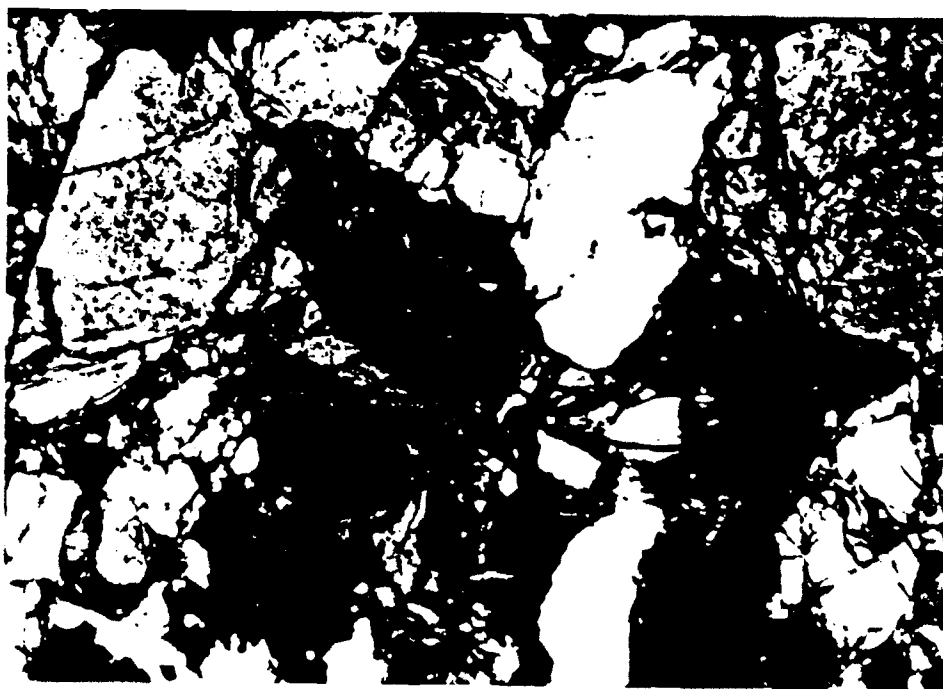
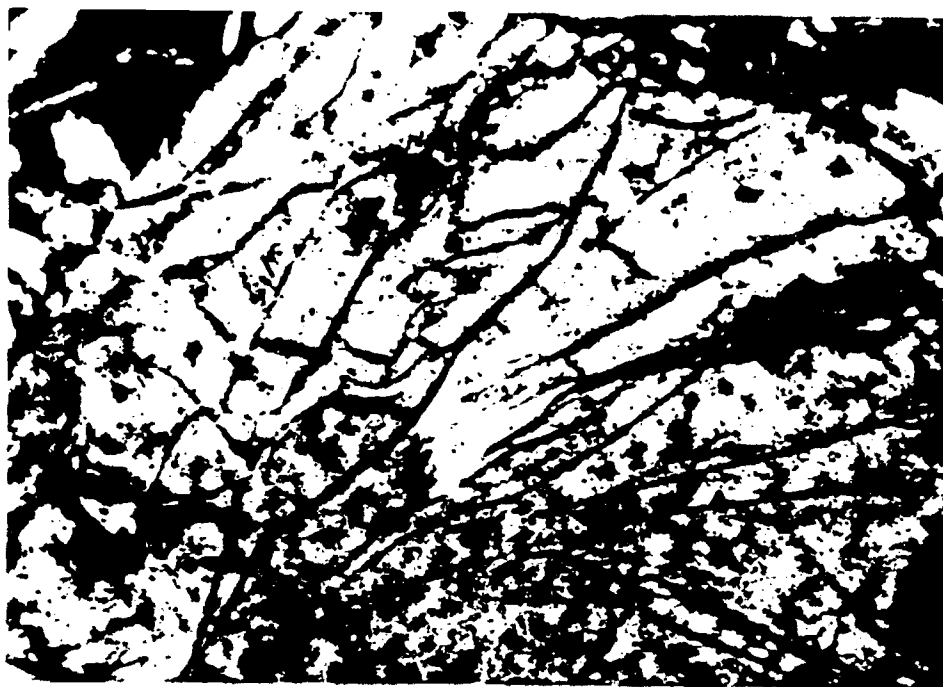


Figure 9-12 Photographs of Thin Section Showing Quartz Sand after Shearing, One-Dimensional Compression Test.

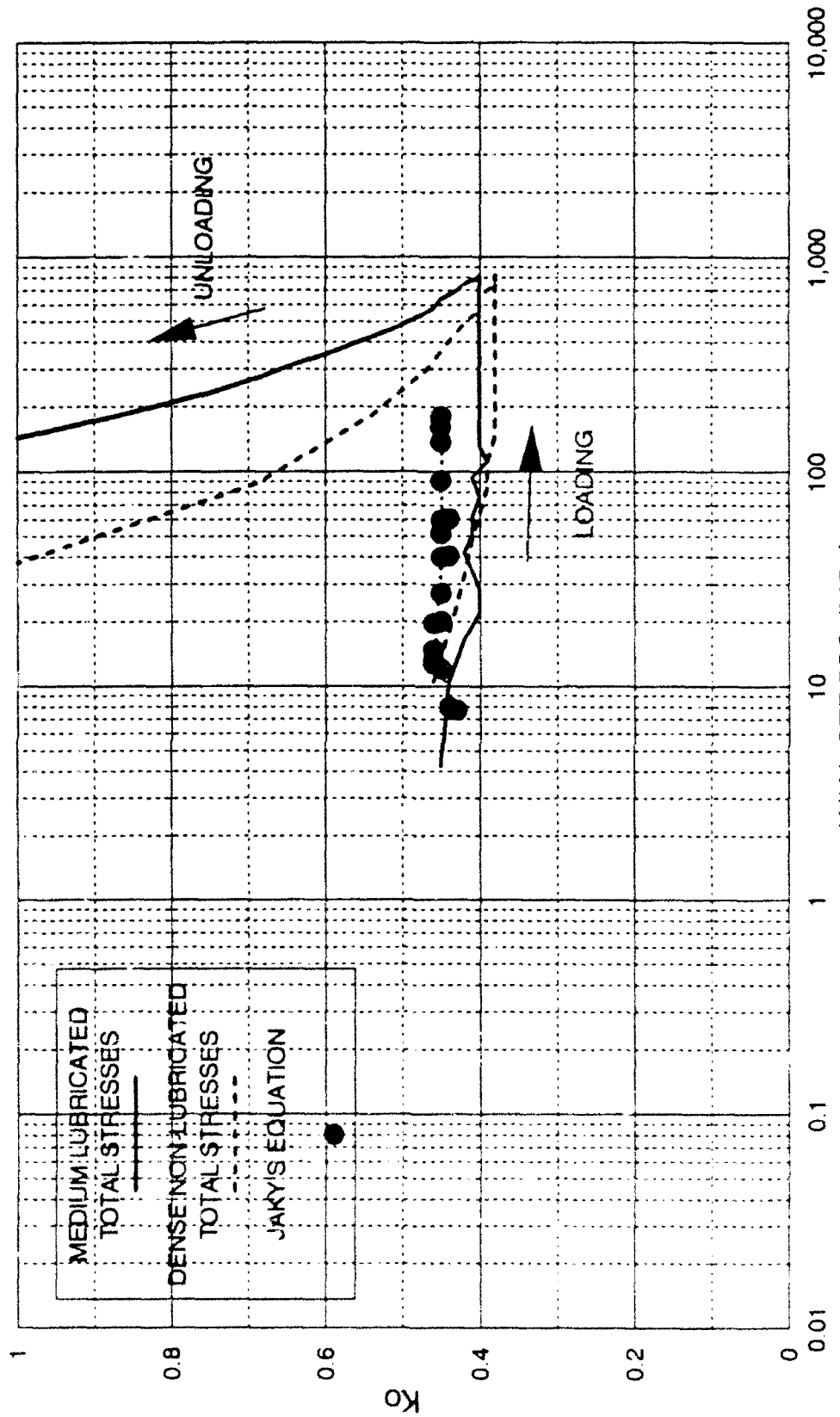
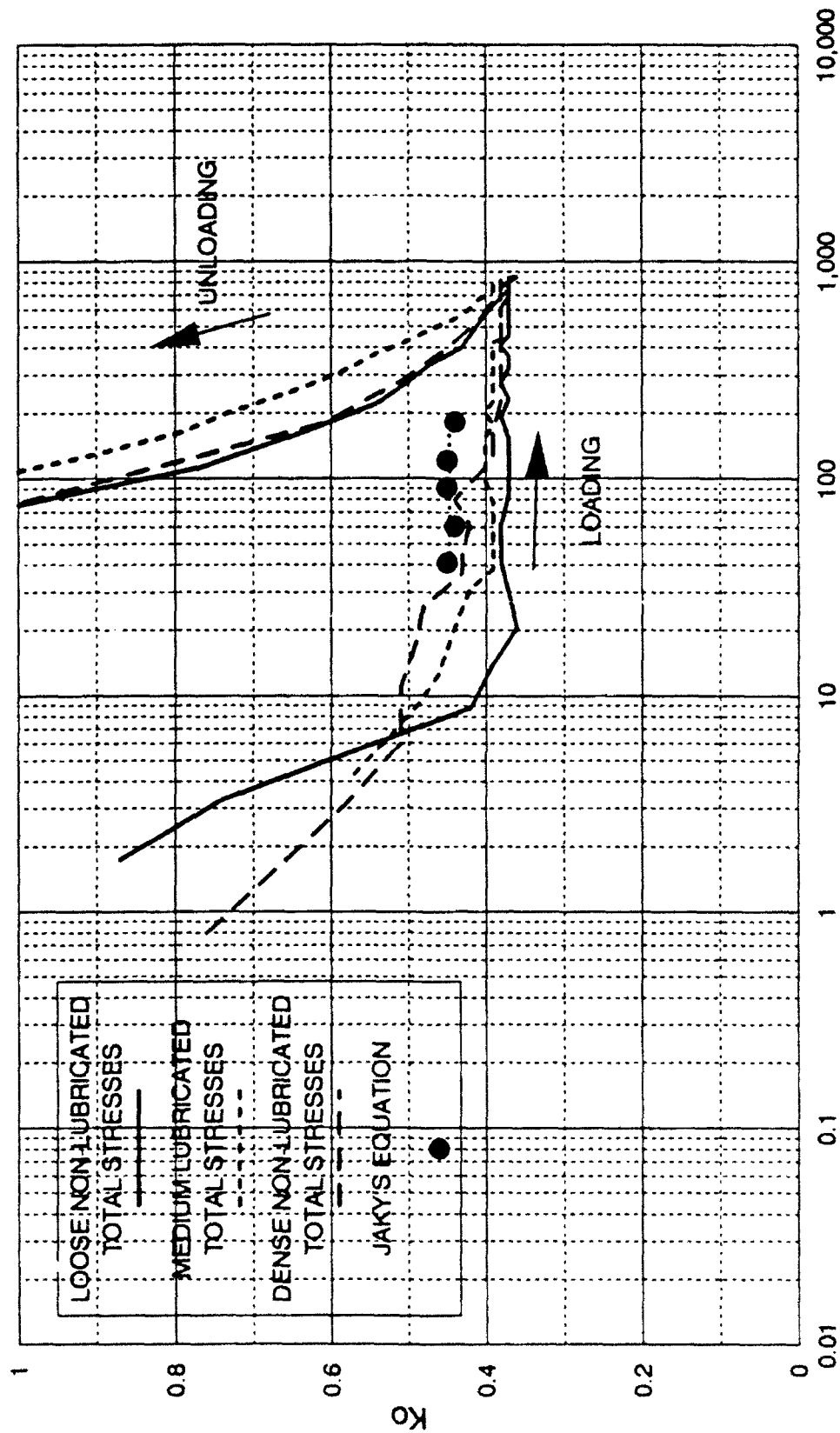


FIGURE 9-14 TOTAL STRESS  $K_0$  vs. AXIAL STRESS  
ONE-DIMENSIONAL AND TRIAXIAL COMPRESSION TESTS  
CAMBRIA SAND



AXIAL STRESS (MPa)

FIGURE 9-15 TOTAL STRESS  $K_0$  vs. AXIAL STRESS  
ONE-DIMENSIONAL AND TRIAXIAL COMPRESSION TESTS  
QUARTZ SAND

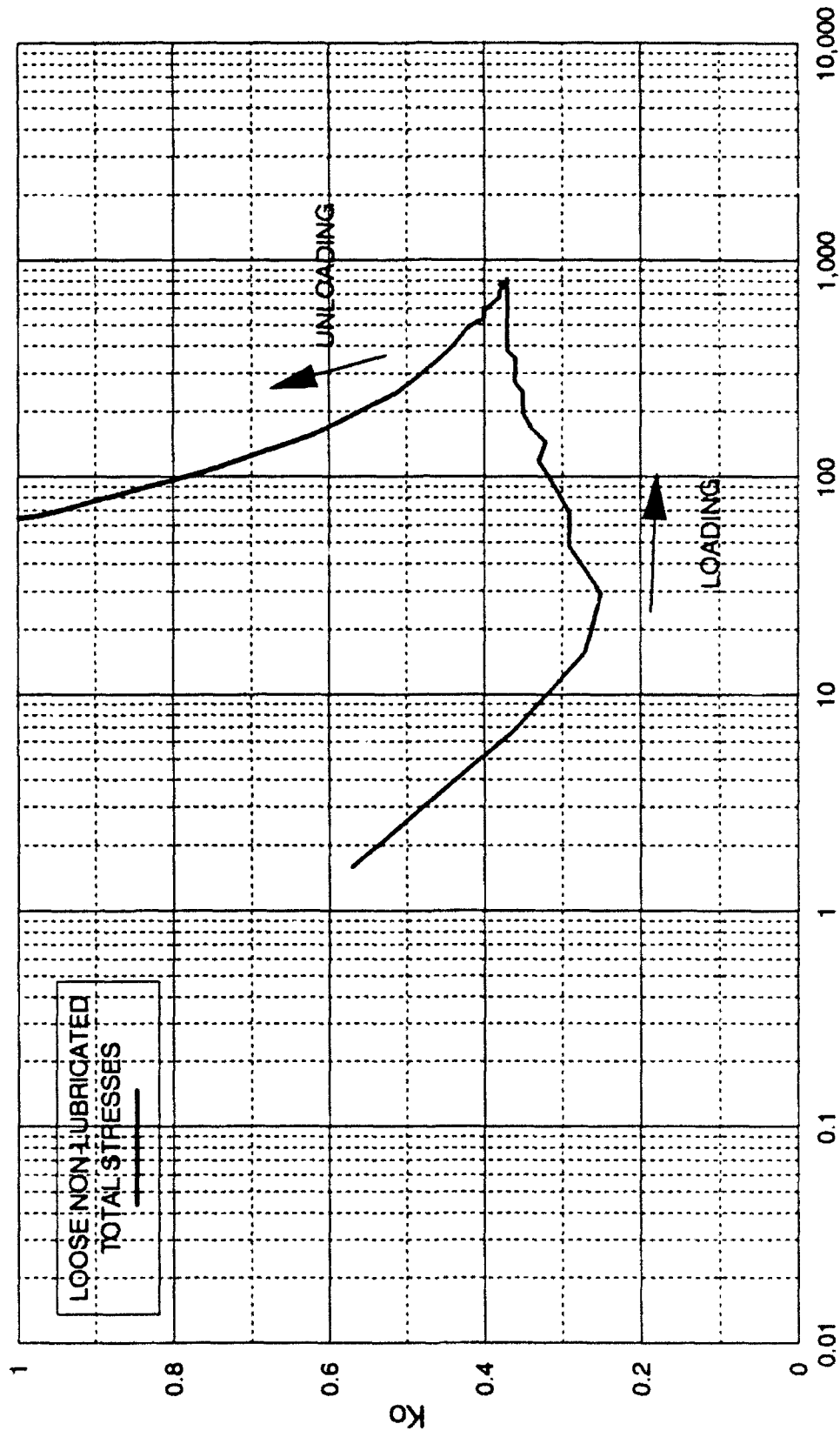


FIGURE 9-16 TOTAL STRESS  $K_0$  vs. AXIAL STRESS  
ONE-DIMENSIONAL COMPRESSION TESTS  
SACRAMENTO RIVER SAND

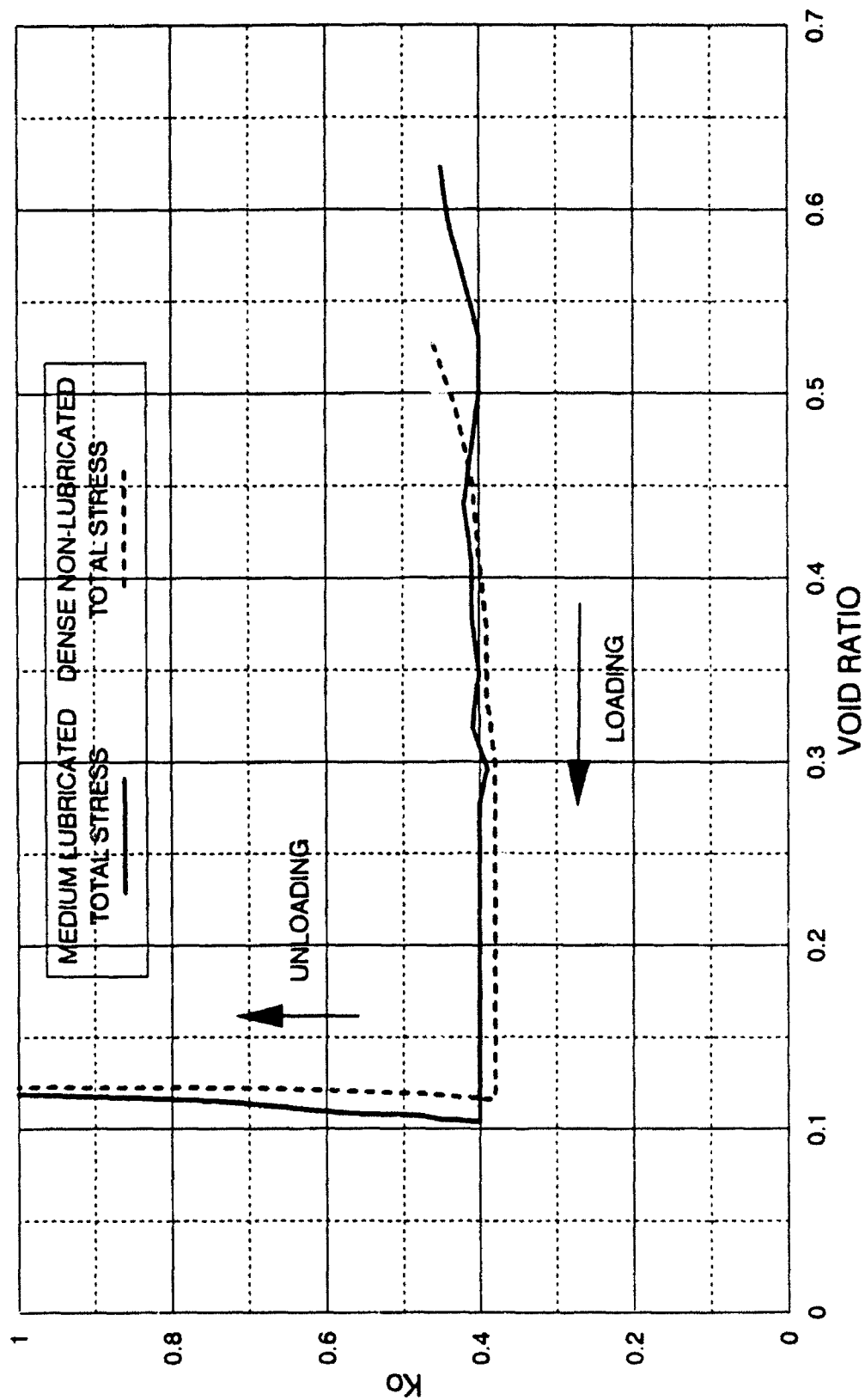


FIGURE 9-20 TOTAL STRESS  $K_0$  vs. VOID RATIO  
ONE-DIMENSIONAL COMPRESSION TESTS  
CAMBRIA SAND

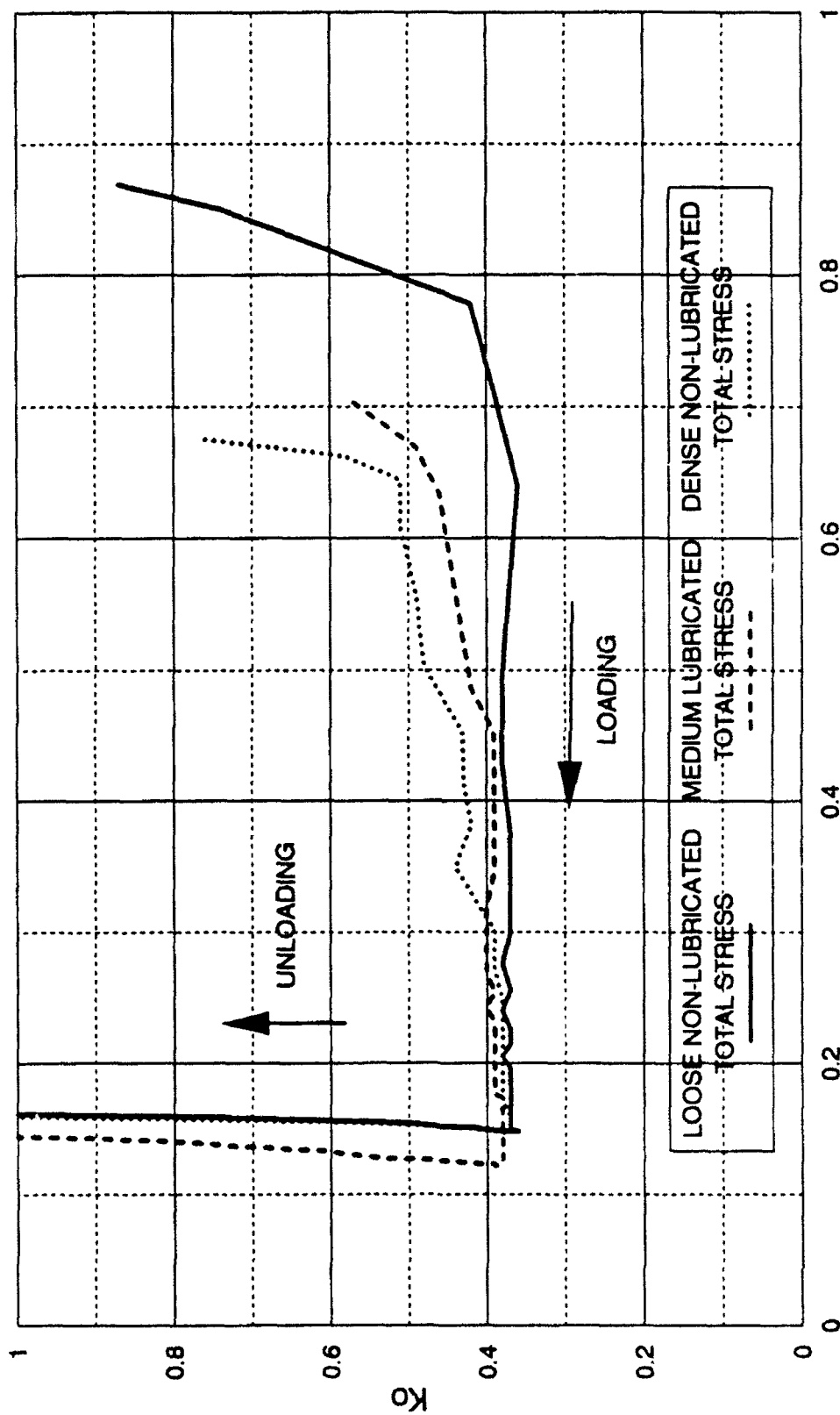


FIGURE 9-21 TOTAL STRESS  $K_0$  vs. VOID RATIO  
ONE-DIMENSIONAL COMPRESSION TESTS  
QUARTZ SAND

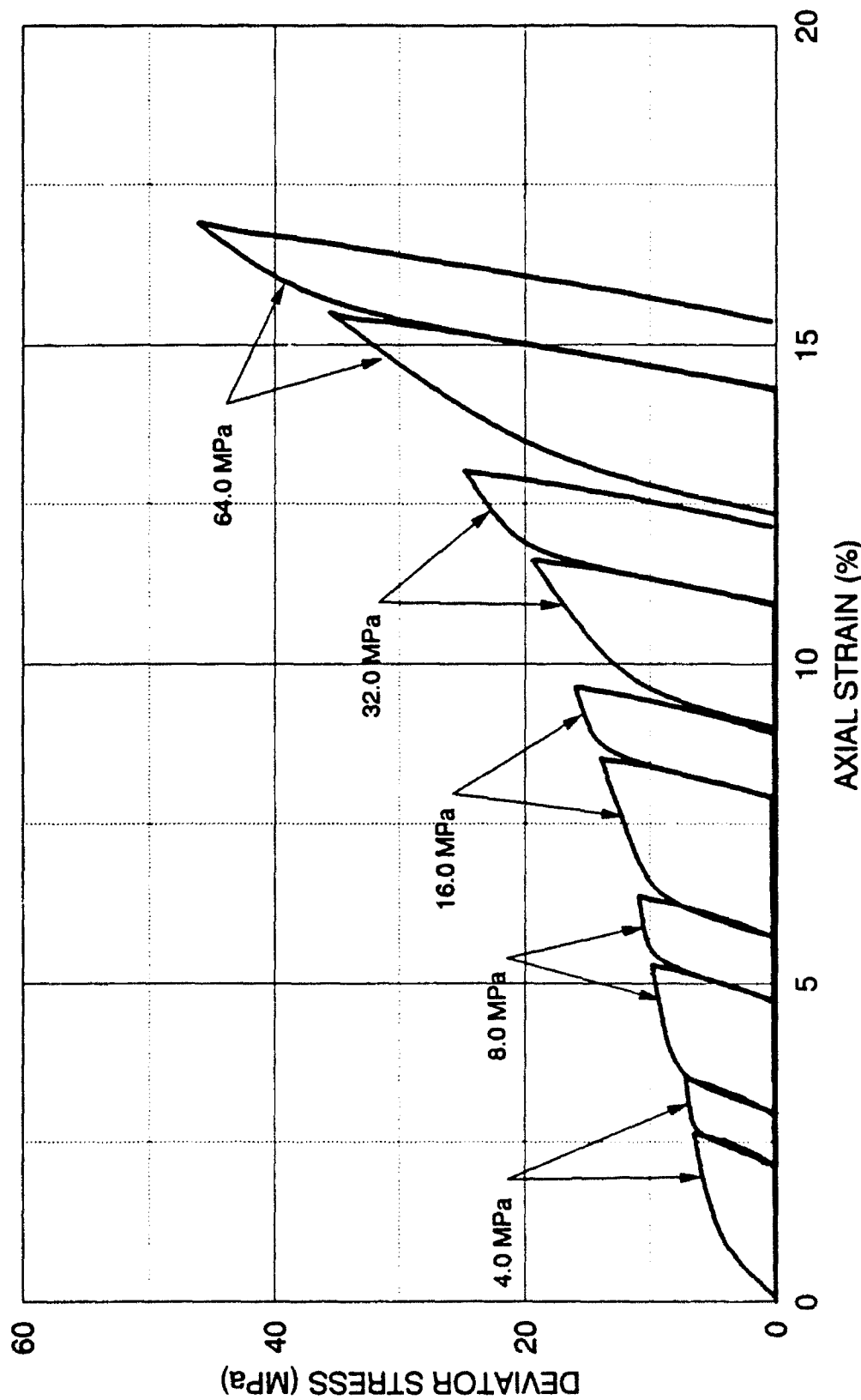


FIGURE 9-26 DEVIATOR STRESS vs. STRAIN  
LOADING-UNLOADING-RELOADING TEST FOR DETERMINATION OF ELASTIC PARAMETERS  
DENSE CAMBRIA SAND

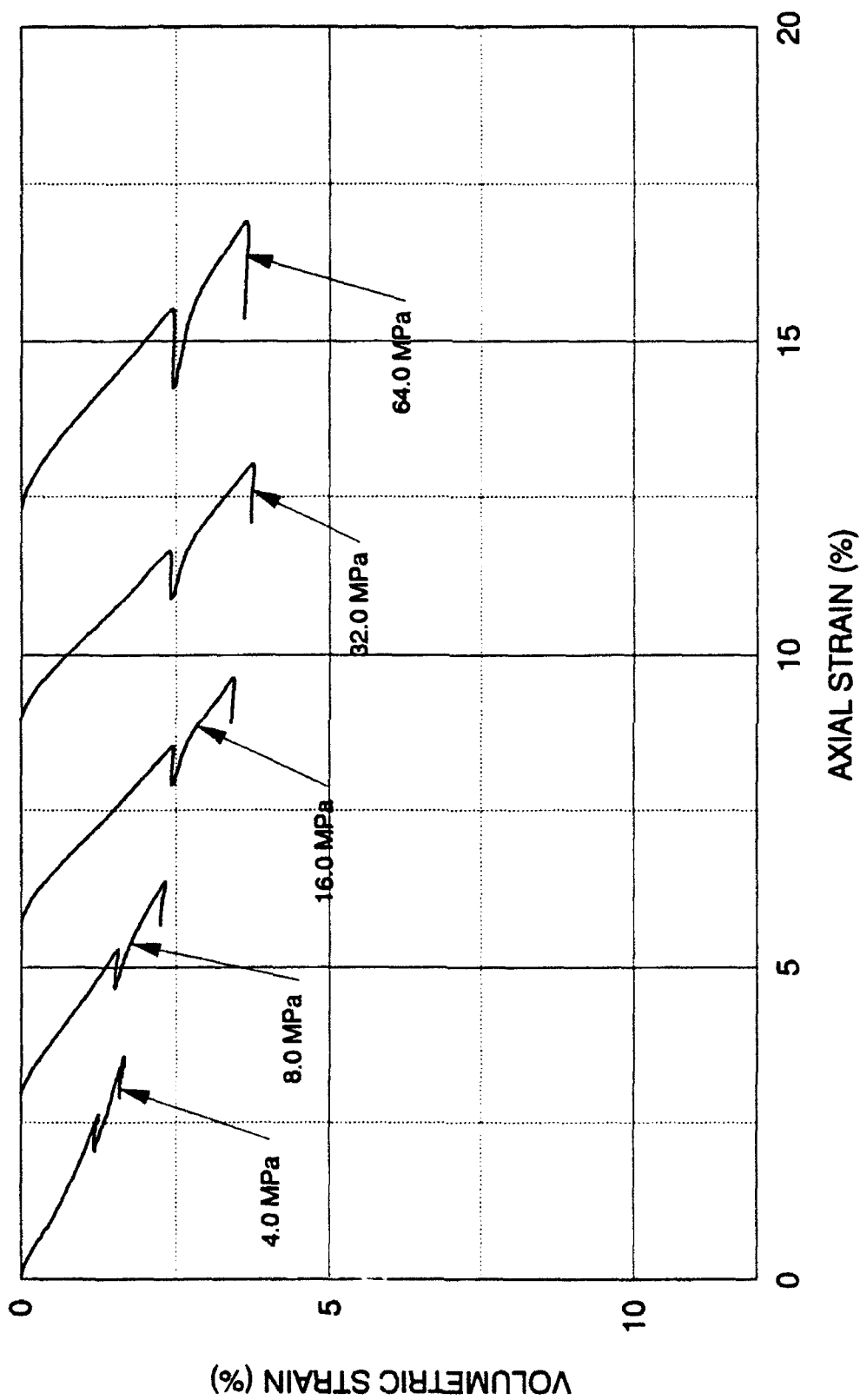


FIGURE 9-27 VOLUMETRIC STRAIN vs. STRAIN  
LOADING-UNLOADING-RELOADING TEST FOR DETERMINATION OF ELASTIC PARAMETERS  
DENSE CAMBRIA SAND

theories for soil behavior at lower pressures. The theories examined were the stress dilatancy theories by Bishop (1954) and Rowe (1962, 1964) and critical state theories by Seed and Lee (1967), Roscoe et al. (1958), and Rutledge (1947). Correlations with total input energy to failure were also presented.

The dilatancy correction equations by Bishop and Rowe ideally should result in a constant friction angle, which Rowe considered to be the basic interparticle friction angle. Both formulations for dilatancy correction involve the rate of dilation at failure. When high pressure test results are applied to Rowe's formulations for compression and extension, the friction angles that result exhibit a large increase at moderately high pressures before decreasing to a constant value at the highest pressures employed (Figure 10-2). The constant friction angle occurs at a stress magnitude where particle crushing is rapidly increasing, and this results in increasing (more compressive) rate of dilation at failure. Bishop's dilatancy correction formulation for triaxial compression tests produces friction angles that exhibit a smoother and more constant value through high pressures. However, when an expression for triaxial extension was derived on the basis of his compression formulation, the reduced friction angles that resulted were apparently incorrect (Figure 10-1): The reduced friction angles at low pressures are much too low and at high pressures excessively large. Both Rowe's and Bishop's formulations for dilatancy corrections were formulated for low pressure applications, where little particle crushing occurs. Implicit in their derivations is the assumption that the soil actually does dilate, even though the expressions have been widely used for volumetrically contracting soils. However, the general concept of stress-dilatancy has been shown to be correct: A soil is measurably stronger when it exhibits more dilatant tendencies.

Seed and Lee's concept of critical state was shown to be inapplicable at high pressures, because the critical void ratio line could not be predicted from drained tests (Figures 10-7 and 10-8). The uniqueness of their critical void ratio line was not confirmed at high pressures, with

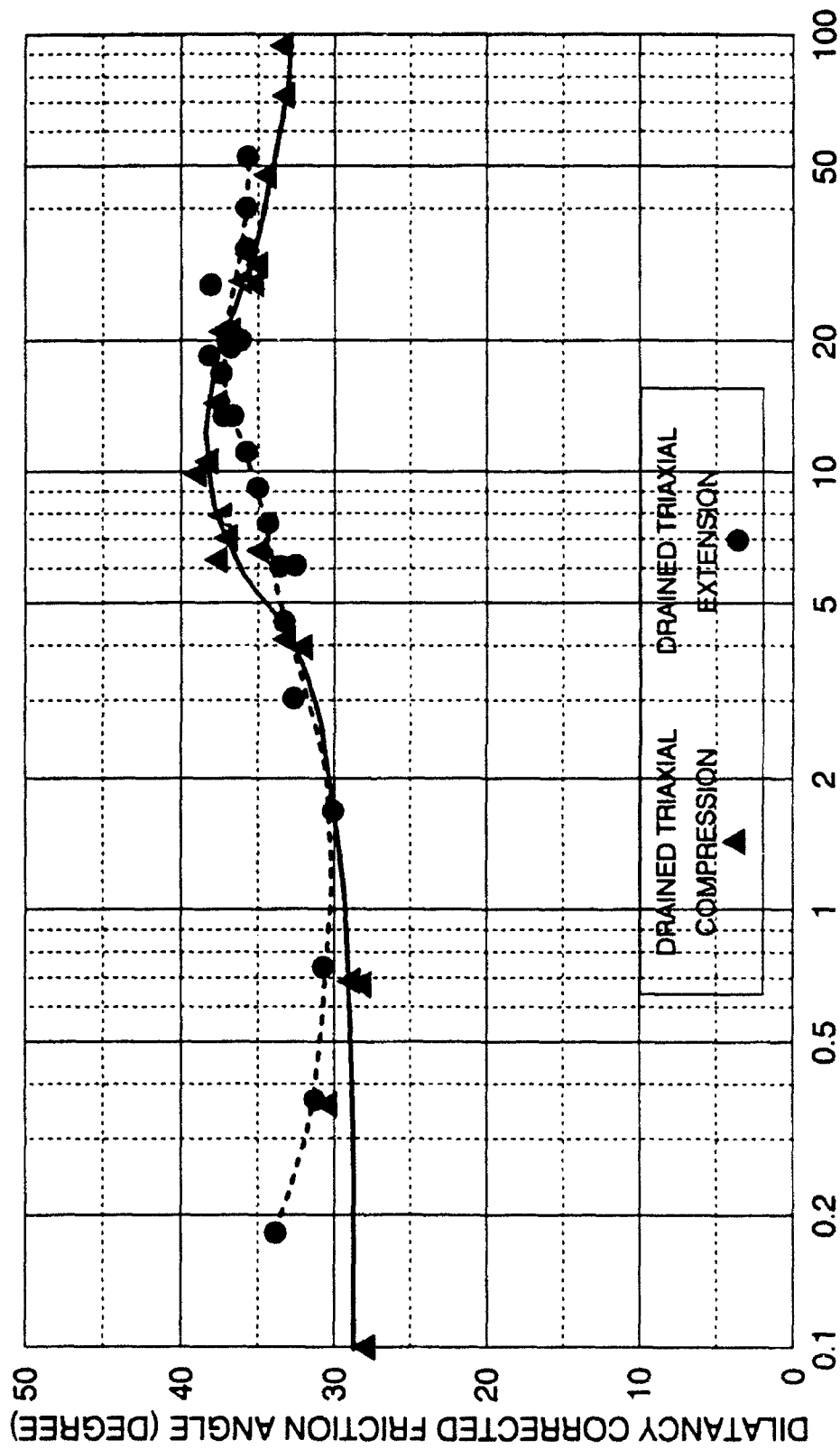


FIGURE 10-2 DILATANCY CORRECTED FRICTION ANGLES USING ROWE'S METHOD  
DENSE CAMBRIA SAND

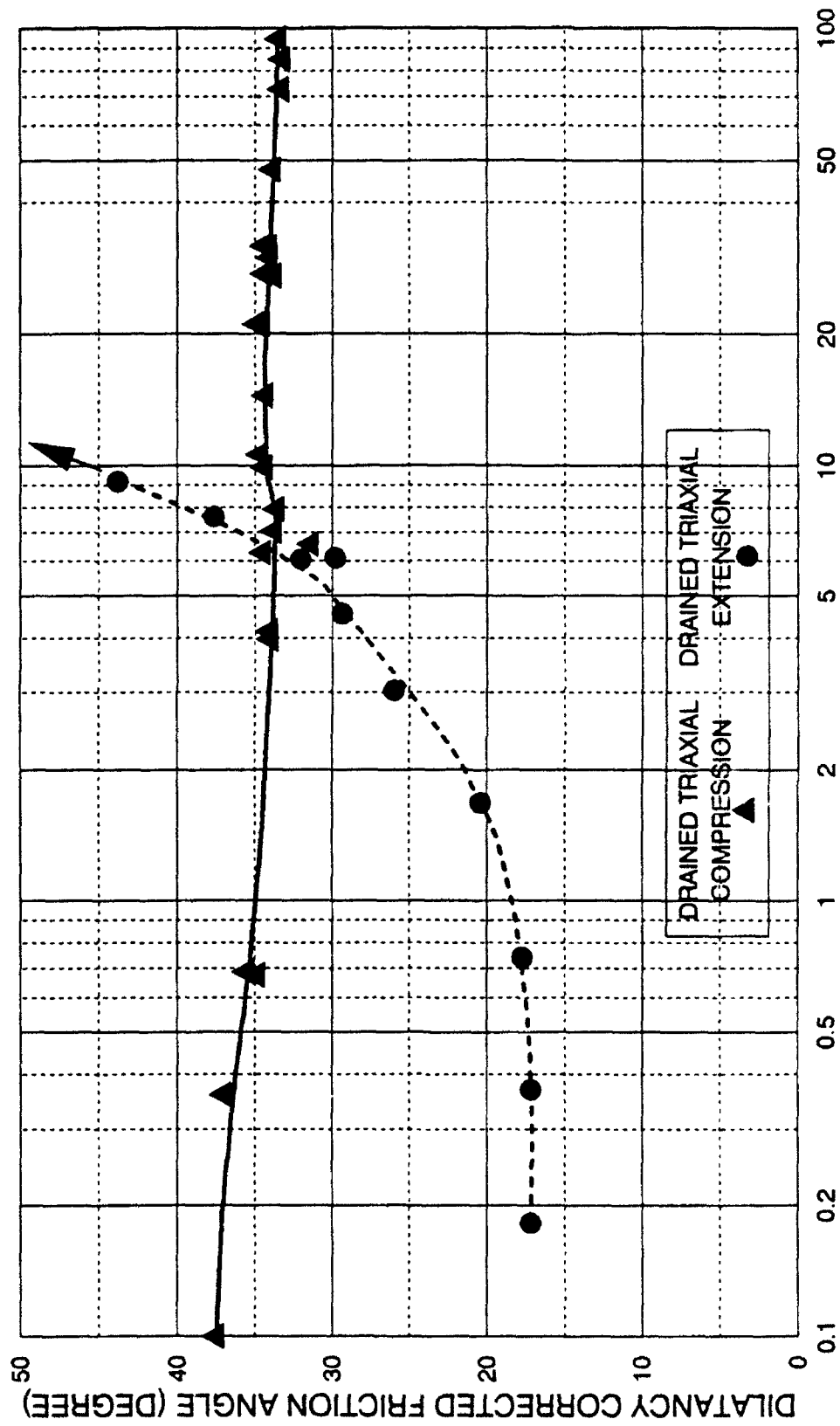


FIGURE 10-1 DILATANCY CORRECTED FRICTION ANGLES USING BISHOP'S METHOD  
DENSE TRIAXIAL COMPRESSION & EXTENSION  
DENSE CAMBRIA SAND

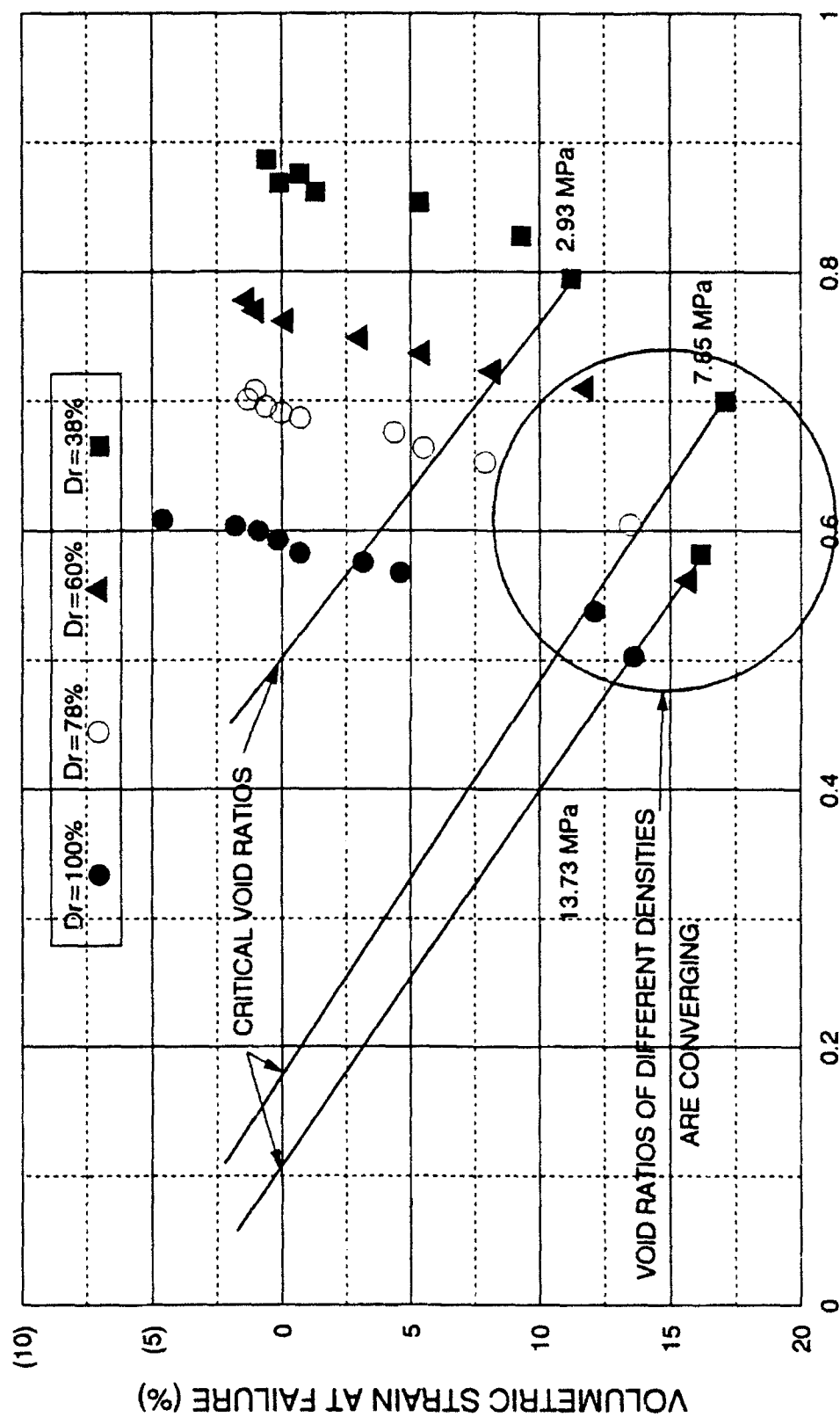


FIGURE 10-7 PROBLEM OF EVALUATION CRITICAL VOID RATIO AT HIGH PRESSURES  
CRITICAL STATE SOIL MECHANICS, DRAINED TRIAXIAL COMPRESSION TESTS  
FOUR DENSITIES OF SACRAMENTO RIVER SAND

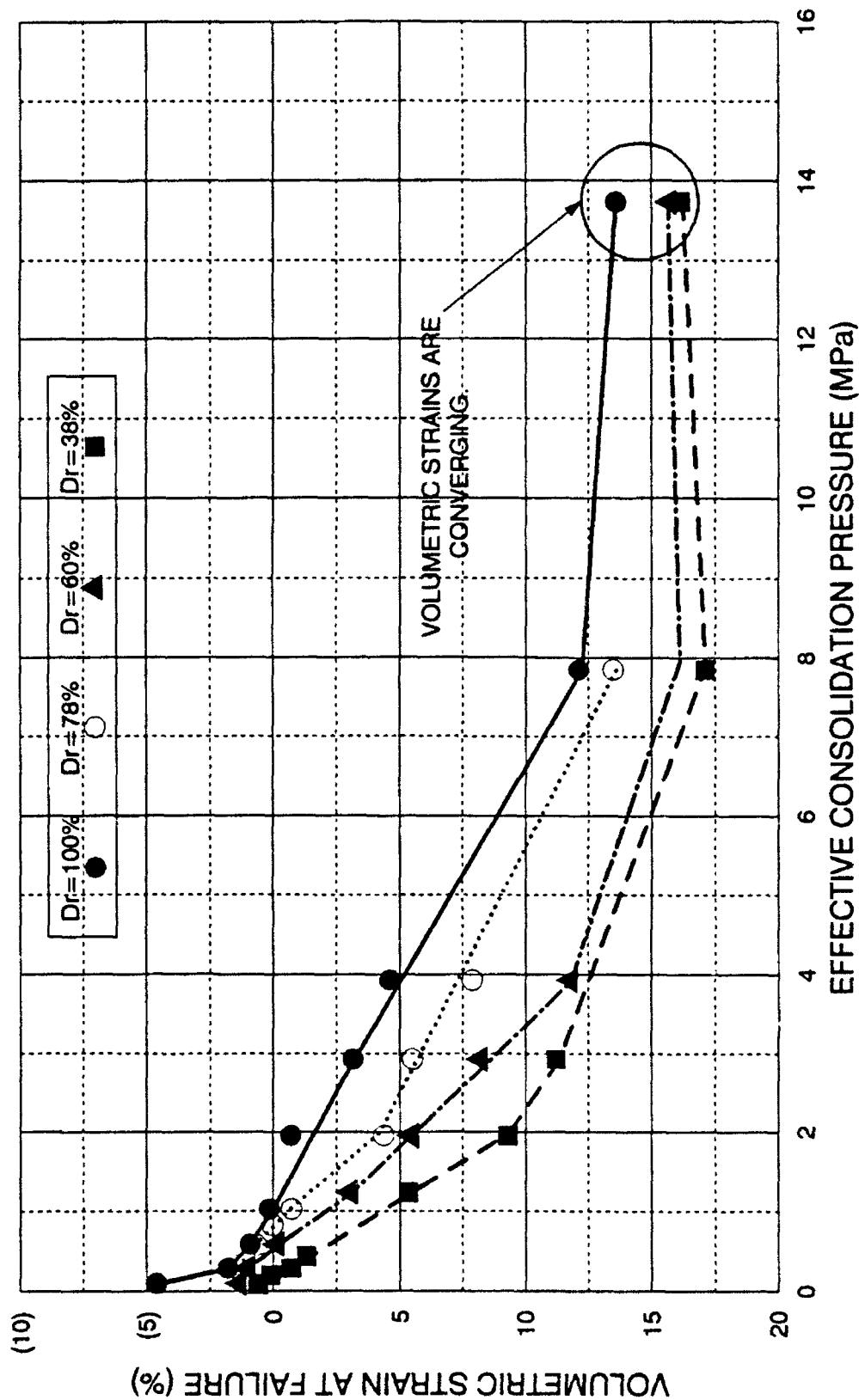


FIGURE 10-8 PROBLEM OF EVALUATION CRITICAL CONFINING PRESSURE AT HIGH PRESSURES  
CRITICAL STATE SOIL MECHANICS, DRAINED TRIAXIAL COMPRESSION TESTS  
FOUR DENSITIES OF SACRAMENTO RIVER SAND

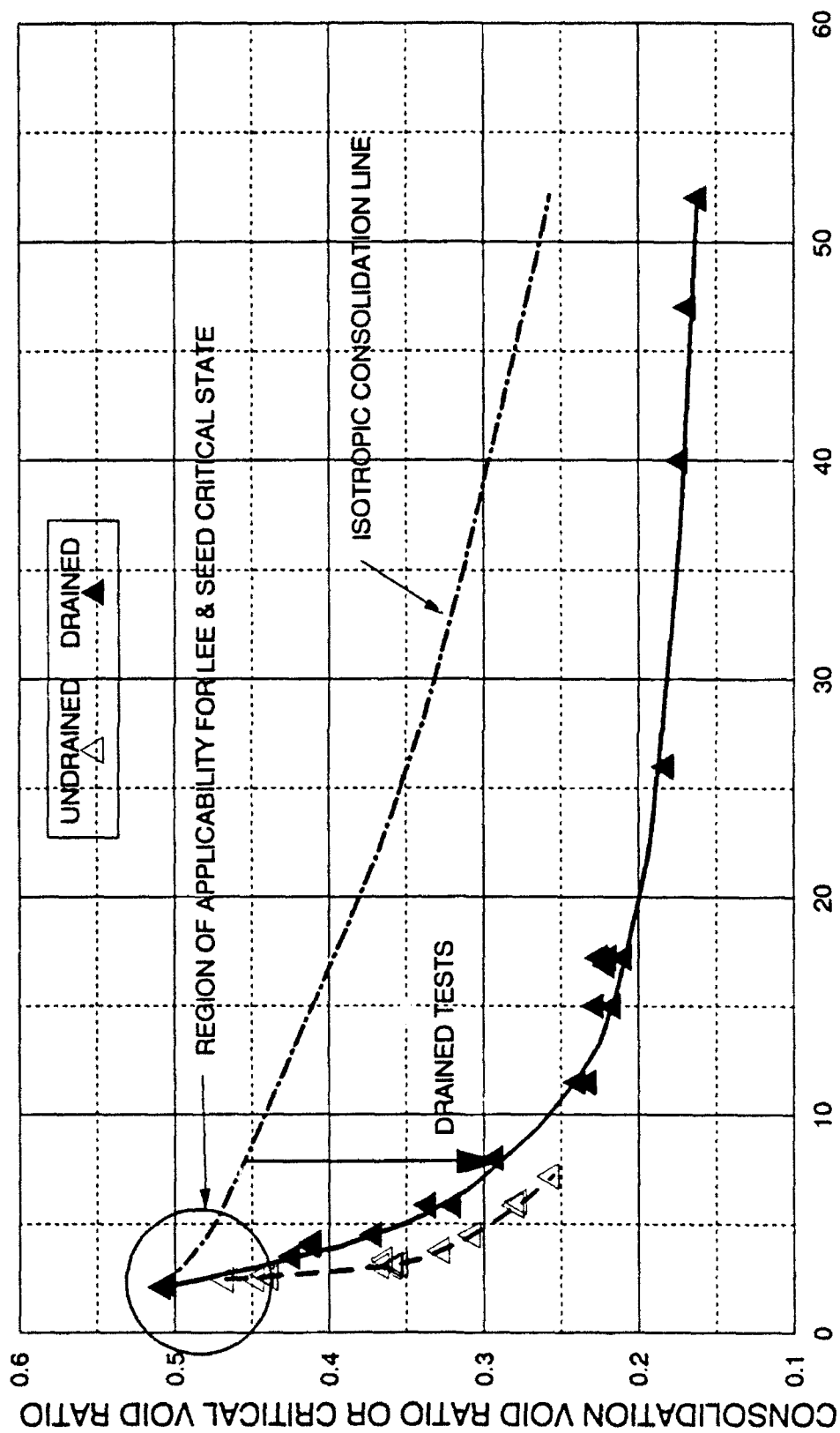


FIGURE 10-9 CRITICAL VOID RATIO LINES

CRITICAL STATE IN DRAINED AND UNDRAINED TRIAXIAL COMPRESSION

DENSE CAMBRIA SAND

drained and undrained tests not appearing on a unique line (Figure 10-9).

Roscoe, Schofield, and Wroth's concept of critical state was also shown to be inapplicable at high pressures. The critical state line was derived from drained tests, and indeed appears to work well for drained tests (Figure 10-11). However, it was determined that the effective stress paths from high pressure undrained tests did not have their maximum stress differences occurring on the derived critical state line, as required by their definition of critical state (Figure 10-12). A line passing through the maximum stress differences correspond to the instability line, not the critical state line.

The Rutledge Hypothesis appears to be valid for granular materials at high pressures. Originally it was only considered applicable to normally consolidated clays at low pressures. The line defined by plotting the void ratio at failure against the maximum deviator stress becomes parallel to the isotropic and one-dimensional compression lines at high pressures on a semilogarithmic plot (Figures 10-13 and 10-14). At low pressures the effect of initial void ratio causes the maximum deviator stresses from drained and undrained tests to be on separate lines. As the effect of initial void ratio is reduced at higher stresses the strength lines start converging toward each other. At higher stresses yet, the strength lines for drained and undrained triaxial compression and extension tests all converge together onto a unique line. The implication of this is that the void ratio at failure essentially controls the strength of soils at high pressures. However, the principal difference with the Rutledge Hypothesis is that the effective stress friction angle for the undrained tests on sands cannot be inferred from the maximum deviator stress, since it occurs well away from effective stress failure condition.

Input energy to failure appears to be useful as a unifying variable when used for comparison with the void ratio at failure and the maximum deviator stress. The correlation with void ratio at failure appears very similar to the void ratio-deviator stress correlation just stated, except the extension and compression tests appear on separate lines until high pressure levels are

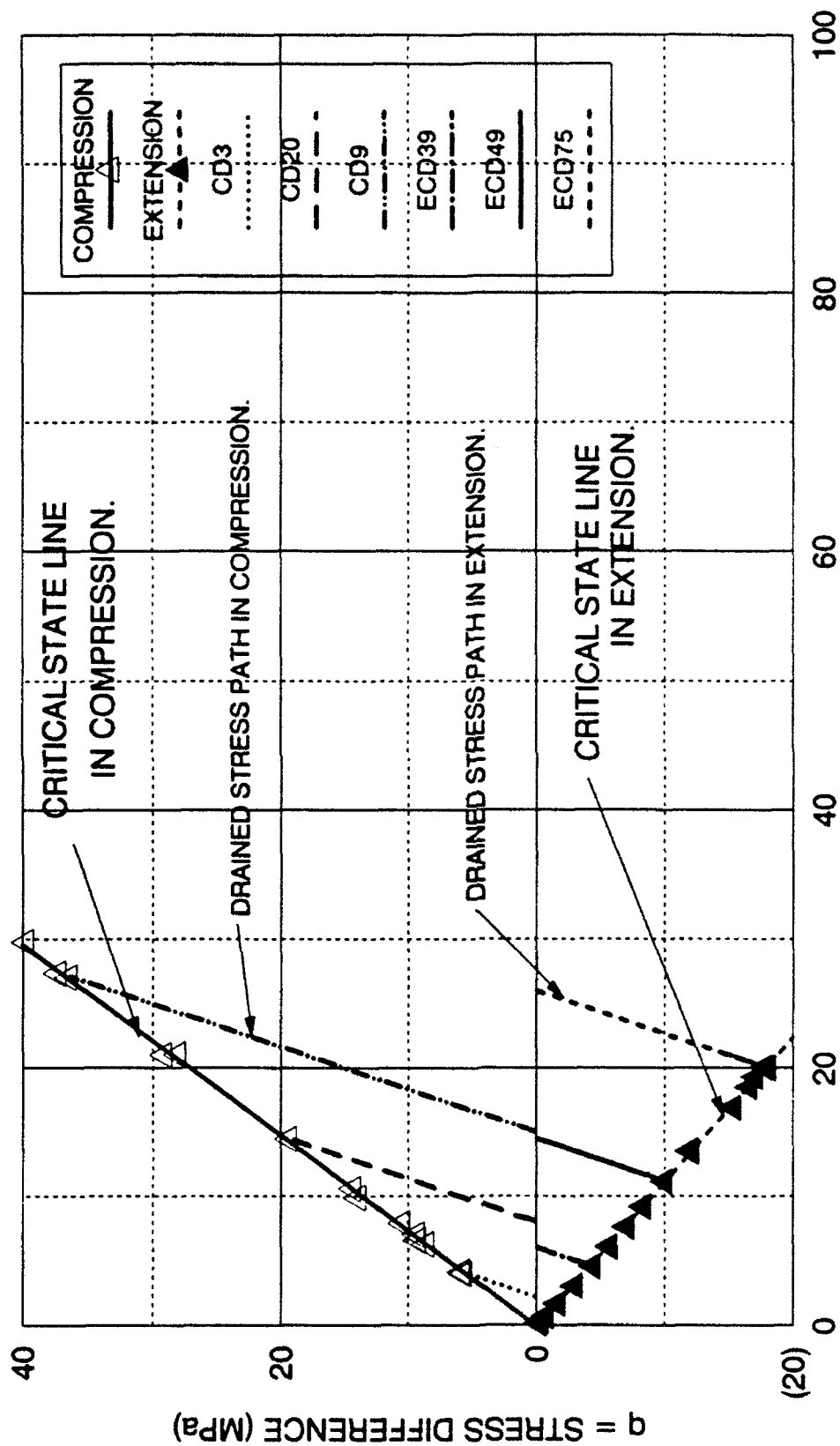
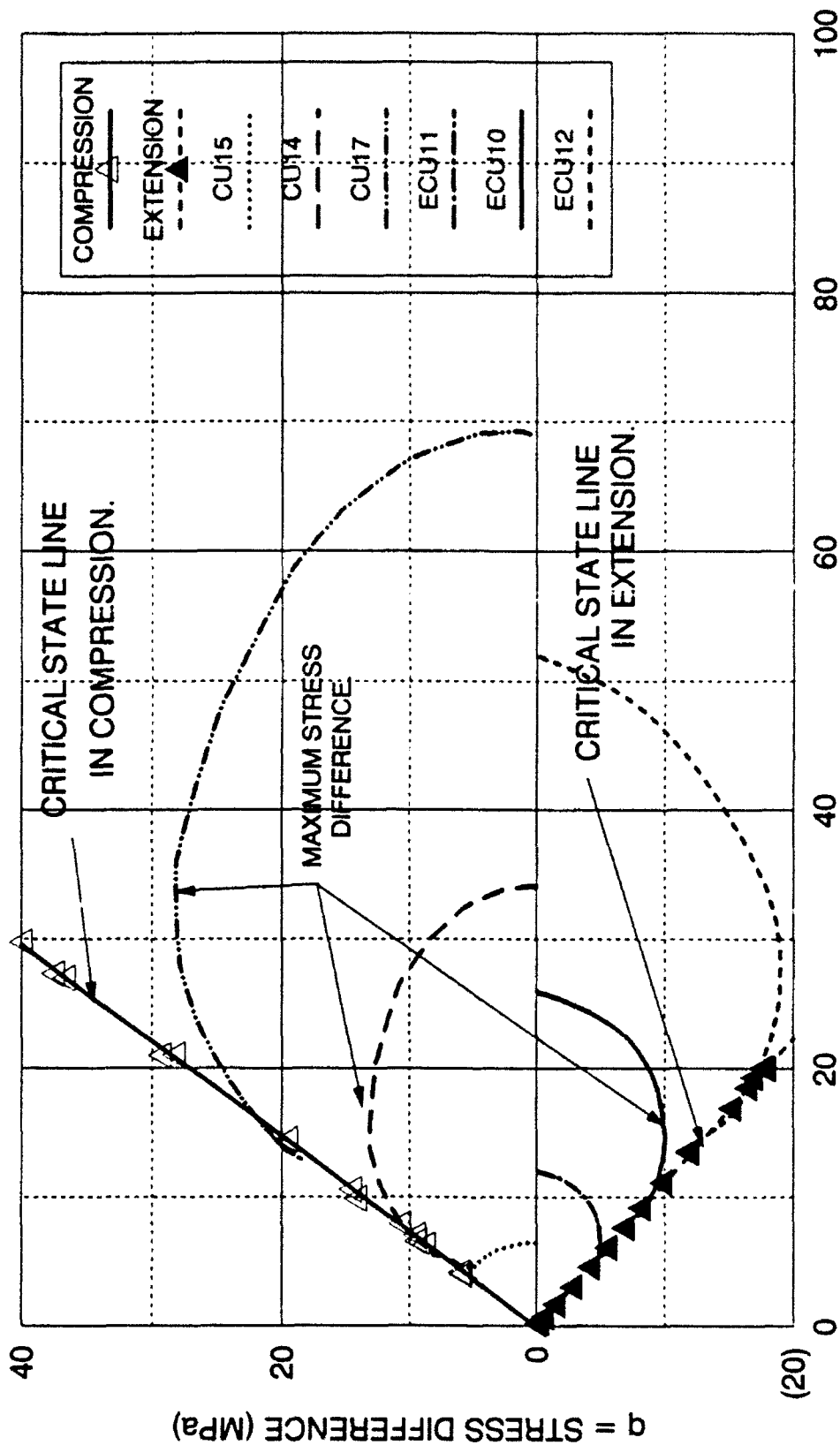


FIGURE 10-11 EFFECTIVE STRESS PATH, CAMBRIDGE  $p'-q$

DRAINED TRIAXIAL COMPRESSION AND EXTENSION

DENSE CAMBRIA SAND



p' = EFFECTIVE MEAN NORMAL STRESS (MPa)  
 FIGURE 10-12 EFFECTIVE STRESS PATH, CAMBRIDGE p'-q  
 UNDRAINED TRIAXIAL COMPRESSION AND EXTENSION  
 DENSE CAMBRIA SAND

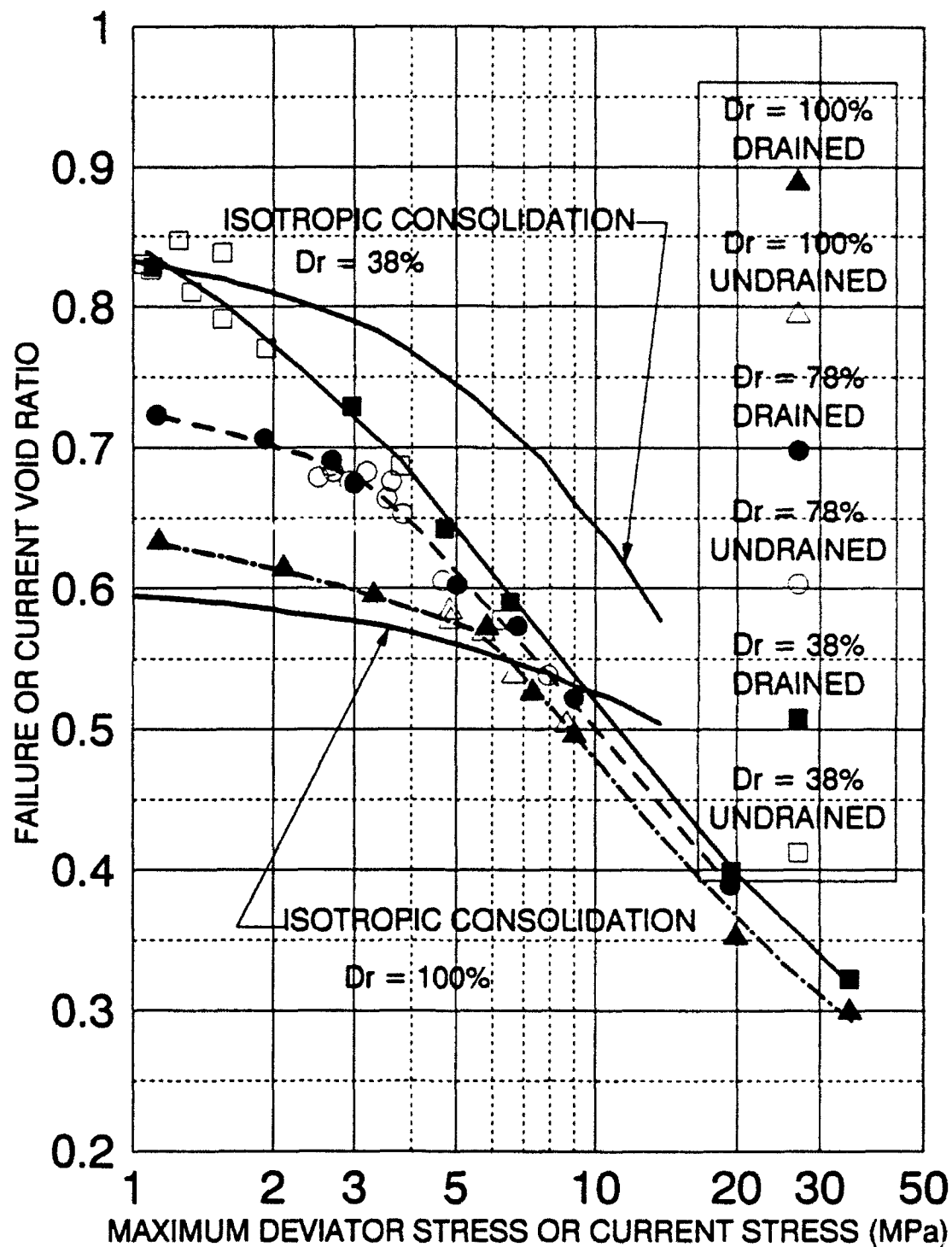


FIGURE 10-13 - VOID RATIO RELATED TO STRESS  
DRAINED & UNDRAINED TRIAXIAL COMPRESSION TESTS  
SACRAMENTO RIVER SAND (from LEE, 1965)

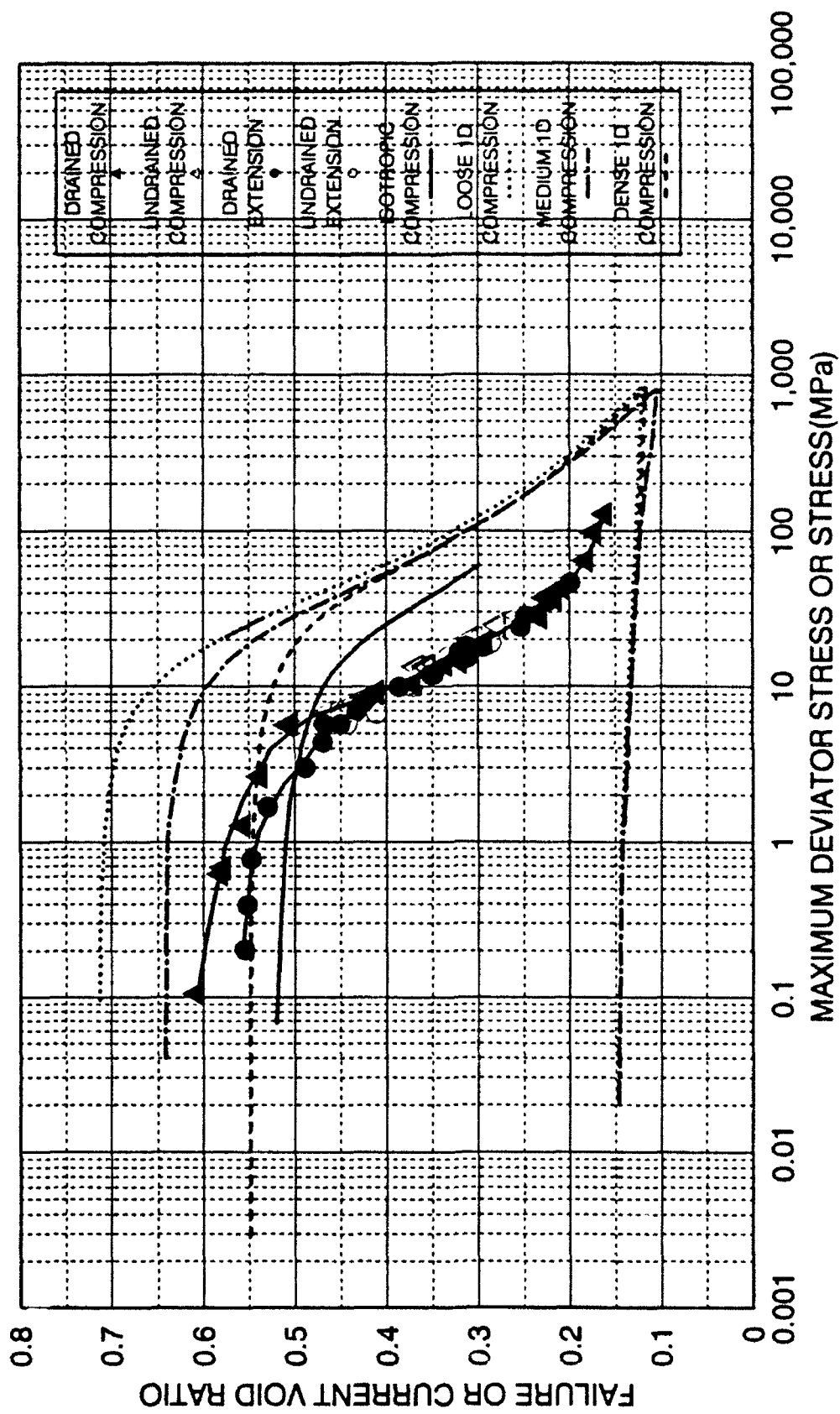


FIGURE 10-14 VOID RATIO VS. STRESS  
DIFFERENT TESTS  
CAMBRIA SAND

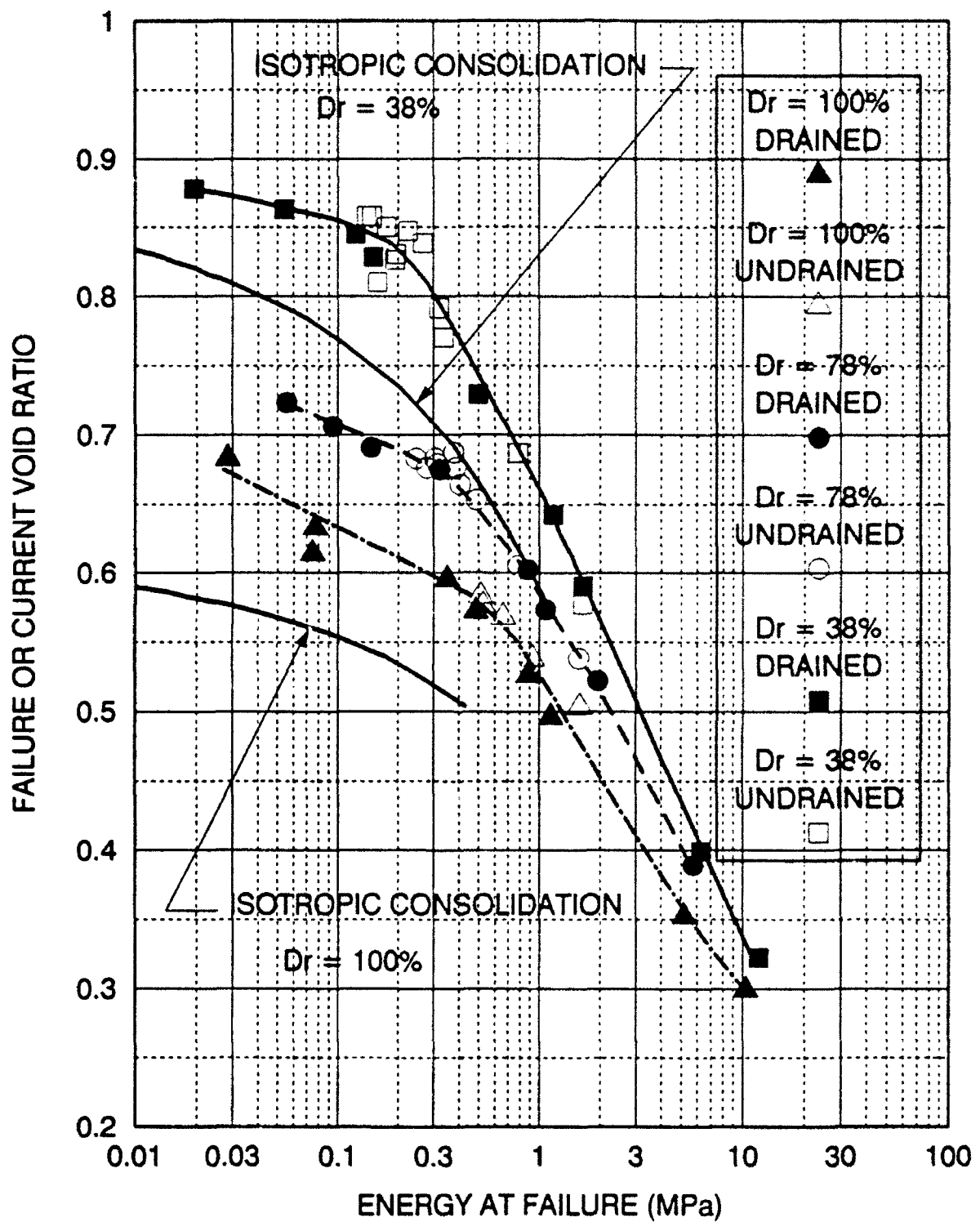
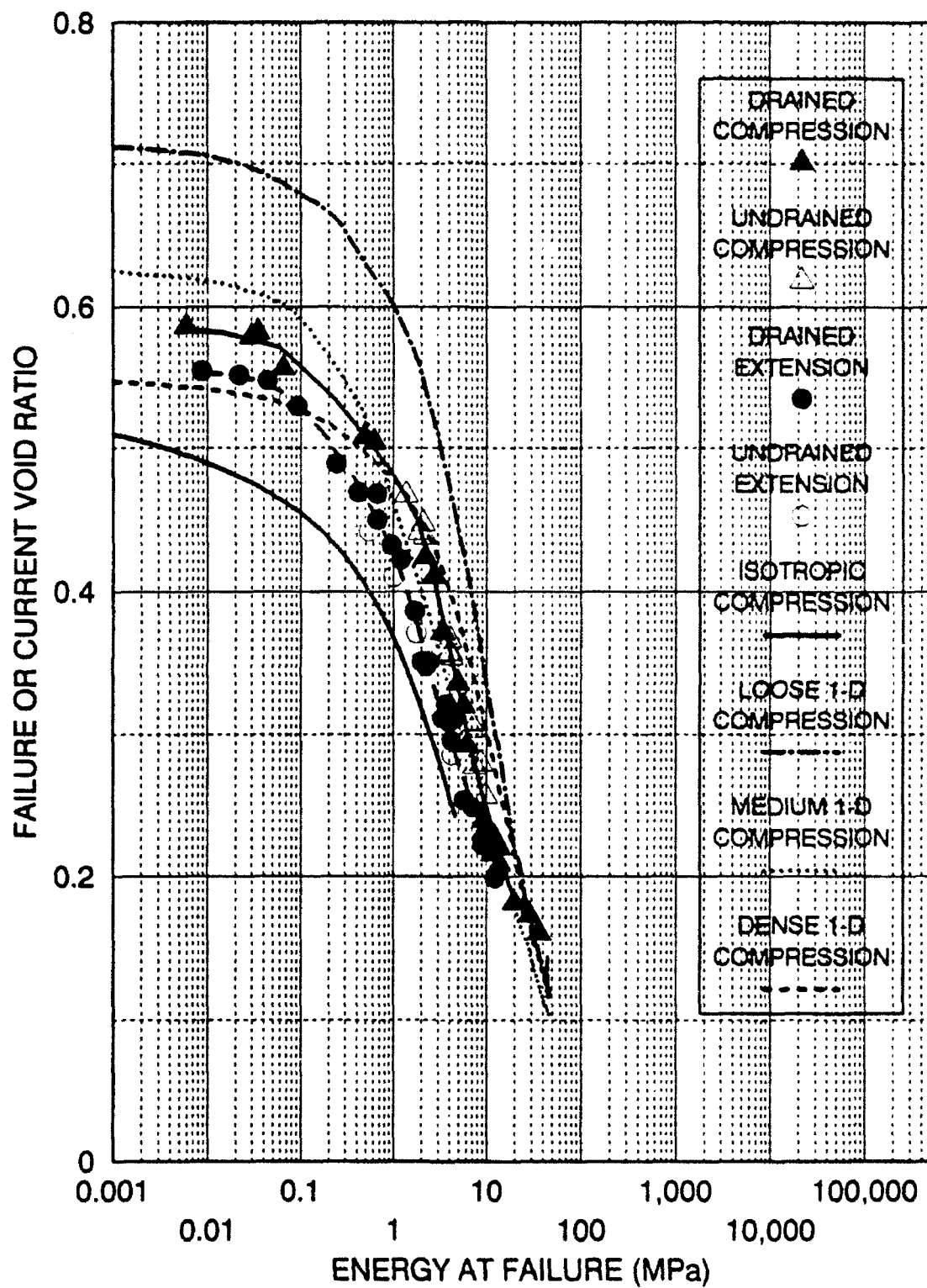


FIGURE 10-16 VOID RATIO VS. ENERGY AT FAILURE  
DRAINED AND UNDRAINED TRIAXIAL COMPRESSION TESTS  
SACRAMENTO RIVER SAND (from LEE, 1965)



achieved (Figures 10-16 and 10-17). This is due to the effect of different stress paths, resulting in different amounts of input energy to failure. The correlation of input energy to failure with maximum deviator stress results in a linear relationship beyond the dilatancy region, and it appears very similar to a classic Mohr-Coulomb failure envelope (Figures 10-18 and 10-19). Extension and compression tests do not appear on a unique line due to stress path effects. Breaking down the total input energy into its separate components of consolidation energy, volumetric strain energy (drained tests only), and deviator stress energy indicates that beyond the dilatancy region the individual component energies appear almost to linearly increase with stress (Figures 10-20 and 10-21).

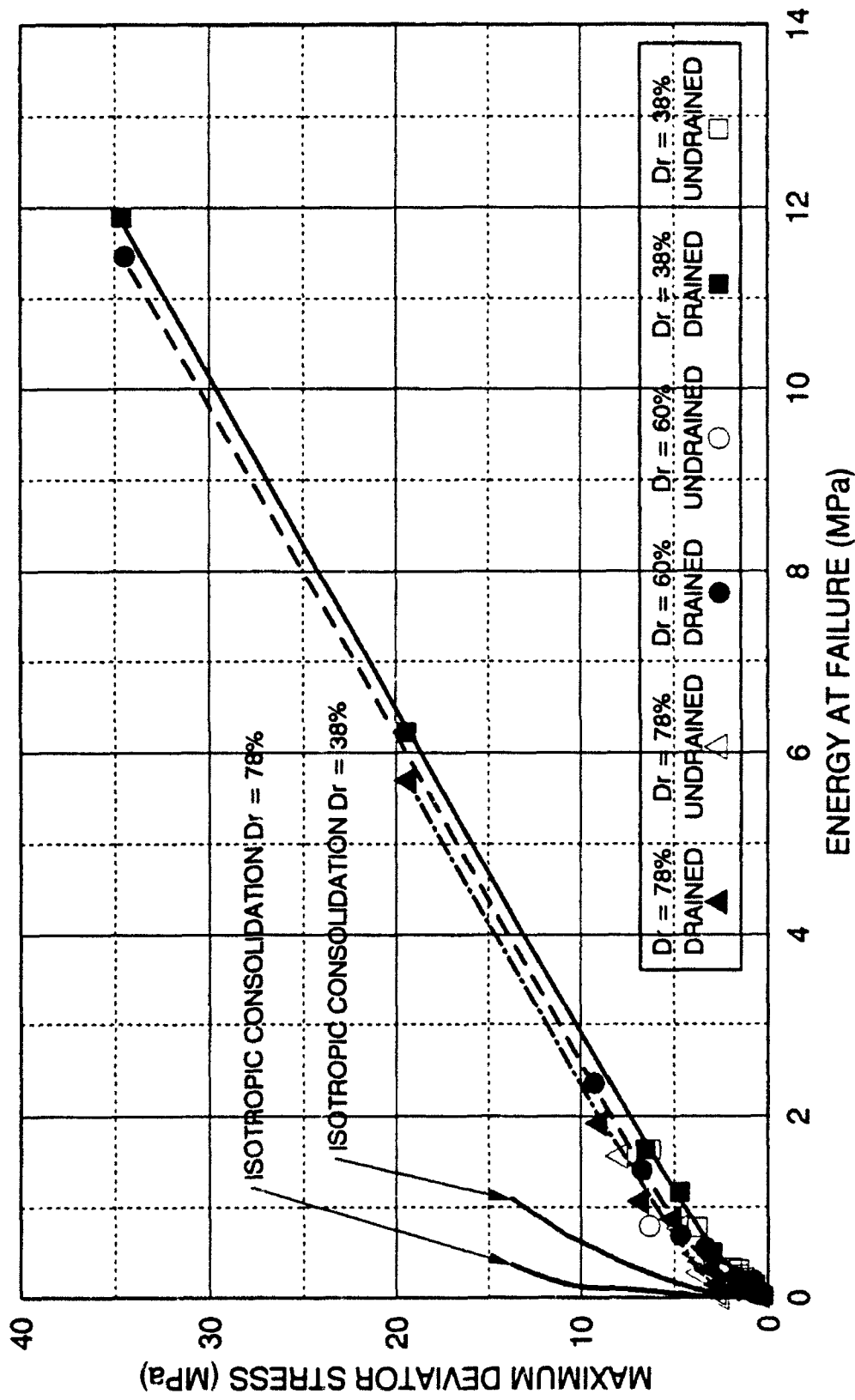


FIGURE 10-18 MAXIMUM DEVIATOR STRESS VS. ENERGY  
DRAINED AND UNDRAINED TRIAXIAL COMPRESSION  
SACRAMENTO RIVER SAND (from LEE, 1965)

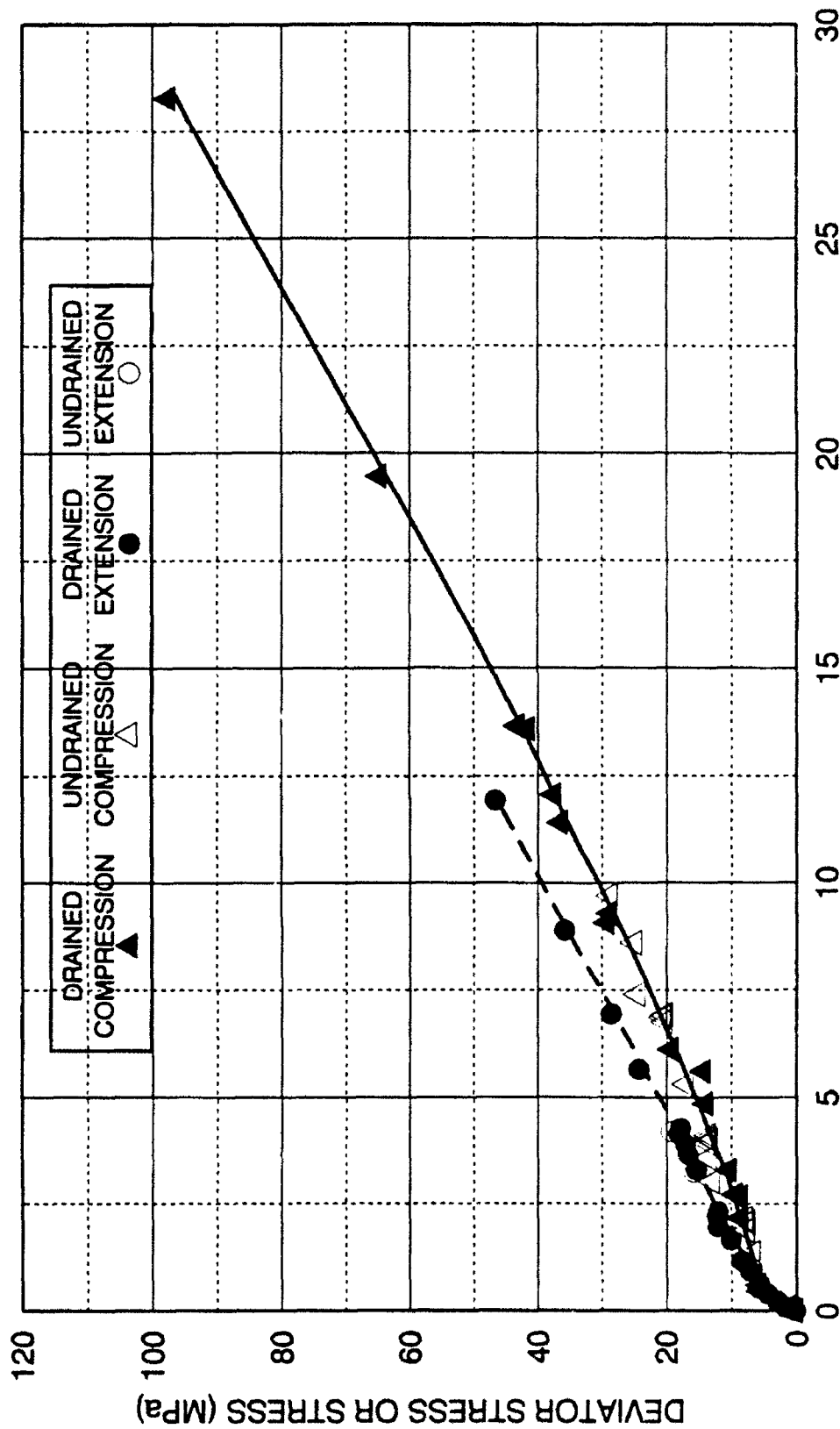


FIGURE 10-19 MAXIMUM DEVIATOR STRESS VS. ENERGY AT FAILURE  
 DRAINED AND UNDRAINED TRIAXIAL COMPRESSION AND EXTENSION TESTS  
 DENSE CAMBRIA SAND

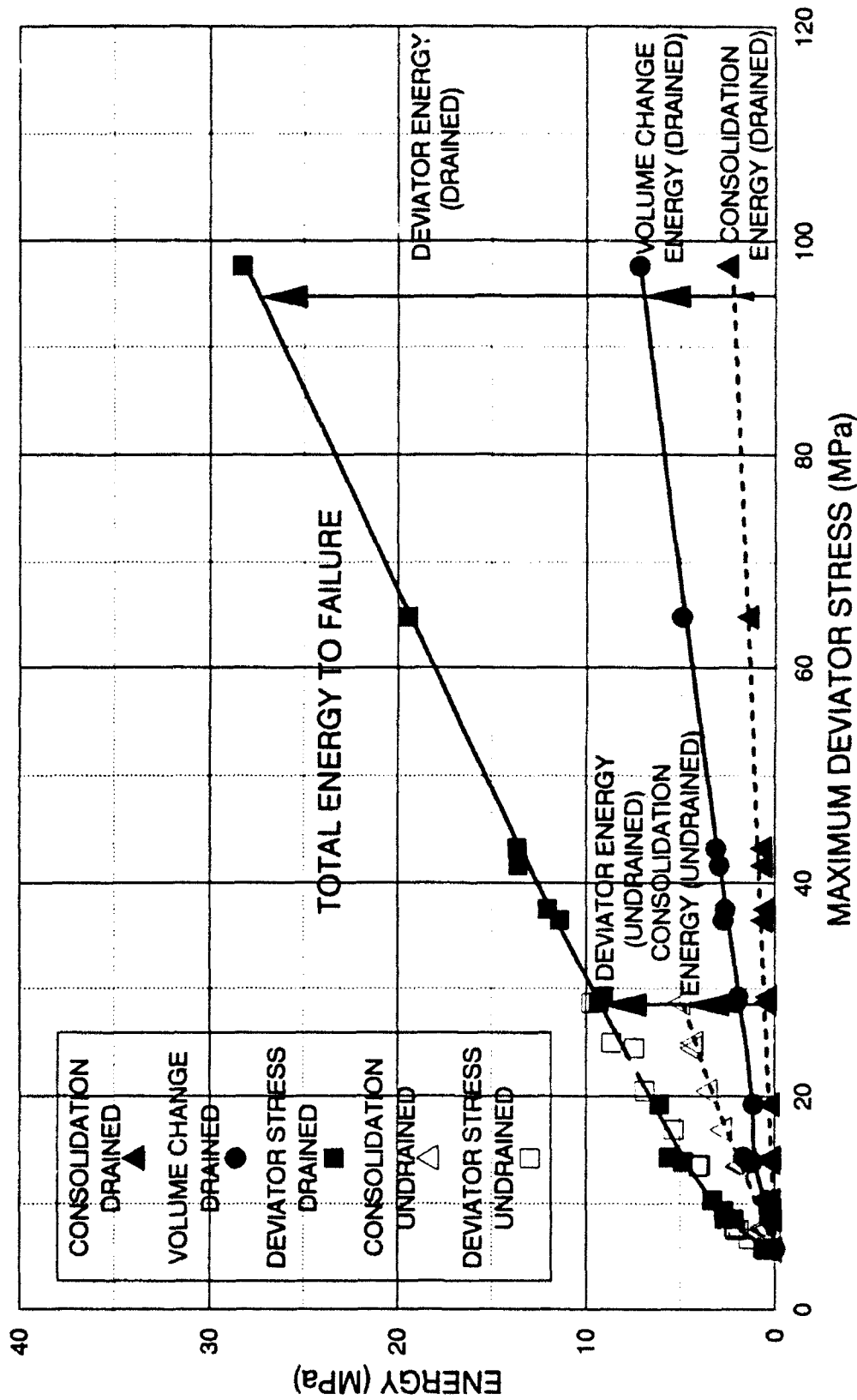


FIGURE 10-20 BREAKDOWN OF TOTAL ENERGY TO FAILURE  
DRAINED AND UNDRAINED TRIAXIAL COMPRESSION TESTS  
DENSE CAMBRIA SAND

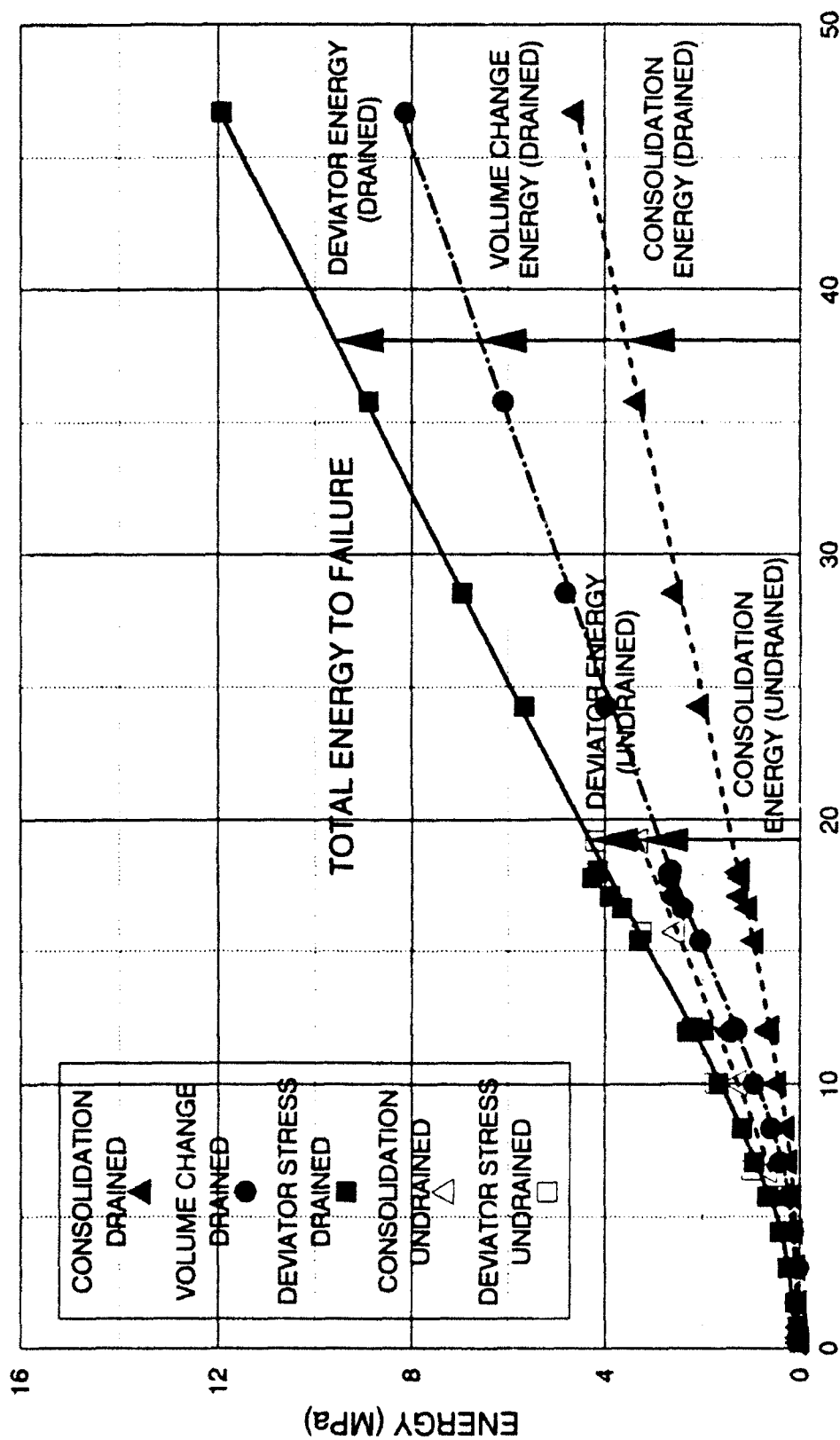


FIGURE 10-21 BREAKDOWN OF TOTAL ENERGY TO FAILURE  
DRAINED AND UNDRAINED TRIAXIAL EXTENSION TESTS  
DENSE CAMBRIA SAND

## SUMMARY OF ATTACHMENT NO. 2

### Static Instability and Liquefaction of Loose Fine Sandy Slopes

Based on previous findings regarding conditions for instability of granular materials, a procedure has been developed for analysis of static instability and liquefaction of loose, fine sandy slopes such as submarine slopes and tailings dams or spoil heaps.

Soils exhibit nonassociated flow and they may therefore become unstable *inside* the effective stress failure surface. Experiments have shown that soils are stable as long as they remain under drained conditions. Instability may be obtained under undrained conditions in the region where the yield surface opens up in the outward direction of the hydrostatic axis. Initiation of instability also requires that the soil tends to compress during undrained shear. Thus, loading (i.e. hardening inside the failure surface resulting in large plastic strains) can occur under decreasing stresses, and this leads to unstable behavior under undrained conditions. The location of the lower boundary for instability, the instability line, is identified. Together with the effective stress failure line it defines the region of potential instability as exemplified in Fig. 8. The instability of a gently inclined submarine slope shown in Fig. 9, and a steeper slope representing a tailings dam or a spoil heap have been analyzed. Conventional stability analyses indicate both slopes to be stable. The analysis procedure clearly show the potential for instability, as actually observed in many submarine deposits of loose, fine sands and silts, and in tailings dams or spoil heaps of granular materials with properties of similar character.

### Stability of Granular Materials in Post Peak Softening Regime

Triaxial compression tests on sand have been performed to study the issue of stability and to investigate the conditions for plastic yielding in the post peak softening regime. The occurrence of softening requires volume dilatation (expansion) and it is observed in drained tests on dense granular materials sheared under low effective confining pressures. It is found that the stability postulates by Drucker and by Hill are not applicable to granular materials in the softening regime. The volume change behavior (dilatancy) plays an important role in the stability of frictional materials.

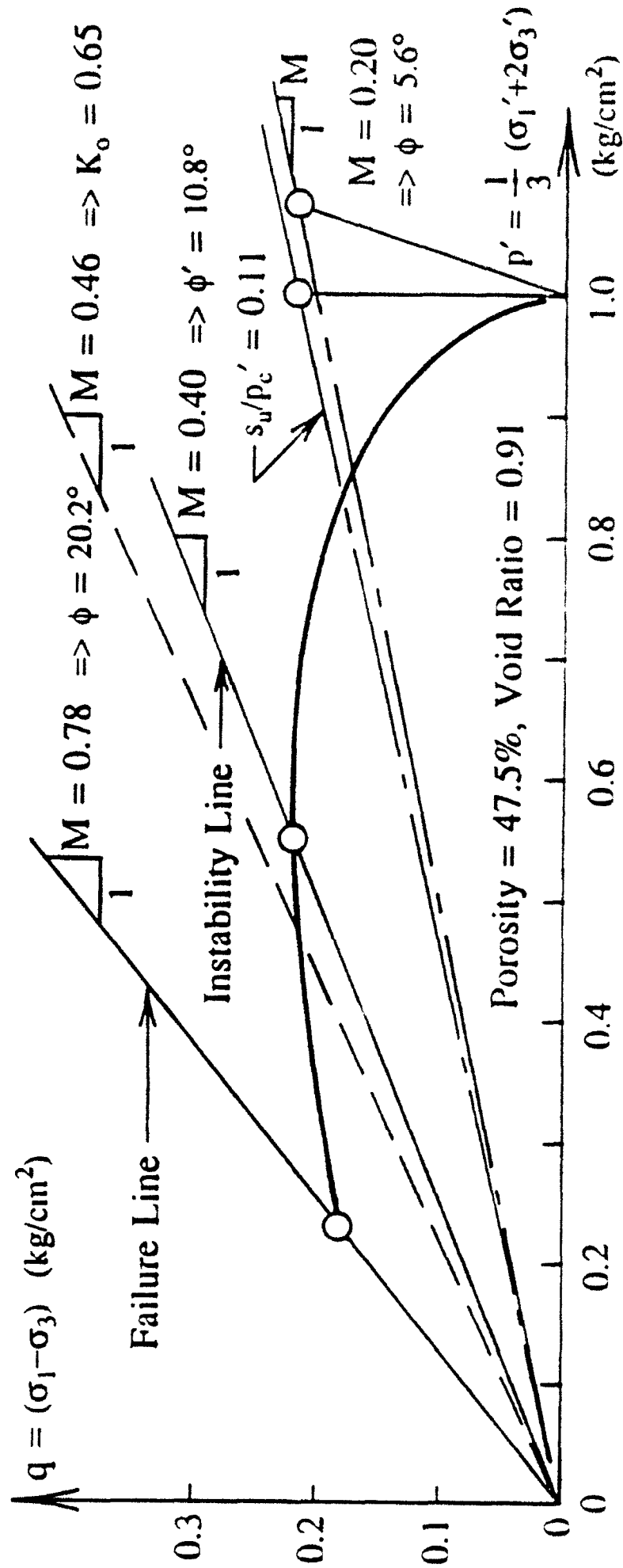


Fig. 8. Effective Stress Path for ICU-Test on Very Loose, Fine Valgrinda Sand (Deduced from Bjerrum et al., 1961).

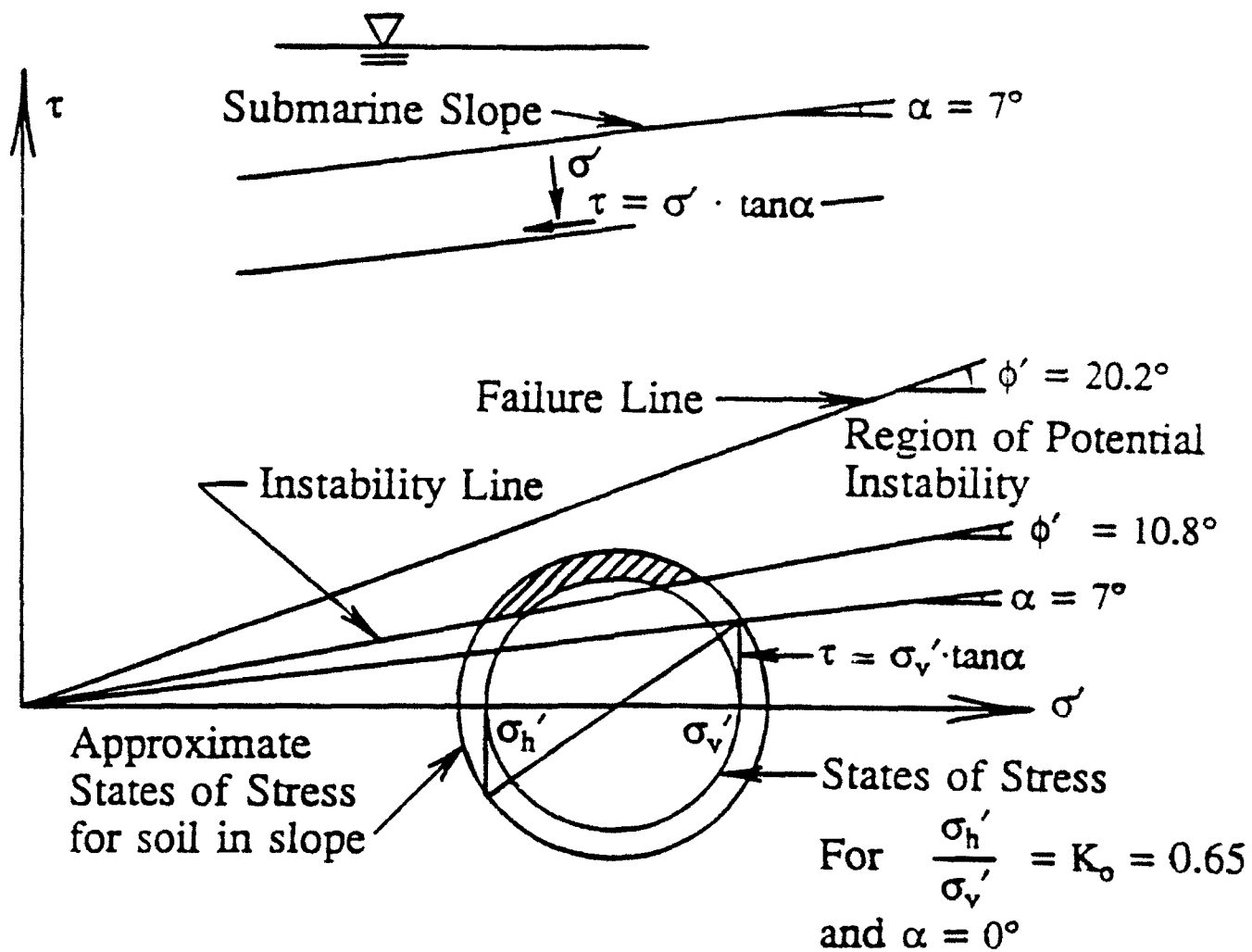


Fig. 9. Analysis of Gently Inclined Submarine Slope. States of Stress on Some Planes are in the Region of Potential Instability.

Plastic yielding can occur along many different stress paths in the softening regime involving increasing, constant, and decreasing stress differences. Elastic behavior (i.e. unloading and reloading) can occur along many similar stress paths. The conventional concept of a yield surface is therefore not applicable in the softening regime. The conventional yield surface may be replaced with a yield fence inside and below which only elastic behavior is observed as shown in Fig 11. The top of the yield fence must be exceeded to produce plastic strains which may then occur for increasing, constant, and decreasing stresses.

Undrained tests, initiated before and after peak failure under drained conditions, show that the stress-strain, pore pressure, and strength behavior is entirely controlled by the capacity of the granular material to dilate. Thus, granular materials that tend to dilate can go through peak failure more than once.

#### **B-Value Measurements for Granular Materials at High Confining Pressures**

This topic was reviewed in connection with Chapter 7 of Attachment no. 1.

#### **Effects of Strain Rate on Instability of Granular Soils**

This topic was reviewed in connection with Chapter 7 of Attachment no. 1.

#### **Instability of Dilating Sand**

With background in the stability conditions proposed by Drucker and by Hill, the stability of granular materials which exhibit nonassociated flow has been investigated on the basis of experimental observations. Several series of triaxial compression tests designed to expose the type of behavior exhibited by granular materials were performed. The variables in these studies were the sign of the work increment (positive or negative), the volumetric strain behavior (compression or dilation), the constraints on the volumetric behavior (free or controlled), and the degree of saturation (fully or partly saturated). It is shown that the conditions for stability proposed by Drucker and by Hill are neither necessary nor sufficient to guarantee stability of granular (frictional) materials as

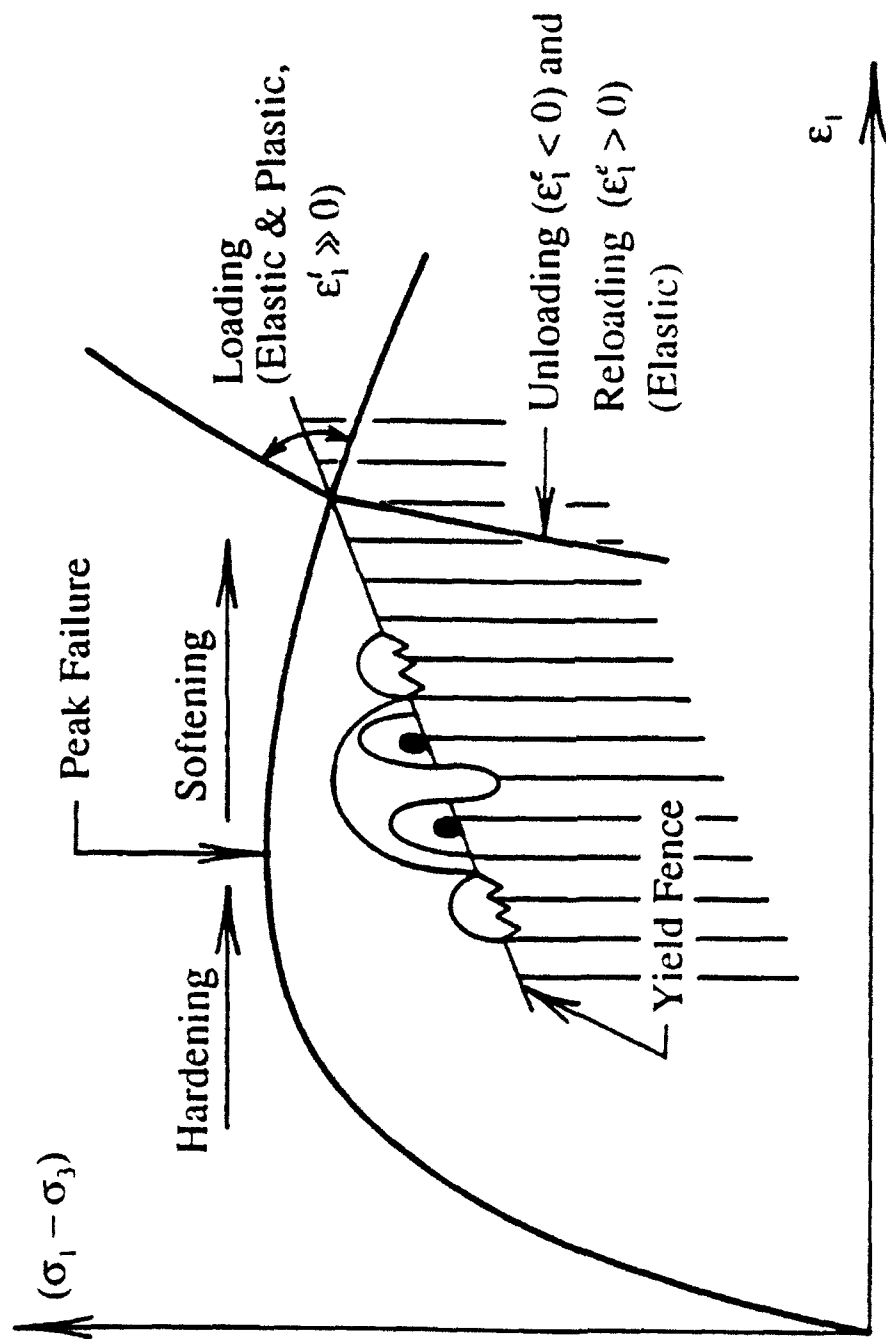


Fig. 11. Schematic Diagram of the Concept of a Yield Fence in the Softening Regime.

may be deduced from Figs. 9 and 10. However, when these criteria are violated, it is possible to create an unstable situation by prescribing a constraint among the kinematic degrees of freedom (e.g. shear and volumetric strain). Conditions for stability are induced on the basis of experimental observations of the behavior of granular materials in triaxial tests.

### Creep Effects on Static and Cyclic Instability of Granular Soils

Observations of soil behavior in conventional consolidation tests indicate that creep results in further compression of the soil beyond that experienced during primary consolidation. This secondary compression causes a stiffening of the soil expressed as an increased quasi-preconsolidation pressure. In order to produce further consolidation (beyond elastic compression) the stress state must exceed the quasi-preconsolidation pressure or the yield pressure. The increase in yield pressure depends on the time the soil is resting under the current pressure. Thus, it appears that the soil becomes stiffer with age.

The aging effect occurs for any soil at any state of stress inside the failure surface. As creep deformation continues, the yield point is pushed out and can be reached by "reloading" beyond the previous maximum stresses. To demonstrate this effect as well as the consequent movement of the point of instability, a series of tests on loose Sacramento River Sand was performed. Five triaxial compression tests were conducted in which the specimens were first isotropically confined at an effective confining pressure of  $\sigma'_3 = 29.9 \text{ kg/cm}^2$  (2,930 kPa) and then loaded under drained conditions to a stress difference of  $(\sigma_1 - \sigma_3) = 43.0 \text{ kg/cm}^2$  (4,220 kPa). At this point the specimens were allowed to creep for 0, 2, 20, 200 and 2,000 minutes, respectively. The drainage valve was then closed and the specimens were further loaded under stress control to study the position of the yield surface and the subsequent unstable behavior.

Figs. 4 and 8 show the results of the five tests. The average stress-strain curve is indicated for the five tests leading up to the point where creep was allowed. To obtain clarity in the diagrams, all creep and subsequent loading test results have been adjusted to begin at the point corresponding to  $t_{\text{creep}} = 0 \text{ min}$ . The figures show that increasing time periods produce increasing amounts of creep, and subsequent undrained loading initially results in elastic "reloading." The plastic yield

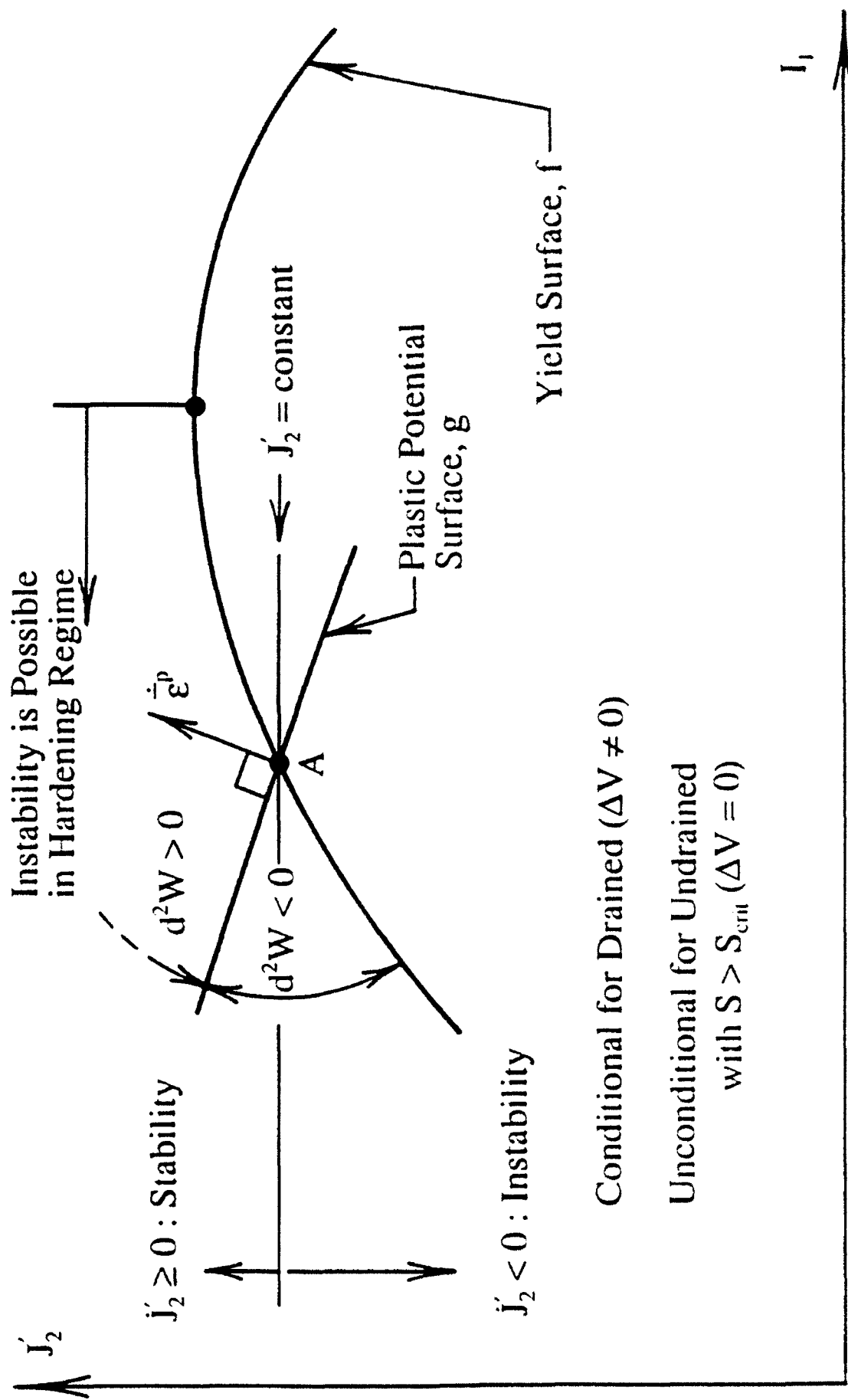


Fig. 9. Schematic Diagram of Conditions for Stability and Instability of Compressing Granular Material.



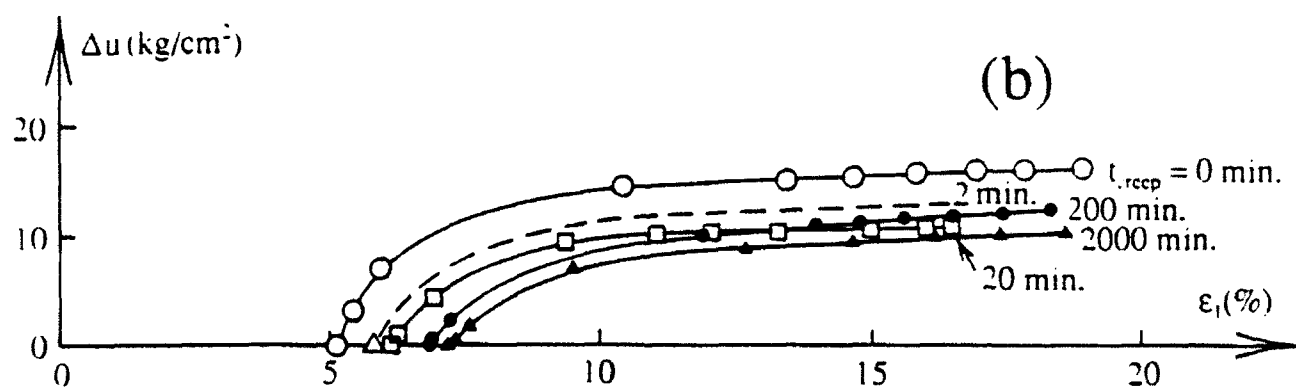
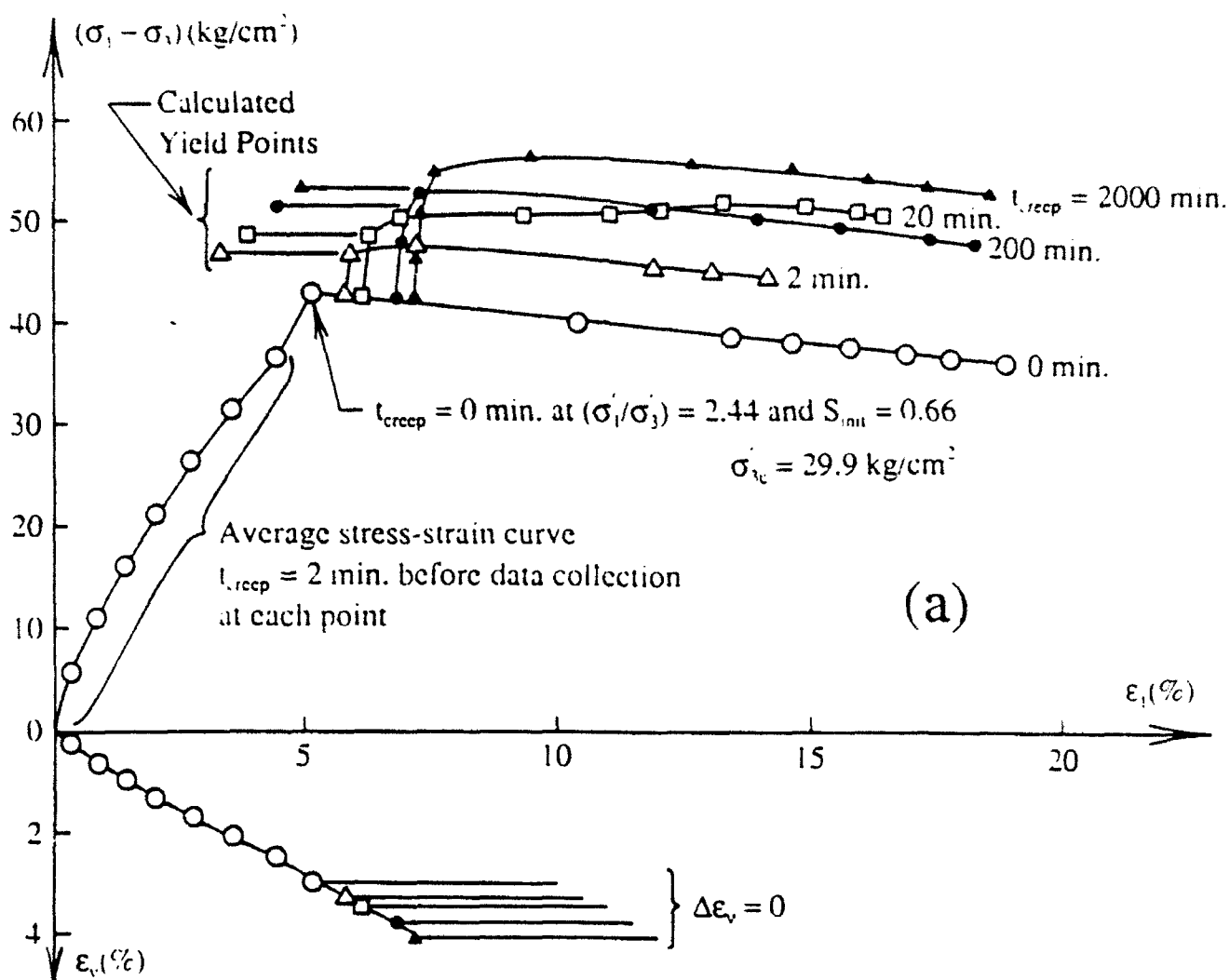


Fig. 4. (a) Stress-strain and volume change, and (b) pore pressure relations for five creep and instability tests on loose Sacramento River sand at  $(\sigma_1 - \sigma_3) = 43.0 \text{ kg/cm}^2$  (4,220 kPa).

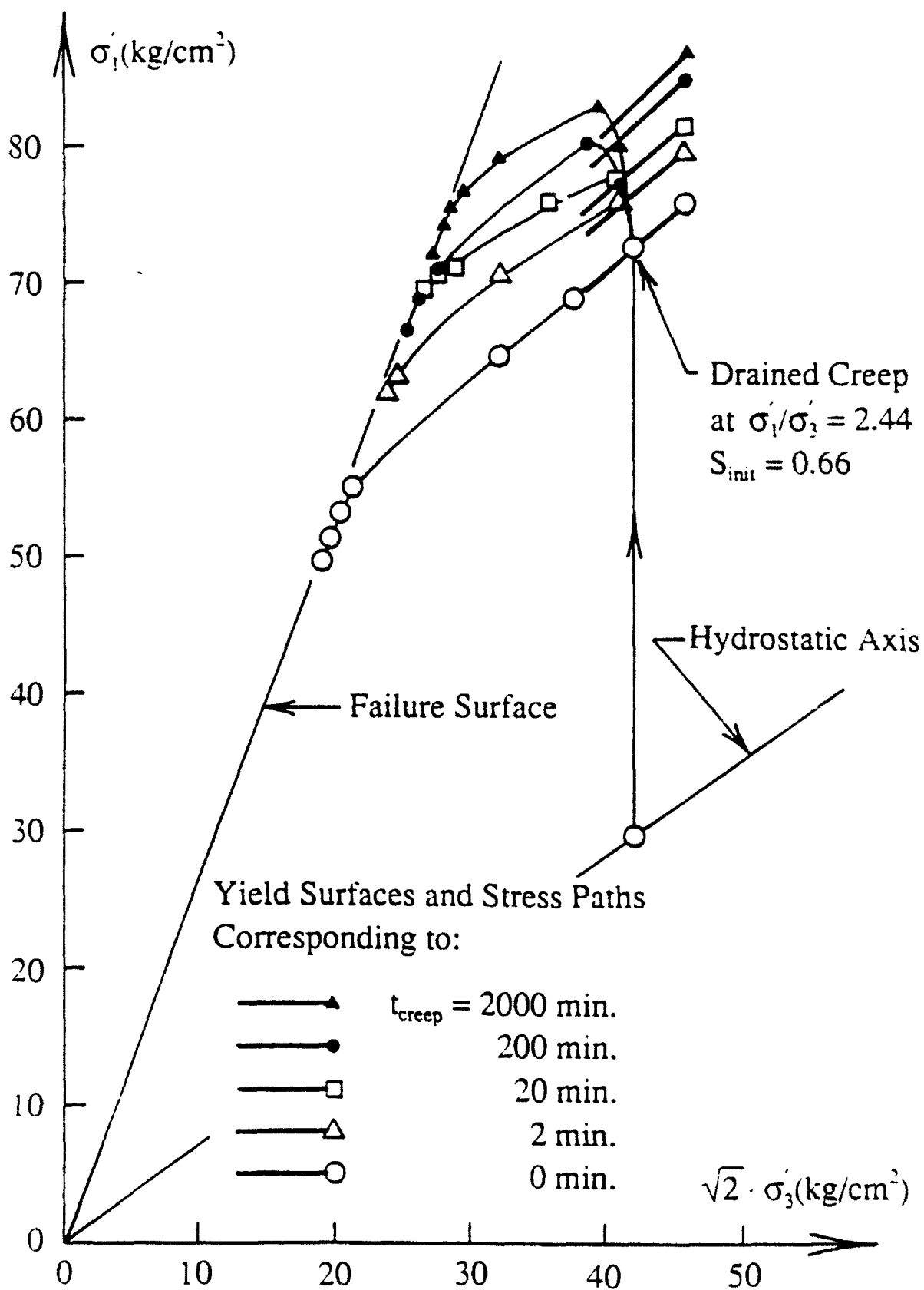


Fig. 8. Effective stress paths in triaxial plane for five creep and instability tests on loose Sacramento River sand at  $(\sigma_1 - \sigma_3) = 43.0$  kg/cm<sup>2</sup> (4,220 kPa).

points also move out with increasing amounts of creep, and instability occurs under the stress controlled loading after the yield surface has been crossed. Thus, the effect of creep is to move the yield surface out and to stabilize the soil, i.e. increasing amounts of creep require increasingly high stress differences to render the sand unstable.

#### Technical journal publications:

- Lade, P.V. (1992) "Static Instability and Liquefaction of Loose Fine Sandy Slopes", *Journal of Geotechnical Engineering*, Vol 118, No. 1 January, pp. 51-71.
- Lade, P.V., and Yamamuro, J.A. (1993) "Stability of Granular Materials in Post Peak Softening Regime," *Journal of Engineering Mechanics*, ASCE, Vol. 119, No. 1, January, pp. 128-144.
- Yamamuro, J.A., and Lade, P.V. (1992) "B-Value Measurements for Granular Materials at High Confining Pressures," *Geotechnical Testing Journal*, ASTM (accepted).
- Yamamuro, J.A., and Lade, P.V. (1992) "Effects of Strain Rate on Instability of Granular Soils," *Geotechnical Testing Journal*, ASTM (accepted).
- Lade, P.V., Bopp, P.A., and Peters, J.F. (1992) "Instability of Dilating Sand," *Mechanics of Materials*, Elsevier Science Publishers (accepted)
- Lade, P.V. (1992) "Creep Effects on Static and Cyclic Instability of Granular Soils," *Journal of Geotechnical Engineering*, ASCE (accepted).

#### Manuscript in Preparation:

- Yamamuro, J.A., and Lade, P.V., "Strain Localization in Extension Tests on Granular Materials," *Journal of Engineering Mechanics*, ASCE.
- Yamamuro, J.A., and Lade, P.V., "Drained Sand Behavior in Axisymmetric Tests at High Pressures," *Journal of Geotechnical Engineering*, ASCE
- Lade, P.V., and Yamamuro, J.A., "Undrained Sand Behavior in Axisymmetric Tests at High Pressures," *Journal of Geotechnical Engineering*, ASCE.
- Lade, P.V., and Yamamuro, J.A., "Significance of Particle Crushing in Granular Materials, *Journal of Geotechnical Engineering*, ASCE.
- Yamamuro, J.A., and Lade, P.V., "One-Dimensional Compression of Sands at High Pressures," *Journal of Geotechnical Engineering*, ASCE.
- Yamamuro, J.A., and Lade, P.V., "Instability of Granular Materials at High Pressures, *Soils and Foundations*, JSSMFE.
- Lade, P.V., and Yamamuro, J.A., "The Angle of Dilation at High Pressures," *Geotechnique*, London, England.

### Professional personnel:

Yamamuro, J.A.	-	Ph.D. student (graduated in Winter 1993)
Bowman, L.	-	M.S. student (graduation expected June 1993)
Bach, O.	-	Postdoctoral Scholar

### Interactions:

Yamamuro, J.A., and Lade, P.V. (1992) "The Effective Stress Path for Soil at High Pressure," Proc. ASCE Ninth Engineering Mechanics Conference, Texas A&M, College Station, Texas, May 25-27, pp. 729-732.

Lade, P.V. (1992) "Instability of Slopes with Nonassociated Flow," Proc. ASCE Ninth Engineering Mechanics Conference, Texas A&M College Station, Texas, May 25-27, pp. 288-291.

Lade, P.V. (1992) "Influence of Creep on Static and Cyclic Instability of Granular soil," presented at a Workshop on "Modern Approaches to Plasticity" held in Horton, Greece, June 12-16, 1992 (invited).

Lade, P.V. (1992) "Instability and Liquefaction of Granular Materials," presented at the 4th International symposium on Numerical Methods in Geomechanics (NUMOG IV) held in Swansea, United Kingdom, August 24-27, pp. 3-13 (invited keynote lecture).

Skyers, B.D., Yamamuro, J.A., and Lade, P.V. (1993) "Effect of Strain Localization in Triaxial Extension Tests," manuscript to be submitted to the Third International Workshop on Localization and Bifurcation Theory for Soils and Rocks, to be held in Aussois, France, September 6-9, 1993.

Lade, P.V. (1992) "Instability Analysis for Tailings Slopes," manuscript accepted for the 13th International Conference on Soil Mechanics and Foundation Engineering, to be held in New Delhi, India, January 1994.